SMOS SSS L2 ATBD

Draft issue 4, 3 Oct., 2005

Deleted: *3.2*

Deleted: *20 Sept*

Table of contents

Deleted: 5

1. Introduction

Purpose, SSS retrieval approach, and explanation of sub-models/options philosophy

to be written for ATBD issue 1

1.2 Definitions, acronyms and abbreviations

Formatted: Font: 12 pt

Formatted: Font: 12 pt

Comment [C1]: From J.B / S.Z

Formatted: Underline

Formatted: Bullets and Numbering

- **Measurement:** brightness temperature measured in one MIRAS polarisation mode, along with relevant information (radiometric noise, observation conditions, contributions as computed by the model, flags, polarisation direction). A measurement is associated with one Grid point, one Snapshot, one WEF and one Footprint .
- **Grid Point:** point on Earth surface where Measurements are available in SMOS L1c product.
- **Dwell line:** ensemble of Measurements at the same Grid Point available in SMOS L1c product.
- **SSS spatial resolution:** Mean Area of Earth surface, centred on a Grid Point, where SSS is retrieved. SSS spatial resolution is deduced from Footprints of Dwell line Measurements deemed valid for SSS retrieval.
- **WEF:** 2D weighting function derived from synthetic antenna gain of MIRAS interferometer, apodization function used at reconstruction and fringe wash factor. Also termed synthetic antenna pattern or equivalent array factor. The two dimensions are differential cosines in the antenna reference frame.
- **Footprint:** 3db contour of WEF once WEF has been projected on Earth surface. Footprint is centred on a Grid point and defined by major and minor axes of an ellipse. Axes lengths are provided by SMOS L1c product.

Now being completed

2. Algorithm overview

A scheme with blocks showing the two approaches and the ensemble of forward models for iterative retrieval.
Historical review and justification for the selected options (sub-models) [WP2100 in ESL proposal]

to be written in detail for ATBD issue 1

A series of physical models (separate modules 4.1 to 4.10 in this ATBD) are applied to auxiliary data (SST, wind, etc.) and a first guess SSS, to compute the brightness temperature that should be measured at a specific polarization and geometric configuration. These values

are transported to SMOS antenna level (module 4.12) and then compared to actually measured Tb. An iterative process (considering all measurements/views of a single grid point obtained in consecutive snapshots, module 4.14) allows minimization of the difference between both values, until identifying a retrieved SSS for this grid point. Three different models are proposed for the effect of ocean surface roughness in L-band emissivity (modules 4.2 to 4.4) and then three retrieval processes will be run in parallel, and three SSS values provided in the L2 Output Product. A selection of the optimal method is expected to be achieved during SMOS commissioning phase and then implemented in the operational L2 processor.

An alternative approach (section 5) uses the neural network technique to retrieve SSS from SMOS measurements and a previous training data set.

The SSS retrieval algorithms described in this ATBD will be applied to all ESEA grid points included in a SMOS L1c product (half-orbit swath).

3. Decision tree

The purpose of the decision tree is to check the conditions of all the grid points coming from L1c to decide processing them or not to retrieve salinity. Additional information will be provided in the Output Product in terms of flags to "processing" grid points to describe some particular conditions that can rise warnings for some L3 applications or indicate that future specific reprocessing could be implemented.

A series of tests, with defined threshold values, have to be run consecutively over each grid point before applying the SSS retrieval algorithm to it:

Subject	*Test*	*Threshold*	*Decision*
L1 flag: Quality check (snapshot, not grid point level)	Percentage of passed quality checks above threshold	TBD at L1	Process snapshot
Ocean/coastal grid point	Applying land mask provided by L1 + computing distance to coast	1) Land: grid point inside the land mask 2) Coast/Land: grid point outside the land mask but land in a radius Rmin from the grid point (40 km TBC). 3) Coast/Ocean: grid point outside the land mask; no land in a radius Rmin but land in a radius Rmax (100 km TBC). 4) Ocean/no_land: grid point outside the land mask; no land in a radius Rmax from the grid point.	1) SSS retrieval is not performed 2) SSS retrieval is not performed and grid point is flagged as land contaminated. 3) SSS retrieval performed, grid point flagged as coast_ocean To minimize land contamination and large ocean inhomogeneities frequently observed in coastal areas, only measurements with semi-major-axis < Rmin (TBC) are used in the retrieval, 4) SSS retrieval performed. only measurements with Elongation < 1.8 and Spatial resolution < 100km (TBC) are used in the retrieval,
Ocean free of ice	Applying sea ice mask (evolving info.)	1) Ice: grid point inside ice mask 2) Ice/Ocean: grid point outside the ice mask; contains ice in a radius Rmin from the grid point 3) Ocean/ice_suspect: grid point outside the	1) SSS retrieval is not performed 2) SSS retrieval is not performed 3) SSS retrieval is performed. If SST less than 2°C, if Tb>Tbflat (SST, SSS_climato) + 20K, for more than N%

Comment [JF2]: Need to take into account the failure of one snapshot in the sequence for dual or full pol snapshots processing JF

Deleted: Approach 1: same as for land mask¶
Approach 2: discard angular measurements above threshold, and flag grid point¶
Alternative approach by JB (see below)

		ice mask, does not contain ice in a radius Rmin from the grid point 4) Ocean/no_ice: other grid points	(TBD) of the measurements used in the retrieval, grid point flagged as ice_suspect. 4) SSS retrieval is performed.
L1 flags: Grid points position within Field of View	Grid points classified as belonging to Alias Free FOV, Extended AF FOV and (being inside) near the border of it	The definition of border will be configurable. First approach considers 30 km *To be discussed: Should the BORDER points be processed?*	1) Grid points outside EAF _FOV will not be processed (if any) 2) A L2 flag can indicate the number of views belonging to each one of these three categories that have been used to compute an SSS value
L1 flag: RFI	L1 will not apply a RFI static mask (difficult due to being angle dependent) but build a table that will be further filled	TBD by L1?	Not process views flagged RFI by L1
Corrupted data (due to RFI or any other reason)	Step 1: Tb values within expected range	TBD	Process
	Step 2: Regression of Tb values vs. incidence angle and check outliers *Or alternative method proposed by JLV at SRR (see below)*	3 sigma or gaussian shape of the Tb distribution	Remove outliers
Galactic noise	If specular reflection goes to center of galaxy … *(SRR: to be written by JB)*	TBD	TBD
Sun glint and other Sun flags from L1	Use model by N. Reul and compare with L1 flags	*To be completed by NR*	TBD
Moon glint	Check if point is affected by specular reflection	If yes	Flag grid point
Num. of observations	Angular data available	By now we decide not to specify a minimum number for flagging	Number = Field in output product (can be completed by FOV information as described above)
Heterogeneity of sea state	TBD		Specific processing: modify sigma in iterative retrieval in function of the ocean area
Sea surface types	TBD		Specific processing. modify sigma in

Formatted: Font color: Auto

Deleted: Pixels

Formatted: Highlight

Deleted: it

Comment [JF4]: Or just measurement? reflection can affect only some views of a single point

Comment [JF3]: Is this provided by L1 as a flag? or contribution will simply be removed?

Comment [JF5]: Only for reprocessing?

Same in flag below

			iterative retrieval in function of the ocean area
Rain	High value of rainfall (ECMWF data)	TBD	Flag: intense rain
Spatial resolution and ellipticity of measurement	*Warning. we might need big and elongated measurements for bias correction*	100km (TBC) Threshold on major/minor axis ratio TBD	Flag or discard? *Now incorporated in land mask issue*

Deleted: them

Formatted: Highlight

Formatted: Font: Italic, Font color: Red

Method to detect outliers (proposed by JLV):

1. For each measurement run forward model with auxiliary data and climatological SSS
2. Remove median of model and data for a grid point (to avoid the scene dependent bias issue)
3. Compare measurements with modeled values and discard those that differ by more than 5 times the radiometric noise

4. Algorithm description

In the following sections it is necessary to take into account that polarised brightness temperature (of a plane wave measured by a radiometer) can be described through the polarisation vector $[T_b] = [T_{hh}, T_{hv}, T_{vh}, T_{vv}]$ in the Earth reference frame and $[T_{xx}, T_{xy}, T_{yx}, T_{yy}]$ in the antenna reference;
or through the Stokes vector [I, Q, U, V], where:
I, first Stokes parameter, is the sum of both perpendicularly polarised T_b, H-pol + V-pol ($T_{hh}+T_{vv}$ or $T_{xx}+T_{yy}$, depending on the reference) and represents the total power transported by the wave
Q, second Stokes parameter, is their difference V-pol – H-pol ($T_{vv}-T_{hh}$ or $T_{yy}-T_{xx}$), and represents the linear polarisation oriented in the reference direction
U, third Stokes parameter, is the difference between linear polarisation components oriented in +45º and -45º; it is related to cross-polarisations by $U = T_{xy}+T_{yx} = T_{hv}+T_{vh}$
V, fourth Stokes parameter, is interpreted as the difference between left-hand and right-hand circularly polarised brightness temperature; all measurements indicate that it is negligible at L-band, so for most applications V is assumed to be 0.

Most of times, instead of the Stokes vector, the modified Stokes vector $[T_1, T_2, T_3, T_4]$ ($[T_{hh}, T_{vv}, U_{Earth}, V_{Earth}]$ or $[T_{xx}, T_{yy}, U_{antenna}, V_{antenna}]$) is used, as it is composed by the quantities actually measured by a fully polarised radiometer:
[modified Stokes vector] = $\lambda^2/kB\eta$ [$<|E_H|^2>$, $<|E_V|^2>$, $2Re<E_V E_H^*>$, $2Im<E_V E_H^*>$]
where λ is the radiometer's wavelength, k the Boltzmann constant, B the bandwidth, and η the medium impedance (air). E_H and E_V are the two orthogonal components of the plane wave.

To avoid any misunderstanding with other parameters used throughout this document we will designate the modified Stokes vector by [A1, A2, A3, A4] in the antenna reference (instead of $[T_{hh}, T_{vv}, U_{Earth}, V_{Earth}]$) and $[T_h, T_v, T_3, T_4]$ in the Earth reference (instead of $[T_{xx}, T_{yy}, U_{antenna}, V_{antenna}]$). This convention was adopted as part of the harmonisation activities in L2 processors development (see in annex ACRI Reqts_L2Draft-2.doc: SMOS L1c product requirements for sea surface salinity retrieval at level 2, 28/4/05**).**

Formatted: English (U.K.)

Note: Need to specify in all modules whether angles are from nadir or zenith, and whether they are provided in degrees or radians

4.1. Flat sea

4.1.1. Theoretical description

4.1.1.1. Physics of the problem

The brightness temperature can be expressed as the sum of two terms; the brightness temperature in the case of completely flat sea and the additional brightness temperature (ΔTb) due to the surface roughness, as follows:

$$T_{b,p}(\theta, SST, SSS, P_{rough}) = T_{b\ Fresnel,p}(\theta, SST, SSS) + \Delta T_{b\ rough,p}(\theta, SST, SSS, \overrightarrow{P_{rough}}) \qquad [4.1.1]$$

The first term is Tb due to the emission of a flat sea surface, which is well described by the Fresnel equations and is polarization dependent (p). The second term is the increment of brightness temperature due to sea roughness, which can be described through several parameters (P_{rough}) related to processes that modify this roughness. θ is the angle under which Tb is measured, SST is the sea surface temperature and SSS the sea surface salinity, understanding as surface the upper fraction of the ocean that contributes to L-band emission (approx. 1 cm).

The brightness temperature is defined as:

$$T_b(\theta) = e(\theta) \cdot SST \qquad [4.1.2]$$

where e(θ) is the flat surface emissivity at L-Band which carries the major information regarding SSS. It can be written, as follows:

$$e(\theta) = 1 - \Gamma(\theta, \varepsilon) \qquad [4.1.3]$$

Formatted: Lowered by 5 pt

where Γ is the Fresnel reflection coefficient, that is dependent on the incident radiation nadir angle θ, and on the complex dielectric constant of sea water ε, and the polarisation.

Deleted: R

The complex dielectric constant of the sea water is dependent on temperature and on the concentration of salt. It can be calculated at any frequency, within the microwave band, from Debye (1929) expression:

$$\varepsilon = \varepsilon_\infty + \frac{(\varepsilon_s - \varepsilon_\infty)}{1 + i\omega\tau} - i\frac{\sigma}{\omega\varepsilon_0} \qquad [4.1.4]$$

in which *i* is the imaginary number, ε_∞ is the electrical permittivity at very high frequencies, ε_s is the static dielectric constant, τ is the relaxation time, σ is the ionic conductivity, and ε_0 is

the permittivity of free space. ε_s, τ and σ are functions of the temperature and salinity of sea-water, and have been evaluated by Klein and Swift (1977), Ellison et al. (1998) and Blanch and Aguasca (2004).

After some comparisons and analysis (Camps et al., 2004; Wilson et al., 2004), the Klein and Swift dielectric constant model has been agreed to be the model that better expresses this parameter.

4.1.1.2. Mathematical description of algorithm

Following Klein and Swift (1977) model, the values of the parameters that describe the dielectric constant of sea water are:

$$\varepsilon_\infty = 4.9 \qquad [4.1.5]$$

$$\varepsilon_0 = 8.854\ 10^{-12} \qquad [4.1.6]$$

$$\varepsilon_s = \left(87.134 - 0.1949T - 0.01276T^2 + 0.0002491T^3\right) \left(1 + 1.613\times10^{-5}TS - 0.003656S + 3.21\times10^{-5}S^2 - 4.232\times10^{-7}S^3\right) \qquad [4.1.7]$$

$$\tau = \left(1.768\times10^{-11} - 6.086\times10^{-13}T + 1.104\times10^{-14}T^2 - 8.111\times10^{-17}T^3\right) \left(1 + 2.282\times10^{-5}TS - 7.638\times10^{-4}S - 7.760\times10^{-6}S^2 + 1.105\times10^{-8}S^3\right) \qquad [4.1.8]$$

$$\sigma = S\left(0.18252 - 0.0014619S + 2.093\times10^{-5}S^2 - 1.282\times10^{-7}S^3\right) \exp((T-25)(0.02033 + 0.0001266(25-T) + 2.464\times10^{-6}(25-T)^2 - S(1.849\times10^{-5} - 2.551\times10^{-7}(25-T) + 2.551\times10^{-8}(25-T)^2))) \qquad [4.1.9]$$

Being S the salinity in psu (practical salinity units, UNESCO, 1978) and T the temperature in ºC. For application in SMOS S will be SSS and T will be SST (note that SST is elsewhere expressed in Kelvin).

The dielectric constant ε is computed following equation [4.1.4] and a complex value results. Then the Fresnel reflection coefficients for a flat sea, for each polarisation, can be calculated as follows:

$$R_H = \left|\frac{\cos\theta - \sqrt{\varepsilon - \sin^2\theta}}{\cos\theta + \sqrt{\varepsilon - \sin^2\theta}}\right|^2$$

$$R_V = \left|\frac{\varepsilon\cos\theta - \sqrt{\varepsilon - \sin^2\theta}}{\varepsilon\cos\theta + \sqrt{\varepsilon - \sin^2\theta}}\right|^2 \qquad [4.1.10]$$

Formatted: Lowered by 41 pt

And finally Th and Tv for a flat surface are computed following [4.1.2] and [4.1.3], as:

$$Th\_flat(\theta, SST, SSS) = (1 - Rh(\theta, \varepsilon)) \cdot SST$$
$$Tv\_flat(\theta, SST, SSS) = (1 - Rv(\theta, \varepsilon)) \cdot SST \qquad [4.1.11]$$

4.1.1.3. Error budget estimates (sensitivity analysis)

ε_∞ has an error of 20% but this is negligible at L-band.

Cox quotes that the ionic conductivity of the sea water, σ, has an error of ± 0.03% for salinities between 30 and 40 psu, which is also negligible.

The static permittivity, ε_s, has a maximum per cent error of 0.49 with respect the measurements, and an average per cent error of 0.11.

The relaxation time, τ, has been derived from measurement with an accuracy of $2.12*10^{-13}$ and this is the assumed error for that parameter.

Ho's estimated error for ε' is 0.2%.

Taking ε =75 + j42, which is the approximate value of the dielectric constant of the sea water at 1.43 GHz when SSS=20 psu and T=20ºC, it then follows that the error associated with this particular choice is:

$$\delta\varepsilon \cong 1.15(\delta\varepsilon' + \delta\varepsilon'')10^{-3}$$

Using the above mentioned values, $\delta\varepsilon' \approx 0.15$ and $\delta\varepsilon'' \approx 0.13$. Hence, the error in the brightness temperature with T=293K is

$$\delta Tb = \delta e * T \cong 0.09 \text{ K}$$

4.1.2. Practical considerations

4.1.2.1. Calibration and validation

S. Blanch, from the Polytechnic University of Catalonia (UPC), is preparing a new laboratory experiment to compute the parameters that describe the dielectric constant following the Debye expression. Results of this experiment will be used to validate the Klein and Swift model. If any change or tuning of the parameters is necessary this should be applied to the model, and the corresponding coefficients file modified accordingly.

4.1.2.2. Quality control and diagnostics

4.1.3. Assumption and limitations

The measurements on which the Klein & Swift model has been based, were obtained from NaCl solutions and some from real sea water samples. Few measurements were done on the

salinity range from 30-40 psu, which are the most common values in the world's ocean. However, until a new model is established and validated, the SMOS and Aquarius communities agreed on using Klein and Swift.

Bibliography

Blanch, S. and Aguasca, A. (2004). Seawater dielectric permittivity model from measurements at l-band. Proceedings of IGARSS 2004, Alaska.

Camps, A., Font, J., Gabarró, C., Miranda, J., Obligis, E., Labroue, S., Boone, C., Sabia, R., Vall-llosera, M., Reul, N., June 2004. WP1100, ESTEC ITT 1-4505/03/NL/Cb

Debye, P. (1929). Polar Molecules. New York: Reinhold.

Ellison, W., Balana, A., Delbos, G., Lamkaouchi, K., Eymard, L., Guillou, C., and Prigent, C. (1998). New Permittivity Measurements of Sea Water. Radio Science, 33(3):639–648.

Klein, L. and Swift, C. (1977). An Improved Model for the Dielectric Constant of Sea Water at Microwave Frequencies. IEEE Transactions on Antennas and Propagation, AP-25(1):104–111.

Swift, C. (1980). Passive Microwave Remote Sensing. Boundary-layer Meteorology, 18:25–54.

UNESCO (1981) The Practical Salinity Scale 1978 and the International Equation of State of Seawater 1980. 10th report of the Joint Panel on Oceanographic Tables and Standards. UNESCO Technical Papers in Marine Science, 36

Wilson, W., Yueh, S., Dinardo, S., and Li, F. (2004). High stability l-band radiometer measurements of saltwater. IEEE Transactions on Geoscience and Remote Sensing, 42(9):1829–1835.

4.2. Surface roughness 1: two-scale model

4.2.1. Theoretical description

For a complete description of the model, the reader should refer to (Yueh, 1997).

4.2.1.1. Physics of the problem

By definition, sea surface brightness temperature, $T_{b\ sea}$, in the direction defined by the incident angle θ and the azimuth angle ϕ is:

$T_{b\ sea}(\theta, \phi) = SST \cdot e(\theta, \phi)$,

where e is sea surface emissivity and SST is sea surface temperature1. Assuming thermodynamical equilibrium, the Kirchhoff law applies and $e = a = 1 - R$, where a and R are sea surface absorptivity and reflectivity respectively. The so-called modified Stokes vector is written as

$$\overrightarrow{\text{Tb sea}} = \begin{bmatrix} T_h \\ T_v \\ T_3 \\ T_4 \end{bmatrix} = SST.\left(\begin{bmatrix} 1 \\ 1 \\ 0 \\ 0 \end{bmatrix} - \vec{R} \right)$$

where Tv and Th are Tb sea in vertical and horizontal polarisations (hereafter V- and H-pol) respectively, related to first and second Stokes parameters by I = Tv + Th and Q = Tv − Th respectively, and T3 and T4 are the third (U) and fourth (V) Stokes parameters respectively. Due to the sea surface not being flat, scattering induced by sea waves slightly modifies the reflectivity from Fresnel's equations. Consequently, R depends not only on incidence angle θ and sea water dielectric constant (and in turn on SST and SSS) but also on ϕ and shape of the surface, i.e. the roughness.

The sea surface is never flat, with roughness at very different scales being created by local and instantaneous wind and/or distant wind (inducing swell), as well as by wave interactions. Roughness at sea surface scatters impinging electromagnetic waves and consequently modifies reflection from Fresnel's equation. Numerical rigorous solution of Maxwell's equations is not considered as they cannot be resolved explicitely. There is two widely-used approximated models, the two scales model and the so-called one-scale small slopes approximation. A simpler approach based on geometric optics (GO) (*Stogryn* (1967), *Prigent and Abba* (1990)) is discarded for use at low frequency. Indeed, whereas at high frequencies (i.e. in the millimeter domain) waves smaller than λ_0 (the radiometer wavelength) have a negligible contribution and all ocean waves can be considered as large-scale, simulations at 21 cm showed that a significant signal is induced by small scales and that a large part of roughness-induced signal is not predicted by GO (*Dinnat et al, 2002b).* Noticeably, GO predicts very small roughness effect on Tb sea at nadir and moderate incidence angles, in contradiction with observations from *Hollinger* (1971), *Swift* (1974), *Webster and Wilheit* (1976), *Camps et al.* (2004a) and *Etcheto et al.* (2004), as well as those from *Blume et al.* (1977) at 2.65 GHz. Note that it is very unlikely that the observed Tb variations correlated with wind speed variations are due to foam only, because they were observed also at small wind speed WS and the trend was close to linear in WS (in the limit of measurements precision).

4.2.1.1.1. Electromagnetic model

In the two-scale model, surface is modelled as the superimposition of small waves upon large waves, roughness scales being parted into small and large scales by a cutoff wavelength λ_c. Small scales are sea waves whose height is small compared to λ_0 and large scales are waves whose curvature radius is large compared to λ_0 . Below we summarize main elements of the two scale model of (*Yueh* (1997). The reader should refer to the original paper for a complete description.

To derive $T_{b\ sea}$, one combines both large and small scales by integrating contributions of all large waves over the slopes domain (S_x, S_y) and weighting contributions by the slopes probability density function (PDF) of the large waves ($P(S_x, S_y)$). It follows that

$$\mathrm{Tb\ sea}\,(\theta,\phi) = \iint T_{b,l}(\theta,\phi)P(S_x,S_y)(1-S'_x\tan\theta)dS_x dS_y$$

where P is assumed to be Gaussian, and its width depends on the mean square slope (MSS) of the large-scale waves, S'x and S'y are the surface slopes along and across the radiometer azimuth observation direction, respectively. Local brightness temperature for a large wave ($T_{b,l}$) differs from $T_{b\ flat}$ because (1) incidence and azimuth angles are modified because of the large wave's tilting, resulting in local incidence and azimuth angles (θ_l, ϕ_l), and (2) diffracting small-scale roughness is present on the large wave. Hence, T_b is expressed as

$$T_{b,l}(\theta_l, \phi_l) = SST \cdot (1 - R_{ss}(\theta_l, \phi_l)) \quad . \quad (6)$$

where $R_{ss} = R_c + R_i$ is reflectivity of small-scale roughness covered surface, separated into a coherent (R_c) and an incoherent (R_i) component. The incoherent term, that accounts for waves impinging from non specular direction and scattered toward the radiometer, according to first order small-perturbation method (SPM1, *Rice* (1951)) is written as:

$$R_i(\theta_l,\phi_l) = \int_0^{\Pi/2}\sin\theta_\alpha d\theta_\alpha \int_0^{2\Pi}\frac{\cos\theta_\alpha}{4\Pi\cos\theta_l}\begin{bmatrix}\gamma_{hhhh}+\gamma_{hvhv}\\ \gamma_{vvvv}+\gamma_{vhvh}\\ 2\,\mathrm{Re}(\gamma_{vhhh}+\gamma_{vvhv})\\ 2\,\mathrm{Im}(\gamma_{vhhh}+\gamma_{vvhv})\end{bmatrix}d\varphi_\alpha$$

where γ functions are the bistatic scattering coefficients, dependent on sea surface power spectrum of small-scale roughness (ψ_{ss}).

The coherent term R_c, that expresses reflection and scattering of the power impinging from specular direction, is modeled using a second order small perturbation method (SPM2, *Yueh et al.* (1988)). Coefficients derived from SPM2 are (*Yueh,* 1997):

$$R_c(\theta_i,\phi_i) = \begin{bmatrix}\left|R_{hh}^{(0)}\right|^2\\ \left|R_{vv}^{(0)}\right|^2\\ 0\\ 0\end{bmatrix} + \int_0^{2\Pi}d\varphi_\alpha\int_0^{\infty}k_0^2 k_{\rho\alpha}\Psi_{ss}(\overrightarrow{k_c})\begin{bmatrix}2\,\mathrm{Re}\left\{R_{hh}^{(0)*}g_{hh}^{(2)}\right\}\\ 2\,\mathrm{Re}\left\{R_{vv}^{(0)*}g_{vv}^{(2)}\right\}\\ 2\,\mathrm{Re}\left\{\left(R_{hh}^{(0)*}-R_{vv}^{(0)*}\right)g_{vh}^{(2)}\right\}\\ 2\,\mathrm{Im}\left\{\left(R_{hh}^{(0)*}+R_{vv}^{(0)*}\right)g_{vh}^{(2)}\right\}\end{bmatrix}dk_{\rho\alpha}$$

Johnson and Zhang (1999) introduce the unified equation that unifies R_i and R_c:

$$R_{ss} = \begin{bmatrix} \left|R_{hh}^{(0)}\right|^2 \\ \left|R_{vv}^{(0)}\right|^2 \\ 0 \\ 0 \end{bmatrix} + \underbrace{\int_0^{\infty} k_0^2 k_\rho' dk_\rho' \int_0^{2\Pi} \Psi\ (k_\rho', \phi') \begin{bmatrix} g_h \\ g_v \\ g_3 \\ g_4 \end{bmatrix} d\phi'}_{\delta R_{ss}} = \begin{bmatrix} R_h^{flat}(\theta_i, \phi_i) \\ R_v^{flat}(\theta_i, \phi_i) \\ 0 \\ 0 \end{bmatrix} + \delta R_{ss}$$

where the first term is the reflectivity of a flat sea, ψ is the surface power spectrum, $k_c = 2\Pi/\lambda_c$ is the cutoff wavenumber and g_p functions (p = v, h, 3 or 4) that account for both coherent and incoherent contributions to δR_{ss}, the correction to Fresnel reflectivity induced by small-scale waves. Expanding physical quantities in a Fourier series with respect to azimuth direction, and under the assumption of even symmetry for surface roughness, one has:

$\delta R_{ss} = \delta R_{ss,0} + \delta R_{ss,2}\, f(2\phi_0)$

$C(k, \phi) = C_0(k) + C_2(k) \cos(2\phi_0)$

$g_p = g_{p,0} + g_{p,2}\, f(2\phi_0)$

where f is cosine function for T_v and T_h and sine function for T_3 and T_4, $C(k, \phi) = k^4 \Psi(k, \phi)$ is the 2D surface curvature spectrum. Therefore, the omnidirectional component ($\delta R_{ss,0}$) and second harmonic amplitude ($\delta R_{ss,2}$) result from weighted integrals of the respective harmonics of the curvature spectrum:

$$\delta R_{ss,0} = \int_{kc/k0}^{\infty} C_0(k_\rho') . \begin{bmatrix} g'_{h,0} \\ g'_{v,0} \\ g'_{3,0} \\ g'_{4,0} \end{bmatrix} d\xi$$

and

$$\delta R_{ss,2} = \int_{kc/k0}^{\infty} C_2(k_\rho') . \begin{bmatrix} g'_{h,2} \\ g'_{v,2} \\ g'_{3,2} \\ g'_{4,2} \end{bmatrix} d\xi$$

where $\xi = k/k_0$ and $g'_{p,n} = g_{p,n}/\xi$ are scattering weighting functions given by *Johnson and Zhang* (1999).

Dinnat and Drinkwater (2004) assessed the relative influence of the various scales on $T_{b\ sea}$ from above weighting functions. Similarly to the radar case, there is a specific range of wavelengths (i.e. typically around λ_0) that contributes most to $T_{b\ sea}$, particularly when θ is small. However, significant additional contributions arise also from various scales especially at large θ. **Therefore, good knowledge of roughness is required over a wide range of scales (typically from 1 m to 2 cm).**

4.2.1.1.2. Sea surface roughness model

In the following Tbsea is decomposed as:

Tbsea=Tbflat + Tbrough

Where Tbflat is Tb modelled for a flat sea and Tbrough is the signal induced by the roughened sea.

Sea surface roughness is described using a 2D surface power spectrum $\psi(k_{p'}, \phi')$, i.e. a Fourier transform of the autocorrelation function of sea surface height, that appears in *Rc* and *Rss* equations and implicitly in *Ri*, or using 2D curvature spectrum $C(k,\phi)$ that appears in $\delta R_{ss,0}$ and $\delta R_{ss,2}$ equations. ψ is also used in the composite model to compute large-scale MSS that defines the slopes probability density function (PDF) of the large waves (P) used in Tbsea equation. There exists in literature many very different wave spectrum models (e.g. *Durden and Vesecky* (1985), *Donelan and Pierson* (1987), *Apel* (1994), *Yueh*(1997), *Elfouhaily et al.* (1997), *Lemaire* (1998), *Kudryavtsev et al.* (1999)...). In the following we focus on DV model as it has been widely used to simulate T_{brough} at L-band and it simulates Tbrough in good agreement with campaign measurements provided it is multiplied by a factor2. Table 1 summarizes Irough (=Tvrough+Through) sensitivity to wind speed, as found from 2-scale model and DV2 spectrum and derived from various campaigns:

Table 1 : Irough sensitivity to wind speed, for wind speed above 3m/s: theoretical models without foam and measurements

	dI/dWS	Incidence angle	Reference
SPM model + 2x Durden and Vesecki wave spectrum	0.45K/m/s	0-50°	ESA 14273/00/NL/DC study
Hollinger measurements	0.35K/m/s	20-70°	[*Hollinger*, 1971]
WISE measurements	0.4K/m/s May decrease to 0.3K/m/s at 55° depending on wind height corrections (*Camps et al.*, 2004)	25-55°	[*Camps et al.*, 2004; *Etcheto et al.*, 2003]
Eurostarrs measurements Mediterranean transit	0.5K/m/s Assuming dTh/dWS=dTv/dWS (NB: if it is not true, dI/dWS should be larger)	21.5 and 38.4°	[*Etcheto et al.*, 2004]
Cape Cod Canal measurements	0.5K/m/s Assuming dTh/dWS=dTv/dWS (NB: if it is not true, dI/dWS should be lower)	23°	[*Sasaki et al.*, 1987; *Swift*, 1974]
JPL Gulf Stream Flights	0.6K/m/s	40°	[*Yueh et al.*, 2001]

The *Durden and Vesecky* (1985) (hereafter DV) model is a semi-analytic spectrum, that relies onwork by *Pierson and Moskowitz* (1964) for gravity waves ranges, on *Phillips* (1977) for general form in equilibrium range, and that is fitted to HH-pol radar data at 13.9 GHz in order to account for deviation from the Phillips spectrum. The model is tuned to agree with *Cox and Munk* (1954) (hereafter CM) measured MSS. *Yueh* (1997) proposes to multiply the DV model by a factor 2 (hereafter DV2) to account for possible underestimation of MSS measured by *Cox and Munk* (1954), as suggested by *Donelan and Pierson* (1987) and *Apel* (1994), and to better fit data at 19.65 and 37 GHz. It should be noted however that, if needed, the multiplying factor is quite uncertain, and Tbrough is directly proportional to this factor.
Upwind/downwind $T_{b\ sea}$ asymmetry is uncertain at L-band: using the empirical model for roughness asymmetry developed by *Yueh* (1997) from high frequency radiometric data, it is estimated to be up to $\pm$ 0.4 K at $\theta = 60°$ and $WS =$ 8 m/s, and very small at moderate

incidence angles. Upwind/crosswind asymmetry is very dependent on the spectrum model. Elfouhaily et al. (1998) model predicts asymmetry 3 times larger than DV2 model (and hence 6 times larger than DV), but still at most ± 0.3 K for WS = 10 m/s.

Sensitivity to roughness and model uncertainty studies are reported in *Dinnat et al.* (2003a). In this model, influence of roughness depends slightly on *SST* and *SSS*. Using a constant *SST* over the global ocean for estimating roughness effect would induce an error on retrieved *SSS* of the order of 0.5 psu between regions having SST differing by 30°C (the SSS effect is less important as a variation of 7 psu on SSS leads to a less than 0.1 psu error on retrieved *SSS* **). Therefore, Tb_{rough} dependence on *SST* should not be neglected in case of *SSS* retrieval in the context of largely variable *SST* , as for example for global ocean measurements** where there is a risk to introduce regional biases.

Comment [EL6]: You should keep in mind that this is true only and only if roughness and SST are decorellated. In Dinnat et al, SST impact on roughness Tb is only considered through changes in the dielectric constant. However, in reality roughness is strongly correlated with SST especially for frontal locations, so that you should be more carefull in your statements here.
(N. Reul)

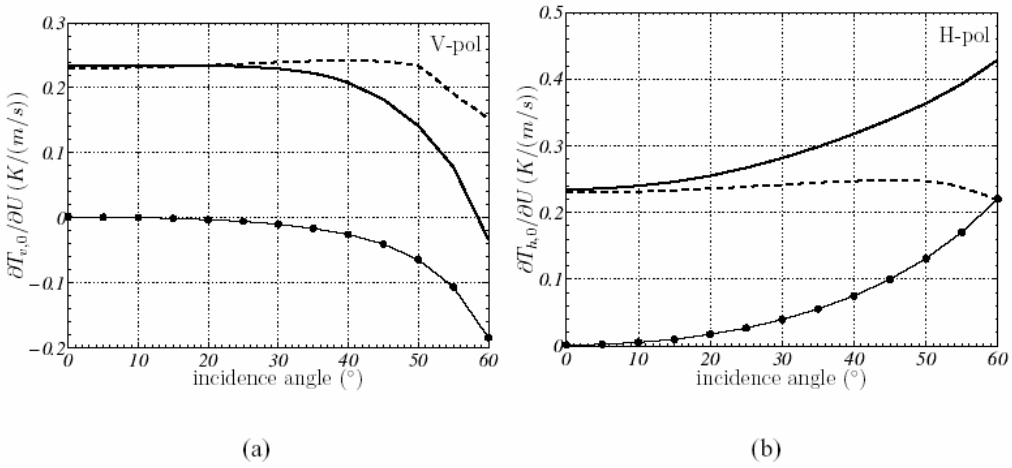

Figure 1: *Sensitivity of omnidirectional* $T_{b\,sea}$ *to wind speed for (a) V-pol and (b) H-pol and SST = 15°C, SSS =36 psu, and* WS = 8 *m/s. Note that this sensitivity depends on* WS*, particularly for small wind speeds. Respective contribution of (dashed line) small and (dotted line) large scales to (plain line) total signal are illustrated. Model for sea spectrum is twice Durden and Vesecky (1985).*

Whatever the sea-surface spectrum model is, wind increases T_v and T_h for most incidence angles, by the order of a few tenths of a Kelvin per meter per second (see fig. 1 derived from DV2 spectrum). Sensitivity of T_v varies very slightly with θ up to 30°, where it starts to decrease to reach 0 close to 55°, and to become negative above. Sensitivity of T_h increases with incidence angle. These large sensitivity differences between V- and H-pol are due to the combination of large- and small-scale effect. Figure 1 also reports Tb_{rough} simulated taking into account only one of the two scales domain. Whereas the effect of small scales is an increase of roughly the same amount in T_v and T_h up to 50°, the effect of large scales is opposite in V and H-pol, and very dependent on θ. Therefore, the increase in T_h sensitivity with θ results from the addition of both scales effects, whereas the decrease in T_v sensitivity at large θ translates the increasing relative importance of large scales effects that counteract small scales effect, θ ~55° being the incidence angle at which both scales effects cancel each other.
Nevertheless, it is of interest to note that **over most of the incidence angles measured by SMOS, the major contributors to Tbrough are the small scales.**
In the studies mentionned above, these small scales have been parametrized using WS assuming a neutral atmosphere (no air-sea temperature difference), i.e. a unique relationship between the friction velocity, U*, and WS. However this is usually not the case in the real

world and atmospheric instability may create variations on the order of 5-10% on U*. Wind speed, WS, at an altitude z, and U* are classically related using
-the Monin-Obukhov equation:

$$WS(z) - u_c = \frac{U*}{\kappa}\left[\ln\left(\frac{z}{z0}\right) + \Psi\right]$$

where u_c is the surface velocity (i.e. the surface current), κ is von Karman's constant (normally assigned to a value of 0.4), z0 is the roughness length (often parametrized as a function of U* and possibly dependent on wave age, in meters), and Ψ is a function of the stabiility parameter z/L where L is the Monin Obhukov length that classically depends on temperature difference between air and sea, on SST and on relative humidity,

-or using a drag coefficient:

$U*^2 / WS(10m)^2 = C_D$

that depends on the above mentionned parameters.
In Dinnat's model, when looking at Tbrough as a function of WS or as a function of U* for variations of Cd of 5 to 12%, we observe that Tbrough better correlates to U* than with WS : on Figure 2 Tbrough simulations are presented for a 50° incidence angle (for which we expect the largest influence of both WS and U* because of the competitive effect of small and large scales (Fig.1)): nevertheless the correlation with U* is still much better than with WS and the scatter induced by the varying Cd is always less than 0.1K for a given U* (which is not true for a given WS).

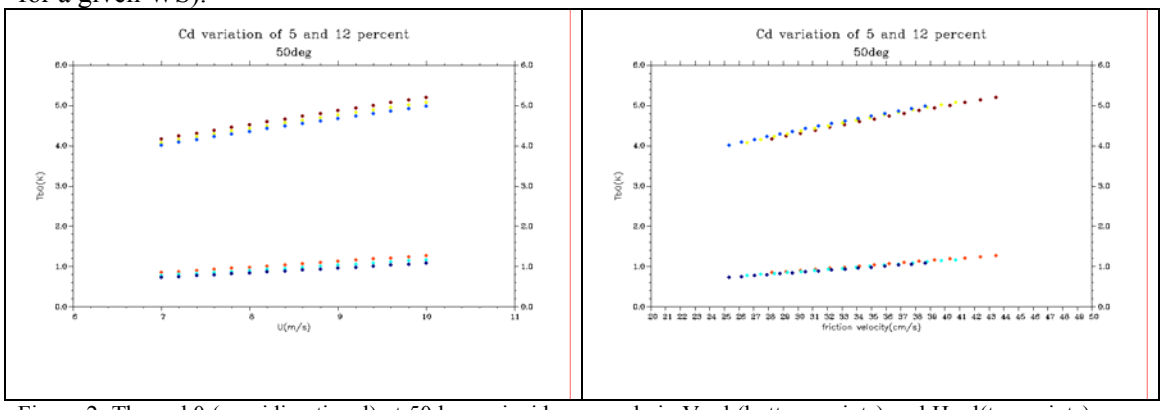

Figure 2: Tbrough0 (omnidirectional) at 50degree incidence angle in Vpol (bottom points) and Hpol(top points) as a function of wind speed (left) and as a function of U* (right) simulated for neutral conditions (blue points) and for Cd varying by 5% (yellow and light blue) and by 12% (red and brown).

Therefore, instead of parametrizing Tbrough variations as a function of WS only, we propose to relate them to U*, and to introduce the neutral equivalent wind speed parameter that is the parameter usually retrieved from scatterometer measurements.
Since scatterometer is primarily sensitive to U*, a neutral equivalent wind speed, WSn, has been introduced in the scatterometer community [*Liu and Tang,* 1996] that represents the wind speed that would be measured at 10m height if the atmosphere were neutral and if the surface speed was zero:

$$WSn = \frac{U*}{\kappa}\left[\ln\left(\frac{10}{z0}\right)\right] \quad (1)$$

Given air-sea temperature differences and relative humidity observed over various regions of the open ocean, systematic differences of 0.5 to 1m/s over some particular regions may occur between WS and WSn [*Liu and Tang,* 1996](e.g. in the equatorial Pacific).

4.2.1.2. Mathematical description of algorithm

Since the model computation is very heavy, a tabulation of Tb_{rough} will be provided.
Tbrough is decomposed as the sum of an omnidirectionnal signal plus first and second harmonics:

$$Tb_{rough} = \begin{bmatrix} Th0 + Th1\cos(\Phi) + Th2\cos(2\Phi) \\ Tv0 + Tv1\cos(\Phi) + Tv2\cos(2\Phi) \\ U1\sin(\Phi) + U2\sin(2\Phi) \\ V1\sin(\Phi) + V2\sin(2\Phi) \end{bmatrix} \quad (1)$$

where ϕ is the azimuth angle between wind direction (ϕw) and the azimuthal observation angle of radiometer look direction (ϕr): $\phi = \phi w - \phi r$ with all these angles counted counterclockwise.
Tabulations of Th0,Th1,Th2,Tv0,Tv1,Tv2, U1,U2,V1 and V2 will be provided, as functions of incidence angle, SSS, SST, wind speed assuming a neutral atmosphere, WSn (TBC). Whether Tbrough can be entirely described using WSn, or whether WS and WSn (or U*) need to be kept, need to be confirmed depending on:
-accuracy of ECMWF WS
-possibility of deducing a reliable U* from ECMWF WS and Tair-Tsea
-sensitivity of Tbrough to WS/U*

It is proposed to deduce WSn from ECMWF U*, using the same z0 formulation as the one used in the ECMWF model, and to make the inversion on WSn as it is the parameter which influences the most Tb_{rough}.(TBC, depending on the reliability on ECMWF z0 parametrization)

The tabulation will be provided at the following geophysical values:

SSS(psu) =[30 40]
SST(°C) = [0 5 10 15 20 25 30]
WSn (m/s)=[2 3 5 7 10 13 15 17 20 25 30]
ϑ (°)=[0 4 8 12 16 20 24 28 32 36 40 44 48 52 56]

and all the Tbrough = 0 for WSn=0.

The extrapolation has to be done linearly in the following order: 1-extrapolation in SSS; 2-extrapolation in SST; 3-extrapolation in WSn; 4-extrapolation in incidence angle; this ensures a precision of 0.05K on each parameter. Extrapolation out of the tabulation ranges has to be made using the coefficients of the linear extrapolations on the last closest points.

4.2.1.3. Error budget estimates (sensitivity analysis)

The advantage of retrieving WSn is that it is comparable to scatterometer derived wind speed. It would be of interest, before launch, to compare ECMWF WSn with scatterometer WS, in order to validate ECMWF WSn, and to decide the order of magnitude of differences between retrieved (from SMOS inversion) and first guess ECMWF WSn that are acceptable.

4.2.2. Practical considerations

4.2.2.1. Calibration and validation

It is likely that the factor 2 applied to the DV spectrum will need to be adjusted during the comissionning phase. Since Tbrough is proportionnal to this factor, the possibility of adjusting it should be kept.
Extrapolation of the tabulated values must be compared with model outputs to validate the extrapolation method.

4.2.2.2. Quality control and diagnostics

Values outside the min/max ranges given in the Tbrough tabulations should be deduced from a linear extrapolation of the two edge values of the tabulations (since most of the dependences are close to linear), except for low wind speed where Tbrough at WS between 0 and 2m/s should be deduced from a linear interpolation between 0 and Tbrough(2m/s).

4.2.3 Assumption and limitations

In the present approach, surface speed (u_c) is neglected while studies like [*Kelly et al.,* 2001] evidence that current speed has an impact on scatterometer measurements in case of strong currents gradients (equatorial Pacific); whether it should be taken into account or not will depend on the confidence we can put on ECMWF surface current speed (TBD).

Roughness is not necessarily related to local and instant wind only, and wind effects also imply itsduration and action distance, as well as the presence of swell. These effects are not included in the present model but may be included in U* computation.
Additional phenomena are likely to cause noticeable modification of $T_{b\ sea}$. The first one is foam,that appears above a threshold wind speed, and whose permittivity largely differs from the one of sea water. During experimental campaigns it is very difficult to separate roughness and foam effect so that it is possible that the factor of 2 applied to DV spectrum is slightly overestimated but it was not possible using WISE and Eurostarrs data to demonstrate that dependence of Tb with respect to WS was non linear, implying that foam effect was weak. The second one, still to be investigated for L-band radiometry, is the presence of surface slicks of natural or non-natural origin. Slicks are known to damp roughness at specific scales, and their permittivity different from that of sea water might change $T_{b\ sea}$.

Bibliography

Blume, H.-J. C., A.W. Love, M. J. V. Melle, and W.W. Ho, Radiometric observations of sea temperature at 2.65 GHz over Cheasapeake Bay, *IEEE Transactions on Antennas and Propagation*, *AP-25*, 121–128, 1977.

Boutin, J., E. Obligis, and E. Dinnat, WP1120, Influence of Surface Roughness on Tb Simulated in L-Band by Yueh-LODYC Emissivity Model and by UCL Model - Analyse of the Differences, in*Scientific requirements and impact of space observation of ocean salinity for modeling and climate studies: final report*, NERSC technical report n_214 under contract n_14273/00/NL/DC European Space Agency, 2002.

Boutin, J., P. Waldteufel, N. Martin, G. Caudal, and E. Dinnat, Salinity Retrieved from SMOS Measurements over Global Ocean: Imprecisions Due to Surface Roughness and Temperature Uncertainties, *Journal of Atmospheric and Oceanic Technology*, *21*, 1432–1447, 2004.

Camps, A., et al., L-band sea surface emissivity: Preliminary results of the WISE-2000 campaign and its application to salinity retrieval in the SMOS mission, *Radio Science*, *38*, 2003.

Camps, A., et al., The WISE 2000 and 2001 field experiments in support of the SMOS mission: sea surface L-band brightness temperature observations and their application to sea surface salinity retrieval, *IEEE Transactions on Geoscience and Remote Sensing*, *42*, 804–823, 2004a.

Cox, C., and W. Munk, Measurement of the roughness of the sea surface from photographs of the sun's glitter, *Journal of the Optical Society of America*, *44*, 838–850, 1954.

Dinnat, E., J. Etcheto, J. Boutin, G. Caudal, A. Weill, A. Camps, J. Miller, and S. Contardo, Sea state influence on L-band emissivity in various fetch conditions, in *Geoscience and Remote Sensing Symposium,2002. IGARSS '02. 2002 IEEE International*, vol. 6, pp. 3632–3634, 2002a, tY - CONF.

Dinnat, E. P., De la d´etermination de la salinit´e de surface des oc´eans `a partir de mesures radiom´etriques hyperfr´equence en bande L, Ph.D. thesis, Universit´e Pierre et Marie Curie, Paris, France, 2003.

Dinnat, E. P., and M. Drinkwater, Optimizing the Active/Passive Synergy in the Frame of Sea Surface Salinity Retrieval from Microwave Measurements at L-Band, in *Proceedings MicroRad'04*, Rome, Italy, 2004.

Dinnat, E. P., J. Boutin, G. Caudal, J. Etcheto, and P. Waldteufel, Influence of sea surface emissivity model parameters at L-band for the estimation of salinity, *International Journal of Remote Sensing*, *23*, 5117–5122, 2002b.

Dinnat, E. P., J. Boutin, G. Caudal, and J. Etcheto, Issues concerning the sea emissivity modeling at L-band for retrieving surface salinity, *Radio Science*, *38*, 25–1–25–11, 2003a.

Dinnat, E. P., J. Boutin, G. Caudal, J. Etcheto, and S. Contardo, On the use of EuroSTARRS and WISE data for validating L-band emissivity models, in *First Results Workshop, EuroSTARRS/WISE/LOSACCampaigns, ESA SP-525*, pp. 117–124, ESTEC/European Space Agency, 2003b.

Donelan, M. A., andW. J. Pierson, Jr., Radar scattering and equilibrium ranges in wind-generated waves with applications to scatterometry, *Journal of Geophysical Research*, *92*, 4971–5029, 1987.

Donelan, M. A., F. W. Dobson, S. D. Smith, and R. J. Anderson, On the dependence of sea surface roughness on wave development, *Journal of Physical Oceanography*, *23*, 2143–2149, 1993.

Durden, S. L., and J. F. Vesecky, A physical radar cross-section model for a wind-driven sea with swell,*IEEE Journal of Oceanic Engineering*, *OE-10*, 445–451, 1985.

Etcheto, J., E. Dinnat, J. Boutin, A. Camps, J. Miller, S. Contardo, J. Wesson, J. Font, and D. Long,Wind Speed Effect on L-Band Brightness Temperature Inferred from EuroSTARRS and WISE 2001 Field Experiments, *IEEE Transactions on Geoscience and Remote Sensing*, *42*, 2206–2213, 2004.

Etcheto, J., E. Dinnat, J. Boutin, A. Camps, J. Miller, S. Contardo, J. Wesson, J. Font, and D. Long, Wind speed effect on L-band brightness temperature inferred from EuroSTARRS and WISE 2001 field experiments, *IEEE Transactions on Geoscience and Remote Sensing*, *42*, 2206-2214, 2004.

Hollinger, J. P., Passive microwave measurements of sea surface roughness, *IEEE Transactions on GeoscienceElectronics*, *GE-9*, 165–169, 1971.

Kelly, K.A., S. Dickinson, M.J. McPhaden, and G.C. Johnson, Ocean currents evident in satellite wind data, *Geophysical Research Letters*, *28*, 2469-2472, 2001.

Liu, W.T., and W. Tang, *Equivalent neutral wind*, 8 pp. JPL/NASA Publ. 96-17, 1 Aug. 1996.

Prigent, C., and P. Abba, Sea surface equivalent brightness temperature at millimeter wavelengths, *AnnalesGeophysicae*, *8*, 627–634, 1990.

Rice, S. O., Reflection of Electromagnetic Waves from Slightly Rough Surfaces, *Communications on Pure and Applied Mathematics*, *4*, 351–378, 1951.

Sasaki, Y., I. Asanuma, K. Muneyama, G. Naito, and T. Suzuki, The dependence of sea-surface microwave emission on wind speed, frequency, incidence angle and polarization over the frequency range 1 to 40 GHz, *IEEE Transactions on Geoscience and Remote Sensing*, *GE-25*, 138-146, 1987.
Stogryn, A., The apparent temperature of the sea at microwave frequencies, *IEEE Transactions on Antennas and Propagation*, *77*, 1658–1666, 1967.
Swift, C. T., Microwave radiometer measurements of the Cape Cod Canal, *Radio Science*, *9*, 641–653,1974.
Webster, W. J., Jr., and T. T. Wilheit, Spectral characteristics of the microwave emission from a winddriven foam-covered sea, *Journal of Geophysical Research*, *81*, 3095–3099, 1976.
Weill, A., T. Besnard, S. Contardo, J. Etcheto, and J. Boutin, WISE results from whitecapping andstereophotogrammetry: a tentative of superposition of topography and foam surface to retrieve active and fossil foam, in *First Results Workshop, EuroSTARRS/WISE/LOSAC Campaigns, ESA SP-525*, pp.89–94, ESTEC/European Space Agency, 2003.
Yueh, H. A., R. T. Shin, and J. A. Kong, Scattering of electromagnetic waves from a periodic surface with random roughness, *Journal of Applied Physics*, *64*, 1657–1670, 1988.
Yueh, S. H., Modeling of wind direction signals in polarimetric sea surface brightness temperatures, *IEEE Transactions on Geoscience and Remote Sensing*, *35*, 1400–1418, 1997.
Yueh, S. H., Estimates of Faraday rotation with passive microwave polarimetry for micrawave sensing of Earth surfaces, *IEEE Transactions on Geoscience and Remote Sensing*, *38*, 2434–2438, 2000.
Yueh, S. H., R. West, W. J. Wilson, F. K. Li, E. G. Njoku, and Y. Rahmat-Samii, Error sources and feasibility for microwave remote sensing of ocean surface salinity, *IEEE Transactions on Geoscience and Remote Sensing*, *39*, 1049–1060, 2001.

4.3. Surface roughness 2: SSA

4.3.1. Theoretical description

4.3.1.1. Physics of the problem

Polarimetric passive remote sensing involves measurement of all four modified Stokes parameters of the microwave thermal emission:

$$\begin{bmatrix} T_h \\ T_v \\ T_U \\ T_V \end{bmatrix} = T_s \left(\begin{bmatrix} 1 - r_h \\ 1 - r_v \\ -r_U \\ -r_V \end{bmatrix} \right) \quad (1)$$

where T_h and T_v are the brightness temperatures measured by horizontally and vertically polarized antennas respectively, and T_U and T_V are proportional to the real and imaginary parts of the correlation between fields in horizontal and vertical polarizations respectively [1] (T_3 and T_4 in the rest of the document).
The second equality follows from Kirchhoff's Law, which relates the emissivity of a medium at constant temperature to the corresponding reflectivity *(r_h, r_v, r_U* and *r_V*) multiplied with the surface physical temperature T_s. Reflectivities are calculated as an integral of bistatic scattering coefficients over the upper hemisphere in the reciprocal active scattering problem [2].

Particular interest in sea surface salinity remote sensing is given to brightness temperature variations with surface salinity and temperature when the sea surface is assumed smooth. In that case, it is straighforward to calculate reflectivities in Equation (1) at a given incidence angle using Fresnel reflection laws provided an accurate dielectric constant model is available at L-band. However, in the various discussions of the Sea Surface Salinity (SSS) retrieval schemes applied to spaceborne L-band radiometer data ([3]-[5]), it is clear that the major uncertainty in the required modelling is the effect of the wind and wave-generated roughness on the emissivity of the ocean's surface at L-band. The purpose of this section is to document one of the three forward models, namely the "SPM/small slope approximation (SPM/SSA)" that will provide roughness impact corrections in the version of the SSS retrieval algorithm used at launch of the ESA's Soil Moisture and Ocean Salinity (SMOS) satellite mission.

Analytical and numerical models for the calculation of the rough ocean surface polarimetric thermal emission have been developed [6]–[11], primarily through application of standard surface scattering approximate methods to calculate surface emissivity using Kirchhoff's law. Models based on both the small perturbation method (SPM) and the physical optics (PO) approximation have been presented. The physical optics (PO) approximation was shown to clearly underestimate the sea surface emissivity observations at L-band [12, 13], particularly in the low incidence angle range (less than about 20-30°). This is mainly because such model does not account for scattering on small roughness elements. Recent works [8-10] has further revealed that use of the SPM for emission calculations results in a small slope, rather than small height, emission approximation identical to that which would be obtained from the small slope approximation of [14], so that the SPM can provide accurate emission predictions even for surfaces with large heights in terms of the electromagnetic wavelength. Numerical tests of the SPM for a set of canonical periodic surfaces have confirmed this statement [15]. Moreover, the success of the SPM/SSA in matching measured brightness temperature [6,16-

19] has shown that the technique should be applicable for rough ocean surface brightness temperature predictions. These results motivate use of the SPM/small slope approximation (SPM/SSA) for the prediction of ocean polarimetric thermal emission at L-band.
The Stokes vector of sea surface brightness temperatures observed at radiometer frequency f, incidence angle θ_i and azimuth angle relative to wind direction ϕ_i can be written:

$$\begin{bmatrix} T_h(f,\theta_i,\phi_i) \\ T_v(f,\theta_i,\phi_i) \\ T_U(f,\theta_i,\phi_i) \\ T_V(f,\theta_i,\phi_i) \end{bmatrix} = T_s \left(\begin{bmatrix} 1-\left|R_{hh}^{(o)}(f,\theta_i)\right|^2 \\ 1-\left|R_{vv}^{(o)}(f,\theta_i)\right|^2 \\ 0 \\ 0 \end{bmatrix} - \begin{bmatrix} \Delta e_h(f,\theta_i,\phi_i) \\ \Delta e_v(f,\theta_i,\phi_i) \\ \Delta e_U(f,\theta_i,\phi_i) \\ \Delta e_V(f,\theta_i,\phi_i) \end{bmatrix} \right) \quad (2)$$

where T_s is the sea surface temperature. $R_\gamma^{(o)}(f,\theta_i)$ are the Fresnel reflection coefficients at polarization γ, and the $\Delta e_\gamma(f,\theta_i,\phi_i)$ are the first prediction of emissivity changes due to the rough sea surface. The physics of the forward problem here is to estimate accurately the wind-excess emissivity Stokes vector $\Delta e_\gamma(f,\theta_i,\phi_i)$ at f=1.4 GHz for the range of (θ_i,ϕ_i) values encountered in L1C SMOS data and for a range of wind and sea state conditions representative of the global ocean.

The SPM/SSA applies standard small perturbation theory to predict the bistatic scattering coefficients of a rough surface, and integrates these scattering coefficients over the upper hemisphere to obtain the reflectivities and hence brightness temperatures. The resonance behaviours observed in the critical phenomena region [20] produce a significant sensitivity of emission harmonics predicted by the SSA to ocean length scales of order equal to the electromagnetic wavelength. However, these emission harmonics are also sensitive (with the exception of the fourth Stokes parameter) to anisotropy in ocean length scale much larger than the electromagnetic wavelength. Use of the SPM/SSA up to 2nd order produces an expansion in surface slope, with zero order terms reproducting flat surface emission results, first order terms identically zero, and second order terms providing the first prediction of changes from flat surface brightnesses.

The second order terms take the form of an integral of a set of weighting functions over the surface directional spectrum, so that the wind-excess emissivity Stokes vector $\Delta e_\gamma(f,\theta_i,\phi_i)$ can be expressed as follows using the second order SPM/Small Slope Approximation theory (e.g., see [19]):

$$\begin{bmatrix} \Delta e_h \\ \Delta e_v \\ \Delta e_U \\ \Delta e_V \end{bmatrix} = \int_0^\infty \int_0^{2\pi} kW(k,\phi) \begin{bmatrix} g_h(f,\theta_i,\phi_i;\varepsilon_{sw};k,\phi) \\ g_v(f,\theta_i,\phi_i;\varepsilon_{sw};k,\phi) \\ g_U(f,\theta_i,\phi_i;\varepsilon_{sw};k,\phi) \\ g_V(f,\theta_i,\phi_i;\varepsilon_{sw};k,\phi) \end{bmatrix} dk d\phi \quad (3)$$

where $\vec{k} = (k,\phi)$ is a surface wavenumber vector, $W(k,\phi)$ is the sea surface directional waveheight wavenumber spectrum, ε_{sw} is the sea water dielectric constant and the g_γ kernels are electromagnetic "weighting" functions given explicitly in [19].

Note, that when deriving an asymptotic solution for EM scattering on the rough ocean surface, a key issue is to determine a tractable statistical description which specifies the sea surface geometry on a very wide range of scales (0.005-200 m). In most practical and/or

theoretical studies, Gaussian statistics are assumed. Under such assumptions, the solution will then only depend upon the definition and the shape of the correlation function. Under Gaussian statistics assumption, which is used as well in the present SPM/Small Slope Approximation theory, the result can be expressed strictly in terms of a roughness spectrum. In the present algorithm, we used the Kudryatsev *et al* model [21] to estimate the sea surface roughness spectrum $W(k,\phi)$ in Equation (3), which was recently developed based on available field and wave-tank measurements, along with physical arguments concerning the dynamics of short-gravity waves. These scales indeed represent particularly important surface components for emissivity at 1.4 GHz, since they belong to the so-called "critical phenomena" region [20] within which surface components are dominant scatterers at L-band. It is important to note that this spectral model was developed without any relation to remote-sensing data. Moreover, by using the Kudryatsev *et al* spectral model, we avoided some deficiencies of the Elfouhaily et al spectral model as found by other (problems at the low to moderate wind speed transition).

In [19], it was shown that using a Fourier expansion in Eq (3), the wind-excess emissivity components can be separated out in individual emission azimuthal terms as follows:

$$\begin{bmatrix} \Delta e_h \\ \Delta e_v \\ \Delta e_U \\ \Delta e_V \end{bmatrix} = \begin{bmatrix} \Delta e_h^{(0)} + \Delta e_h^{(2)} \cos(2\phi_i) \\ \Delta e_v^{(0)} + \Delta e_v^{(2)} \cos(2\phi_i) \\ -\Delta e_U^{(2)} \sin(2\phi_i) \\ -\Delta e_V^{(2)} \sin(2\phi_i) \end{bmatrix} \quad (4)$$

where the $\Delta e_\gamma^{(n)}$ terms represent the *n*th azimuthal harmonics of the wind-excess emissivity.

Note that due to the assumption of gaussianity in the sea surface statistics, the solution can be expressed strictly in terms of a roughness spectrum. Properties of a directional spectrum result in no first azimuthal harmonic variations being obtained; introduction of non-gaussianity is required to obtain first azimuthal harmonics. As second azimuthal harmonics were measured to be already very small at L-band [22, 23], only the second order SSA/SPM expansion is considered here and no first azimuthal harmonic variations are neglected.

4.3.1.2. Mathematical description of algorithm

The *n*th azimuthal harmonics of the wind-excess emissivity $\Delta e_\gamma^{(n)}$ terms in Eq (4) can be determined numerically by calculating integrals of the products of the *n*th azimuthal harmonics of the surface curvature spectrum $k^4 W(k,\phi)$ by the *n*th azimuthal harmonics of the electromagnetic weighting function g_γ .

Typically, the Kudryavtsev curvature spectrum model $k^4 W(k,\phi)$ is determined as function of the following geophysical parameters:

- The wind friction velocity U* [m/s],
- The inverse wave age parameter $\Omega=\frac{WS}{C_p}$ [no unity] for the wind sea, where *WS* is the wind speed module at 10 meter height [m/s] and C_p is the phase speed at the peak of the wind-sea spectrum [m/s]. Note that $\Omega=\frac{WS}{C_p}=\frac{2\pi WS}{gT_p}$ where g is the acceleration of gravity [m/s^2], and T_p is the peak period of wind-sea [s].

The electromagnetic weighting functions g_γ can be determined as function of

- the incidence angle θ_i at SMOS pixel, and,
- ε_{sw}, the complex sea water dielectric constant, which is itself function of Sea Surface Temperature T_s and Sea Surface Salinity *SSS*.

Therefore, the mathematical description of the SSA roughness brightness temperature corrections includes 4 major parts:

(1) A five-dimension Look-Up Table (LUT) of the $\Delta e_\gamma^{(n)}$ coefficients.

Two options for the look-up table are foreseen as ε_{sw} will be already calculated by the flat-sea surface module of the processor:
Option 1: LUT1 as function of

- the wind friction velocity U* [m/s],
- the inverse wave age parameter Ω
- the incidence angle θ_i at SMOS pixel,
- the real part of ε_{sw}, and,
- the imaginary part of ε_{sw}.

Or
Option 2: LUT2 as function of

- the wind friction velocity U* [m/s],
- the inverse wave age parameter Ω
- the incidence angle θ_i at SMOS pixel,
- the sea surface temperature T_s [K] and,
- the prior sea surface salinity SSS [psu].
- In case of option 2, the same dielectric constant model than the one used in the processor [24?] is used in the generation of the LUT.

Parameter or variable ranges

- For the wind friction velocity U*: 0→ 1 [m/s],
- For the inverse wave age parameter for wind sea Ω: 0.5 →2.5 [m/s],
- For the incidence angle θ_i at SMOS pixel [degrees]: 0→ 75°
- For the sea surface temperature T_s : 269.15→ 309.15 K
- For the prior sea surface salinity SSS : 0 → 40 psu
- For the azimuth angle relative to wind direction ϕ_i [in rad] : 0→ 2π
- For the real part of the dielectric constant ε'_{sw} [no unit]: 65→ 90
- For the imaginary part of the dielectric constant ε''_{sw} [no unit] 0→100

(2) A multi-dimensional interpolation step.
Given the four values of the "geophysical" auxiliary parameters estimated at a given SMOS pixel, namely u*$_i$, Ω_i, Real(ε_{sw}), Imag(ε_{sw}) where Real and Imag denote real and imaginary parts (respectively, u*$_i$, Ω_i, T_{si} and SSS$_i$), plus the series of incidence angles ($\theta_{i=1,\ldots,N}$) associated to the L1C product considered, a cubic spline interpolation is performed from the LUT1 (resp LUT2) to evaluate, the values of $\Delta e_{\gamma,i=1,\ldots,N}^{(n)}$, the underlying multidimensional functions $\Delta e_{\gamma}^{(n)}$ at the pixel considered.

(3) Total roughness-induced emissivity correction.
From the value of azimuth angle relative to wind direction ϕ_i estimated at the pixel [in rad], the total wind-excess emissivity Stokes vector is calculated using Equation (4).

(4) Total roughness-induced brightness temperature correction.
From the estimated values of the total wind-excess emissivity Stokes vectors for each L1C incidence angles, the corresponding brightness temperature changes are derived by multiplying the results by the sea surface temperature at the pixel $T_{si.}$ [K].

4.3.1.3. Error budget estimates

In Figure 1, we show the comparison between currently available experimental data collected at L-band over water surfaces [4; 13; 22; 25-29] and the SSA/SPM model predictions of the wind speed sensitivity of surface emissivity at H and V polarization. The figures reveal that the model emissivity dependencies with wind speed are in agreement with the data to roughly about ±5 x10^{-4}, in both vertical and horizontal polarizations. This translates into an error in brightness temperature of about 1 K at SST=15°C and WS =7 m/s. Note that this is a very maximized error estimate. In general, the model is found to correctly reproduce the averaged trends observed at both polarization also it often slightly underestimates the data, particularly in V-polarization and around nadir. Discrepancies might be due to either foam, currents, slicks and swell impacts not accounted for in the model or to radiometric uncertainties in the experimental data (see error bars given for some of the data). It is however expected that using auxiliary wind friction velocity data, a measure of wind stress that implicitly carries a response to near-surface phenomena, instead of wind speed at 10 meter height, shall improve the error budget estimate.

There are no evidence of clear azimuthal/wind direction related signatures in the few available measured brightness temperature signals at L-band [22, 23] so that it is now very difficult to estimate errors due to the wind stress directionality.

Therefore, we estimate an overall error budget on the roughness correction factor $\Delta e(\theta_i)$, as predicted by the SSA/SPM model (without accounting for wind direction impacts), of about:

$$\text{Error}\left(\begin{bmatrix}\Delta e_h(\theta_i)\\ \Delta e_v(\theta_i)\end{bmatrix}\right) = \pm 5\times 10^{-4}\cdot U_{10}$$

An additional error will be introduced by the multi-dimensional interpolation scheme from the LUT table. The error is not provided yet in the draft ATBD but will be given later.
Note that no error budget can be estimated for the third and fourth Stokes parameters as no data as function of wind speed are currently available for validation.

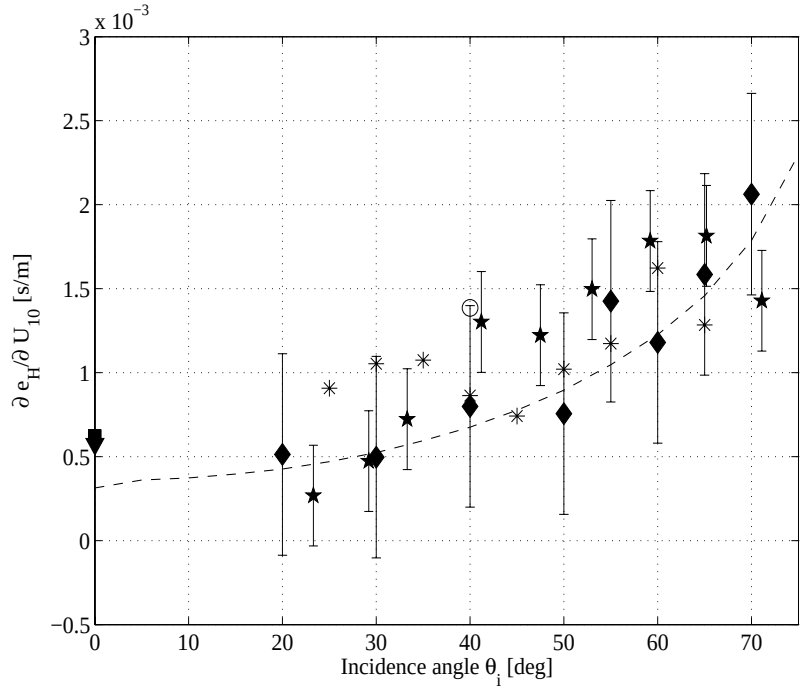

Figure 1a : for legend see next figure.

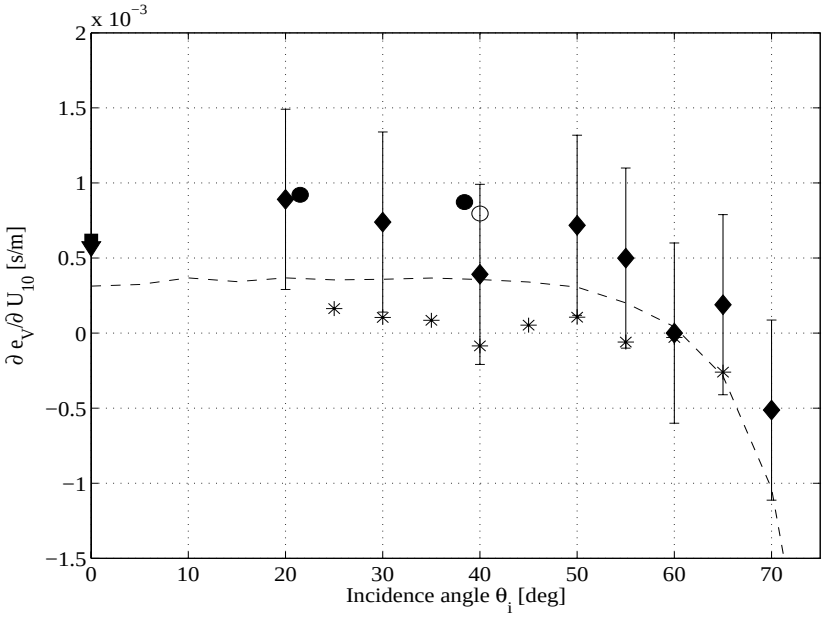

Figure 1b Comparison between measured and calculated sensitivities of the sea surface emissivity at L-band to wind speed at 10 meter height as function of incidence angle. Figure 1a: horizontal polarisation; Figure 1b: vertical polarisation. (★): Cape Code Canal data [13]; (■): Data from Skylab S-194 [25]; (✳): WISE 2000-2001 [22], [26]; (♦) : Argus Island Tower data [27]; (▼): Bering Sea Experiment [28]; (○):

JPL experiment [4]; (●)EuroSTARRS [29]; (--): predictions from the SSA/SPM model at SST=15°C and SSS=35 psu. Error bars show uncertainties in the data of [13] and [27].

4.3.2. Practical considerations

4.3.2.1. Calibration and validation

Calibration and validation of the forward SSA/SPM emissivity model for roughness correction will be done during the commissioning phase and later-on by perfoming residual analysis of the future SMOS measurements and using a formalism proposed for and applied to NASA scatterometer (NSCAT), Special Sensor Microwave Imager (SSM/I) and ESA/ERS scatterometer measurements [see 30].

Using in situ SSS, SST and wind (TAO, Argo drifter+ satellite SST and winds and ECMWF model winds) and SMOS co-localized data, the first step will be to remove the flat sea surface contribution from the SMOS surface brightness temperature data (i.e., corrected for atmospheric, ionospheric, galactic and sunglint contribution) in order to estimate the residual Stokes vector of roughness impact $\Delta e_B(\theta_i)$. The in situ and satellite SSS, SST and wind data will be the chosen reference. In addition, ECMWF analysis winds will be used as a thrid data source to completely determine the errors via a multiple collocation analysis. The main objective will be to present observed correlations between regional and seasonal model roughness correction factors $\Delta e_B(\theta_i)$ errors and nonwind oceanic and atmospheric factors such as the surface current and sea state. Following the methodology applied in [30], we shall explicitly take into account the errors in the reference datasets as well as in the roughness correction factors retrieved estimates. The gain shall come in more accurate assessment of bias and variance and less possible systematic contamination that can obscur geophysically driven impacts not accounted for by the SSA/SPM model.

4.3.2.2. Quality control and diagnostics

As explained in section 4.3.3 below, the SSA/SPM model is not expected to provide correct results for wind seas generated by winds less than about 2 m/s and larger than 15 m/s . This corresponds roughly to wind friction velocity u* less than 0.6 cm/s and larger than 0.5 m/s.
The model can be applied as it is at launch for conditions out of this range however, we expect that the CAL/VAL activities will provide after commissioning phase a variability estimate at low winds and a residual foam impact at high winds which will be used to correctly tune the model.

4.3.2.3. Exception handling

There is no particular exception handling in the mathematical algorithm except if the following auxiliary data are not provided by the processor or exceed the ranges anticipated*:*

- the wind friction velocity u* [m/s], (which can be estimated from auxiliary U_{10}, the wind speed module at 10 meter height and the auxiliary parameter “Coefficient of drag with waves C_d “defined by : u*= $\sqrt{C_d} \times |U_{10}|$)

- the inverse wave age parameter Ω for the wind sea (which can be deduced from estimates of both U_{10} and the mean period of wind waves T_p: $\Omega = \frac{2\pi U_{10}}{g T_p}$),
- the incidence angles θ_i at SMOS pixel,
- the sea surface temperature T_s,
- the prior sea surface salinity SSS, and,
- the azimuth angle at SMOS pixel relative to wind direction ϕ_i.

4.3.3. Assumption and limitations

SSA/SPM approximation is by essence a first-order small slope perturbation approximation so that it is not expected to correctly estimate the roughness impact for sea surfaces exhibiting large slopes and most importantly, large curvature. Therefore, it is expected to fail in strong frontal conditions (strong wave-wave, wave-current or wind-wave interaction conditions). Moreover, the sea surface state model (i.e. Kudryavtsev et al) is only accounting for wind seas. Moreover, it should be valid for wind seas generated by winds stronger than about 2 m/s and less than 15 m/s. Out of these limits, it is not expected that the physics of air-sea interaction is correctly accounted for.

Deleted: s

Deleted: t

Therefore, we do not expect the model to perform well in presence of either strong swells, strong currents, very small and unsteady winds as well as stormy conditions. We expect however that accounting for the impact of waves on the drag coefficients will better characterize impact of these parameters on roughness.

References

[1] S. H. Yueh, R. Kwok, F. K. Li, S. V. Nghiem, and W. J. Wilson, "Polarimetric passive remote sensing of ocean wind vectors," *Radio Sci.*, vol. 29, pp. 799–814, 1994.

[2] L. Tsang, J. A. Kong, and R. T. Shin, *Theory of Microwave Remote Sensing*. New York: Wiley, 1985.

[3] G. S. E. Lagerloef, C. T. Swift, and David M. Le Vine, Sea surface salinity : The next remote sensing challenge, *Oceanography*, vol. 8, no. 2, pp. 44-49, 1995.

[4] S. H. Yueh, R. West, W. J. Wilson, Fuk K. Li, E. G. Njoku, and Y. Rahmat-Samii, Error sources and feasibility for microwave remote sensing of ocean surface salinity, *IEEE Trans. Geosci. and Remote Sens.*, vol. 39, no. 5, pp. 1049-1060, 2001.

[5] E. P. Dinnat, J. Boutin, G. Caudal, J. Etcheto, and A. Camps, Issues concerning the sea emissivity modeling in L-band for retrieving surface salinity, *Radio Sci.*, vol. 38, no. 4, 2003.

[6] S. H. Yueh, "Modeling of wind direction signals in polarimetric sea surface brightness temperatures," *IEEE Trans. Geosci. Remote Sensing*, vol. 35, pp. 1400–1418, 1997.

[7] D. B. Kunkee and A. J. Gasiewski, "Simulation of passive microwave wind direction signatures over the ocean using an asymmetric-wave geometrical optics model," *Radio Sci.*, vol. 32, p. 59, 1997.

[8] V. G. Irisov, "Small-slope expansion for thermal and reflected radiation from a rough surface," *Waves Random Media*, vol. 7, pp. 1–10, 1997.

[9] J. T. Johnson, ``A study of rough surface thermal emission and reflection using Voronovich's small slope approximation," IEEE Trans. Geosc. Rem. Sens., Feb 2005.

[10] A. B. Isers, A. Puzenko, and I. M. Fuks, The local perturbation method for solving the problem of di_raction from a surface with small slope irregularities," J. Electromagn. Waves Appl., vol. 5, no. 12, 1991.
[11] V. G. Irisov, "Microwave radiation from a weakly nongaussian surface," in *Proc. IGARSS'98* vol. 5, pp. 2329–2332.
[12] J. P. Hollinger, Passive microwave measurements of sea surface roughness, IEEE Trans. Geosci. Electron., vol. GE-9, no. 3, pp. 165-169, 1971.
[13] C. T. Swift, Microwave radiometer measurements of the Cape Cod Cannal, Radio Sci., vol. 9, no. 7, pp. 641-653, 1976.
[14] A. G. Voronovich, *Wave Scattering from Rough Surfaces*. Berlin, Germany: Springer-Verlag, 1994.
[15] M. Zhang and J. T. Johnson, "Theoretical studies of ocean polarimetric brightness signatures," in *Proc. IGARSS'98*, vol. 5, pp. 2333–2335.
[16] J. T. Johnson and Y. Cai, ``A theoretical study of sea surface up/down wind brightness emperature differences," IEEE Trans. Geosc. Remote Sens, 2002.
[17] J. T. Johnson, ``Comparison of the physical optics and small slope theories for polarimetric thermal emission from the sea surface," IEEE Trans. Geosc. Remote Sens, 2002.
[18] M. Zhang and J. T. Johnson, ``Comparison of modeled and measured second azimuthal harmonics of ocean surface brightness temperatures," IEEE Trans. Geosc. Remote Sens, 2001.
[19] J. T. Johnson and M. Zhang, ``Theoretical study of the small slope approximation for ocean polarimetric thermal emission," IEEE Trans. Geosc. Remote Sens., 1999.
[20] V. S. Etkin, N. N. Vorsin, Y. A. Kravtsov, V. G. Mirovskii, V. V. Nikitin, A. E. Popov, and I. A. Troitskii, Critical phenomena with the thermal radio irradiation of a periodically uneven water surface, *Izvestiya: Radiophysics and Quantum Electronics*, vol. 21, pp. 316-318, 1978.
[21] V. N. Kudryavtsev, V. K. Makin, and B. Chapron, "Coupled sea surface atmosphere model. 2. spectrum of short wind waves," J. Geophys. Res., vol. 104, no. C4, pp. 7625-7639, 1999.
[22] A. Camps, J. Font, M. Vall-llossera, C. Gabarro, R. Villarino, L. Enrique, J. Miranda, I. Corbella, N. Duo, F. Torres, S. Blanch, J. Arenas, A. Julia, J.Etcheto, V. Caselles, A. Weill, J. Boutin, S. Contardo, R. Niclos, R. Rivas, S. Reising, P. Wursteisen, M. Berger, and M. Martn-Neira, The WISE 2000 and 2001 Campaigns in support of the SMOS Mission: Sea surface L-band Brightness Temperature Observations and their application to Multi- Angular Salinity Retrieval, *IEEE Trans. Geosci. Remote Sensing*, vol. 42, no. 4, pp. 1039-1048, 2004.
[23] S. Sobjaerg and N. Skou, An Airborne Campaign measuring wind signatures from the Sea Surface using an L-band polarimetric radiometer, in *Proceedings of the International Geoscience and Remote Sensing Symposium, IGARSS*, Toulouse, 2003.
[24] L. A. Klein and C. T. Swift, ìAn Improved model of the dielectric constant of sea water at microwave frequencies,î *IEEE Trans. Antennas Propag.*, vol. AP-25, pp. 104-111, 1977.
[25] R. M. Lerner and J. P. Hollinger, ìAnalysis of 1.4 GHz Radiometric measurements from Skylab,î *Remote Sens. Environm.*, vol. 6, pp. 251-269, 1977.
[26] A. Camps, J. Font, J. Etcheto, V. Caselles, A. Weill, I. Corbella, M. Vall-llossera, N. Duffo, F. Torres, R. Villarino, L. Enrique, A. Julia, C. Gabarro, J. Boutin, E. Rubio, S. C. Reising, P. Wursteisen, M. Berger, and M. Martin-Neira, ìSea surface emissivity observations at L-band: First results of the wind and salinity experiment wise 2000, *IEEE Trans. Geosci. and Remote Sens.*, vol. 40, no. 10, pp. 2117-2129, 2002.
[27] J. P. Hollinger, Passive microwave measurements of sea surface roughness, *IEEE Trans. Geosci. Electron.*, vol. GE-9, no. 3, pp. 165-169, 1971.

[28] W. J. Webster, T. T. Wilheit, D. B. Ross, and P. Gloersen, Spectral characteristics of the microwave emission from a wind-driven covered sea, *J. Geophys. Res.*, vol. 81, no. 18, pp. 3095-3099, 1976.
[29] J. Etcheto, E. P. Dinnat, J. Boutin, A Camps, J. Miller, S. Contardo, J. Wesson, J. Font, and D. Long, Wind speed effect on L-band brightness temperature inferred from EuroSTARRS and WISE2001 field experiments, *IEEE Trans. Geosci. and Remote Sens.*, vol. 42, no. 10, pp. 2206-2213, 2004.
[30] Y. Quilfen, B. Chapron and D. Vandemark, "The ERS Scatterometer Wind measurement accuracy: evidence of seasonal and regional biases", *Journal of Atmopsheric and Oceanic Technology*, vol 18, p 1684-1697, 2001.

4.4. Surface roughness 3: empirical

4.4.1. Theoretical description

4.4.1.1. Physics of the problem

The brightness temperature can be expressed as the sum of two terms; the brightness temperature in the case of completely flat sea and the brightness temperature (ΔT_b) due to the surface roughness:

$$T_{b,p}(\theta_i, SST, SSS, P_{rough}) = T_{bflat,p}(\theta_i, SST, SSS) + \Delta T_{b\ rough,p}(\theta_i, SST, SSS, \overrightarrow{P_{rough}}) \qquad [4.4.1]$$

where the first term is T_b due to specular reflection, which is well described by the Fresnel equations. The second term is the increment of brightness temperature due to sea roughness indicated here by a vector $P_{rough,}$ which includes the effect of some of the parameters that modify the surface roughness, like wind speed (WS), significant wave height (Hs), wave age (Ω)… Furthermore, T_b is polarization dependent.

Comment [EL7]: Be careful there is already p parameter for polarization. Another notation should be used NR

No confusion possible: polarization always lower case, parameter upper case CG

Several models describe this increment on T_b in a theoretical basis as in the modules 2 and 3. However, these theoretical models are not fully well validated.

This module proposes to use an empirical model describing ΔT_b through several physically measurable parameters and coefficients which are derived from measurements.

The most important parameter that affects the roughness of the sea is the wind speed, due to the stress on its surface and then this is the main (and usually the only) parameter used in the description of the sea roughness. However, this impact is not linear with all wind speeds as shown in several works (Etcheto et al, 2004, Vall-llossera et al., 2003).

A good approximation can be done by using three linear approximations, each with a different slope, that form a continuous function. These three segments are defined in the regions of 0-3 m/s, 3-12 m/s, and > 12 m/s, when the foam factor begins to be important at L-band (Camps et al., 2005).

Miranda et al. (2003), using several wind speed sequences recorded during WISE 2000 and 2001 campaigns (Camps et al, 2004, Camps et al, 2002), found large differences between measured spectra and theoretical fully-developed spectra obtained with the measured local wind speed. This can produce errors on T_b of about a fraction of a Kelvin in both polarizations with opposite sign (therefore, these errors could be minimized by using the first Stokes parameter).

This is the case when swell is present, where some events of low local wind speed and high wave height are possible and therefore roughness can not be properly described only by the wind speed.

In Gabarró et al, 2004a, a new empirical model is proposed to describe the increment of T_b due to the roughness of the sea as function of wind speed and also significant wave height.

That model is derived from WISE 2001 campaign measurements. Gabarró, 2004b compares the behaviour of this model with respect to other models which are only dependent on WS, and better performances are observed when the proposed model is used.

Another parameter that describes the degree of development of the waves is the so-called inverse wave age, Ω. It is defined Ω=WS/Cp, where WS is the surface wind speed at 10 meter height and Cp the phase speed at the peak of the wave spectrum. Ω=2.5 corresponds to very young seas at short fetches while Ω=0.8 corresponds to fully-developed sea state. Since the peak phase speed Cp can be deduced from a measure of the peak wave period Tp via the deep-water dispersions relationship for surface waves, Ω might be correctly evaluated from auxiliary peak wave period values. The inverse wave age is computed by oceanographic models like WAM, from ECMWF. Once the satellite will be flying, the impact of these parameters will be evaluated.

In Camps et al., 2004 authors have observed that azimuthal variations of the measured T_b during WISE 2000 at 25°, 35°, 45°, and 55° incidence angles, and at both polarizations, are within 0.5 K. However, they can be due to differences between calibrations, and the authors do not think there is any measurable azimuthal signature below 10 m/s. Only during very large storms (as the case of WISE2001, with a wind speed of 11m/s and very large waves (3 m < Hs < 5 m)), the azimuthal signature has been observed. Therefore, wind direction is not considered in the empirical model.

The coefficients that weight the contributions of the different parameters in the ΔT_b model will be determined and tuned once the MIRAS instrument will have measured brightness temperatures during the commissioning phase. With those measurements and the auxiliary geophysical parameters, the relations can be derived. Therefore, the software code should be flexible enough to allow these modifications.

The model should accomplish the condition that at nadir the contribution on T_b due to sea roughness is the same for H and V polarization. This assumption can be done since no azimuthal dependence (wind direction dependence) is considered in this model. Several campaigns and measurements have shown that at L-band this dependence is negligible.

A set of different models can be necessary (TBC), as different sea and meteorological conditions can change the relationship between T_b and the different parameters, this is, the coefficients (and so the model) can have spatial variability.

4.4.1.2. Mathematical description of algorithm

Taking into account the results from Etcheto et al., 2004, and Camps et al., 2005, a set of three different models is proposed. The first one will be valid for WS ≤ 3 m/s, the second one for 3 m/s < WS ≤ 12 m/s, and the last one for WS > 12 m/s.

The three models proposed in this module permit to consider several parameters that influence the roughness, or to make them null (by putting the coefficients equal to 0). Also the coefficients should be easily changeable, since once the satellite will be flying the model will be adjusted. Therefore, the general equation for each polarization is as follows (where x is the model used, from 1 to 3):

Comment [JF8]: Please note that the writing of coefficients has been changed

$$\begin{cases} T_{b\ h\ rough} = (C_{1.x} + Z_{1,x}\theta_i)\ WS + (C_{2.x} + Z_{2.x}\theta_i)\ Hs + (C_{3.x} + Z_{3.x}\theta_i)\ \Omega + \\ + (C_{4.x} + Z_{4.x}\theta_i)\ U^* + (C_{5.x} + Z_{5.x}\theta_i)\ MSQS + (C_{6.x} + Z_{6.x}\theta_i)\ T_{air-sea} \\ T_{b\ v\ rough} = (C_{1.x} + Z_{7.x}\theta_i)\ WS + (C_{2.x} + Z_{8.x}\theta_i)\ Hs + (C_{3.x} + Z_{9.x}\theta_i)\ \Omega + \\ + (C_{4.x} + Z_{10.x}\theta_i)\ U^* + (C_{5.x} + Z_{11.x}\theta_i)\ MSQS + C_{6.x}\ (C_{6.x} + Z_{12.x}\theta_i)\ T_{air-sea} \end{cases}$$

[4.4.2]

where the brightness temperature due to roughness can be described by the wind speed (WS), the significant wave height (Hs), the inverse wave age (Ω), the wind friction velocity (U^*), the mean square slope of waves (MSQS), and the air-sea temperature difference ($T_{air\text{-}sea}$). The wind speed WS is the module of the wind speed components vector (WC_U, WC_V). θ_i is the incidence angle, measured from the nadir. It should be defined in degrees.

These parameters can be obtained from ECMWF analysed data directly or indirectly. The wave age parameter is defined as $\Omega = \frac{WS}{C_p}$, where Cp is the phase speed at the peak of wind sea spectrum [m/s]. Note that $\Omega = \frac{WS}{C_p} = \frac{2\pi WS}{1.1 g T_p}$, where g is the acceleration of gravity [m/s^2], and T_p is the mean period of wind waves [s], which is given by ECMWF analysis. It is multiplied by 1.1 to obtain the peak period (usually peak = mean + 10%), the parameter actually needed in the computation and not provided by ECMWF. The wind friction velocity U* [m/s], can be estimated by $U^* = \sqrt{C_d} \times |WS|$, where C_d is the coefficient of drag with waves which is given by the ECMWF data. Air-sea temperature difference should be obtained by subtracting one from the other both given by ECMWF. The rest of the parameters are directly given by models.

The coefficients $C_{i.x}$ represent the slope of the sensitivity of ΔT_B to the parameters when incidence angle is 0. $Z_{i.x}$ are the coefficients that adjust the values to the different incidence angles. All these coefficients (Ci,x and Zi,x) express the empirical relationship between $T_{b\ rough}$ measured by SMOS and the descriptors of surface roughness, therefore they have to be obtained by fitting during the satellite commissioning phase. Consequently they should be written in an external file, so that they could be easily changed.

It has to be noted that no discontinuities should be introduced in the $T_{b\ rough}$ equation at the edge values of WS (3 and 12 m/s).

In Gabarró et al., 2004, the model derived from WISE 2001 data set, which considers the WS and Hs parameters, has the following coefficients:

$C_{1.1} = C_{1.2} = C_{1.3} = 0.12$ $\quad$ $Z_{1.1} = Z_{1.2} = Z_{1.3} = 0.005$
$C_{2.1} = C_{2.2} = C_{2.3} = 0.59$ $\quad$ $Z_{2.1} = Z_{2.2} = Z_{2.3} = 0.012$

$C_{3.1} = C_{3.2} = C_{3.3} = 0$ $\quad$ $Z_{3.1} = Z_{3.3} = Z_{3.3} = 0$
$C_{4.1} = C_{4.2} = C_{4.3} = 0$ $\quad$ $Z_{4.1} = Z_{4.3} = Z_{4.3} = 0$
$C_{5.1} = C_{5.2} = C_{5.3} = 0$ $\quad$ $Z_{5.1} = Z_{5.3} = Z_{5.3} = 0$
$C_{6.1} = C_{6.2} = C_{6.3} = 0$ $\quad$ $Z_{6.1} = Z_{6.3} = Z_{6.3} = 0$

$Z_{7.1} = Z_{7.2} = Z_{7.3} = -0.003$
$Z_{8.1} = Z_{8.2} = Z_{8.3} = -0.012$
$Z_{9.1} = Z_{9.2} = Z_{9.3} = 0$
$Z_{10.1} = Z_{10.2} = Z_{10.3} = 0$
$Z_{11.1} = Z_{11.2} = Z_{11.3} = 0$
$Z_{12.1} = Z_{12.2} = Z_{12.3} = 0$

The roughness model should be continuous and derivable according to the retrieved parameters.

This empirical model is a linear fit to incidence angle. As will be discussed in section 14 (iterative convergence), not more than two parameters can be simultaneously retrieved per equation. Then, after a series of tests we have to decide what roughness parameters will be used in the model, but for sure not all six of them.

Note: It is not possible here to use the components of the wind speed, WC_U and WC_V, since they can have positive or negative values, depending on the wind direction. Therefore the contribution of Tb due to the wind components could have negatives values, which is physically inconsistent.

4.4.1.3. Error budget estimates (sensitivity analysis)

In Camps et al., 2004, authors observe that the uncertainty of the brightness temperature sensitivity to wind speed is on the order of 0.1 K/(m/s) for all incidence angles, when using the model only dependent on WS. Therefore, for WS=10 m/s, the uncertainty of the brightness temperature T_b is about 1 K. Taking into account the brightness temperature sensitivity to SSS (0.35-0.8 K/psu at V-pol, and 0.20-0.6 K/psu at H-pol), it translates at 10 m/s into a ΔSSS within 1.2-5 psu.

In the case of using a model dependent not only on WS, as part of the contribution on the brightness temperature are explained with other parameters, the sensitivity of the model to the WS will be smaller.

4.4.2. Practical considerations

4.4.2.1. Calibration and validation

During the commissioning phase, half of the measures could be used to adjust the coefficients of the three models. The rest of measures would then be the input for the validation of the model.

4.4.2.2. Quality control and diagnostics

When a significantly strong rain is present in the FOV, the model cannot be applied. This information will be known from the ECMWF data.

4.4.3. Assumption and limitations

We assume that wave and wind directions are negligible. This is argued in Camps et al., 2004 of the Synergy study.

Bibliography

Camps, A., Font, J., Vall-llossera, M., Gabarró, C., Villarino, R., Enrique, L., Miranda, J., Corbella, I., Duffo, N., Torres, F., Blanch, S., Arenas, J., Julià, A., Etcheto, J., Caselles, V., Weill, A., Boutin, J., Contardo, S., Niclòs, R., Rivas, R., Reising, S., Wursteisen, P., Berger, M., and Martín-Neira, M. (2004a). The WISE 2000 and 2001 Campaigns in Support of the SMOS Mission: Sea Surface L-band Brightness Temperature Observations and their Application to Multi-Angular Salinity Retrieval. IEEE Transactions on Geoscience and Remote Sensing, 42(4):804–823.

Camps, A., Font, J., Etcheto, J., Caselles, V., Weill, A., Corbella, I., Vall-llossera, M., Duffo, N., Torres, F., Villarino, R., Enrique, L., Julià, A., Gabarró, C., Boutin, J., Rubio, E., Reising, S., Wursteisen, P., Berger, M., and Martín-Neira, M. (2002b). Sea Surface Emissivity Observations at L-band: First Results of the Wind and Salinity Experiment WISE-2000. IEEE Transactions on Geoscience and Remote Sensing, 40(10):2117–2130.

Camps, A., Font, J., Gabarró, C., Miranda, J., Obligis, E., Labroue, S., Boone, C., Sabia, R., Vall-llosera, M., Reul, N., June 2004. WP1100, ESTEC ITT 1-4505/03/NL/Cb

Camps, A., Vall-llossera, M., Villarino, R., Reul, N., Chapron, B., Corbella, I., Duffo, N., Torres, F., Miranda, J.J., Sabia, R., Monerris, A., and Rodríguez, R. (2005c). The Emissivity of Foam-Covered Water Surface at L-Band: Theoretical Modeling and Experimental Results From the Frog 2003 Field Experiment. IEEE Transactions on Geoscience and Remote Sensing, 43(5):925-937.

Etcheto, J., Dinnat, E., Boutin, J., Camps, A., Miller, J., Contardo, S., Wesson, J., Font, J., and Long, D. (2004). Wind speed effect on L-band brightness temperature inferred from EuroSTARRS and WISE 2001 field experiments. IEEE Transactions on Geoscience and Remote Sensing (in press).

Gabarró, C., Font, J., Camps, A., Vall-llossera, M., and Julià, A. (2004a). A New Emprical Model of Sea Surface Microwave Emissivity for Salinity Remote Sensing. Geophysical Research Letters, 31(L01309):1–5.

Gabarró, C. (2004b). Study of salinity retrieval errors for the SMOS mission. PhD thesis, Universitat Politècnica de Catalunya.

Miranda, J., Vall-llossera, M., Camps, A., Duffo, N., Corbella, I., and Etcheto, J. (2003). Sea State on the Sea Surface Emissivity at L-Band. IEEE Transactions of Geoscience and Remote Sensing, 41(10):2307–2315.

Vall-llossera, M., Miranda, J., Camps, A., and Villarino, R. (2003). Sea Surface Emissivity Modeling At L-Band: An InterComparison Study. Proceedings of the WISE/LOSAC/EuroSTARRS campaigns Workshop. ESA, SP-525:143–154.

4.5. Foam Contribution

4.5.1. Theoretical description

4.5.1.1. Physics of the problem

Although foam generated by breaking waves typically covers only a few percent of the sea surface, it has a profound effect on the average microwave brightness of the ocean surface [1-8]. For surface wind speeds greater than 15 m/s, foam-induced effects may provide as much as half of the total sea surface signature to an orbiting microwave radiometer [9;10].
At L-band, WISE [11] and FROG [12] experiments have provided detailed L-band emissivity measurements of the sea foam over a wide range of incidence angles and salinities at both polarizations. Although foam as a weaker impact at 1.4 GHz than at higher frequencies, it was shown that the presence of foam also increases the emitted brightness temperature at L-band, since it acts as a transition layer that adapts the wave impedance of the two media: water and air. The increase depends on the fraction of the sea surface covered by foam and its thickness, which can be parameterized in terms of the local wind strength, but it depends as well on other factors, such as the air-sea temperature difference, the sea water temperature, the fetch, etc… FROG 2003 experiments revealed that at a salinity of 37 psu, the foam-induced emissivity increase is ~0.007 per mm of foam thickness (extrapolated at nadir), increasing with increasing incidence angles at vertical polarization, and decreasing with increasing incidence angles at horizontal polarization. According to the model developed by [13], for a 12 m/s wind speed, one should expect in average a coverage-weighted foam thickness of about 0.5 cm: this translates to an increase in brightness temperature of about 0.2 K at an SST of about 15°C. At 20 m/s, the calculation predicts a 0.5 K increases: this might have a non negligible impact for salinity retrieval accuracy.

In [12], it was shown that the emissivity model proposed by [14] correctly predicts the measured foam emissivities at L-band provided some auxiliary parameter describing the foam-water system are tuned. The purpose of this section is to document this forward foam emissivity model, which is used here to provide foam impact corrections in the version of the SSS retrieval algorithm used at launch of the ESA's Soil Moisture and Ocean Salinity (SMOS) satellite mission.
As proposed by [13], foam formations contribute to the total sea surface brigthness temperature measured by a radiometer as function of wind speed WS following:

$$T_{b,foam}(f,p,\theta_i,WS) = T_s \cdot \int e^{\mathrm{typ}}{}_{\mathrm{foam;p}}(f,p,\theta_i,h) \cdot F(WS,h)dh \quad (1)$$

where

- f, p and θ_i are the receiving electromagnetic frequency, polarization and incidence angle of the radiometer respectively,
- $F(WS, h)$ is the fraction of sea surface area covered by whitecaps with thickness h at wind speed WS,
- T_s is the physical tempearture of foam, usually assumed the same as the bulk sea surface temperature and,
- e^{typ}_{foam} is the emissivity of typical sea foam-layer with thickness δ.

This model is used in the present algorithm to provide foam impact corrections for SMOS. It contains two submodels: one to parametrize the emissivity of typical sea foam-layer with

thickness h and the second to model the fraction of sea surface area covered by whitecaps with thickness h at wind speed WS. Both of them are successively detailed hereafter.

4.5.1.2. Emissivity modeling of the foam-water system

Following Guo et al. [6], it is assumed that foam on the ocean surface is composed of nearly spherical coated bubbles described by an outer radius r, made of an air core with permittivity ε_a, surrounded by a shell of sea water with thickness δ and permittivity ε_W. The foam covered ocean is modeled by the succession of three media: the air (region 0), a foam layer defined as a region of effective permittivity $\varepsilon_{N\alpha}$ with a layer thickness d (region 1), and the underlying seawater with some air bubbles (region 2) with permittivity ε_W. Boundaries between each region are assumed flat.

The emissivity of a typical foam-water system at incidence angle θ_i and polarization p= h (horizontal) or v (vertical) is given by:

$$e^{\mathrm{typ}}{}_{\mathrm{foam;p}} = 1 - \left|\mathrm{R_p}(\theta_\mathrm{i})\right|^2 \tag{2}$$

where the coefficient R_p is the spectral reflection coefficient of the foam layer medium with the effective dielectric constant $\varepsilon_{N\alpha}$ and is given by

$$R_p(\theta_i) = \frac{R_p^{01}(\theta_i)e^{-j2\psi} + R_p^{12}(\theta_i)}{e^{-j2\psi} + R_p^{01}(\theta_i)R_p^{12}(\theta_i)}, \tag{3}$$

where ψ is an attenuation factor that depends on the foam layer thickness d, the electromagnetic wavelength λ_0, and the effective permittivity $\varepsilon_{N\alpha}$:

$$\psi = \frac{2\pi d}{\lambda_0}\sqrt{\varepsilon_{N\alpha} - \sin^2\theta_i}\,, \tag{4}$$

Note that for the foam-covered ocean, Stokes 3 and Stokes 4 = 0.

In Eq.(3), R_p^{01} are the Fresnel reflection coefficients between the air (region 0) and the foam (region 1):

$$R_h^{01}(\theta_i) = \frac{\cos(\theta_i) - \sqrt{\varepsilon_{N\alpha} - \sin^2\theta_i}}{\cos(\theta_i) + \sqrt{\varepsilon_{N\alpha} - \sin^2\theta_i}}, \tag{5a}$$

and

$$R_v^{01}(\theta_i) = \frac{\varepsilon_{N\alpha}\cos(\theta_i) - \sqrt{\varepsilon_{N\alpha} - \sin^2\theta_i}}{\varepsilon_{N\alpha}\cos(\theta_i) + \sqrt{\varepsilon_{N\alpha} - \sin^2\theta_i}}, \tag{5b}$$

and R_p^{12} are the Fresnel reflection coefficients between foam (region 1) and water (region 2):

$$R_h^{12}(\theta_i) = \frac{\sqrt{\varepsilon_{N\alpha} - \sin^2(\theta_i)} - \sqrt{\varepsilon_w - \sin^2\theta_i}}{\sqrt{\varepsilon_{N\alpha} - \sin^2(\theta_i)} + \sqrt{\varepsilon_w - \sin^2\theta_i}}, \tag{6a}$$

and

$$R_h^{12}(\theta_i) = \frac{\varepsilon_w\sqrt{\varepsilon_{N\alpha} - \sin^2(\theta_i)} - \varepsilon_{N\alpha}\sqrt{\varepsilon_w - \sin^2\theta_i}}{\varepsilon_w\sqrt{\varepsilon_{N\alpha} - \sin^2(\theta_i)} + \varepsilon_{N\alpha}\sqrt{\varepsilon_w - \sin^2\theta_i}}. \tag{6b}$$

Region 2 consists of air bubbles embedded in the ocean background and is assumed to be absorptive. To solve the previous equations (2-6), one needs to define an effective permittivity for region 1, namely $\varepsilon_{N\alpha}$, and for region 2, namely ε_w.

The main parameter of the previous multi-layer emissivity model for foam is the effective permittivity $\varepsilon_{N\alpha}$ of the foam-layer considered. To define this parameter, the well-known *Lorenz-Lorentz* and *Hulst* equations can be used and modified for the poly-dispersed system of bubbles. The first formula takes into account *dipole interaction* of bubbles in a close-packed dispersed system (the quasi static approximation). The Hulst equations describe the contribution of the *multi-pole moment* of bubbles into effective permittivity of the system. Spectral calculations by Cherny and Raizer [15] show that first resonant electromagnetic effects by Hulst's mechanism occur for bubbles radius $a \approx \lambda_o/4$. At L-band (λ_0=21 cm), this corresponds to bubble diameters on order of 10 cm. Such very large bubbles are extremely rare at the sea surface and therefore, the multi-pole mechanism may be neglected at L-band for which the dipole term might be considered only. In the present work, we use the dipole approximation model developed by Dombrovskiy and Raizer [16] to describe the effective permittivity of the system. It involves the use of a modification of the Lorenz-Lorentz equation and yields to the following simple formula for the complex effective permittivity $\varepsilon_{N\alpha}$ of a foam-layer [15, 16]:

$$\varepsilon_{N\alpha} = \frac{1+\frac{8}{3}\pi\overline{N\alpha}}{1-\frac{4}{3}\pi\overline{N\alpha}}, \tag{7}$$

where

$$\overline{N\alpha} = \frac{\kappa\int \alpha(r)\, p_f(r)\, dr}{\frac{4}{3}\int r^3 p_f(r)\, dr}, \tag{8}$$

and N is the volumetric concentration of the bubbles, $\alpha(r)$ is the complex polarizability of a single bubble with external radius r, κ is the so-called packing coefficient or *stickiness parameter*, and $p_f(r)$ is the normalized probability distribution function of the bubbles' size. In natural media such as foam, the densely packed particles can have adhesive forces that make them adhere to form aggregates. This effect is accounted for in the model by the *stickiness parameter* κ, which is inversely proportional to the strength of the attractive forces between bubbles [17].

According to Dombrovskiy and Raizer [16], the complex polarizability depends on the external radius of the bubbles r, the complex permittivity of the shell medium (salt water) ε_w, and the bubble's filling factor $q = 1-\delta/r$ following

$$\alpha(r) = r^3 \frac{(\varepsilon_w - 1)(2\varepsilon_w + 1)(1-q^3)}{(\varepsilon_w + 2)(2\varepsilon_w + 1)(1-q^3) + 9\varepsilon_w q^3}. \tag{9}$$

Experimental measurements on stable foam reveal that the effective permittivity might be dependent on the vertical position within the foam layer, i.e, $\varepsilon_{N\alpha} = \varepsilon_{N\alpha}(z)$. In the simplest case, the foam-water system may be modeled as a succession of elementary foam-layers, each of them having a homogeneous effective dielectric constant. However, the exact dependence of such function with the vertical position, which depends on the vertical distribution of the bubble's size, is very poorly known. It is very likely that the vertical distribution of the

bubble's size $p_f(r,z)$ is a function of the intensity and scale of the underlying breaking event. Moreover it will certainly strongly evolve during a transient breaking event. Nevertheless, in order to keep a tractable number of parameters in the present model, we choose to consider a uniform vertical distribution of bubbles sizes $p_f(r,z) = p_f(r)$ within the foam layer.

The foam void fraction (i.e., the ratio of the volume of air to the total volume of the foam) depends on the distribution of the bubble's filling factor *q*. Therefore, the distribution of bubbles radii $p_f(r)$ together with the distribution of coating thicknesses $f(\delta)$ determine the foam layer void fraction. In the present simplified model, we fixed the value of the shell thickness δ, but the outer bubble radius *r* is randomly distributed. According to Dombrovskiy [18], this approximation reflects an experimentally established fact for an emulsion layer of foam (young foam), but it requires verification for a foam with honeycomb structure (aged foam). Numerous observations of oceanic bubble size distributions are reported in the literature based on acoustic, photographic, optical, and holographic methods [19]. Currently, it is not clear how to parameterize the ocean surface bubble size distribution. Following Bordonskiy et al. [18] and Dombrovskskiy and Raizer [16], we used a Gamma distribution for the size distribution function of the bubbles:

$$p_f(r) = \frac{A^{B+1}}{\Gamma(B+1)} r^B e^{-Ar}, \tag{10}$$

where *A* and *B* are parameters of the distribution defined with $r_p = A/B$ being the most probable radius. Finally, to calculate ε_w, a simple physical model based on induced dipoles is used. Let ε_{sw} denote the permittivity of the seawater at L-band, and f_a the fractional volume occupied by the air bubbles. Then, the effective permittivity ε_w, is given by the Maxwell-Garnett mixing formula [6]:

$$\varepsilon_w = \varepsilon_{sw} \frac{1+2f_a y}{1-f_a y}, \tag{10}$$

where

$$y = \frac{1-\varepsilon_{sw}}{1+2\varepsilon_{sw}}. \tag{11}$$

Note that the effective permittivity ε_w here does not include scattering extinction, which is small due to the fact that the seawater is heavily absorptive.

According to our simplified model, the emissivity induced by a typical sea foam layer at L-band is a function of:

$$e^{typ}{}_{Bf} = function(\theta_i, p, T_s, r_p, \delta, \kappa, f_a, d, SSS, SST) \tag{12}$$

where θ_i is the radiometer incidence angle, *p* is the polarization, T_s is the foam physical temperature, r_p is the most probable radius, δ is the bubble's water coating thickness, κ is the bubble's packing coefficient, *d* is the foam layer thickness, f_a is the void fraction beneath the foam layer, and finally, SSS and SST are the sea surface salinity and temperature respectively.

4.5.1.3. Foam coverage Model

In [13], it was shown that the fractional sea surface covered by foam-layers with thicknesses between *h* and *h+dh* at wind speed *WS,* namely, the term *F(WS,h)dh* in Equation (1), can be decomposed as follows:

$$dF(WS,h)=F(WS,h)dh= dF_c(WS,h)+ dF_s(WS,h) \quad (13)$$

where $dF_c(WS,h)$ and $dF_s(WS,h)$ are the contributions to the coverage of actively breaking crests or active foam and of the passive foam, or static-foam formations (see [7] for detailed terminology), respectively.

The model with used for these two terms is described in detailed in [13], wher the following empirical expression for $dF_c(WS,h)$ was derived:

$$dF_c(WS,h) = \left[2.9\times10^{-5}\cdot WS^3\sqrt{h}\cdot e^{-4.48\sqrt{h}}dh\right]\times e^{(\alpha_c\Delta T-\beta_c)} \quad (14)$$

where *WS* is the 10 meter height wind speed, α_c and β_c are numerical constants and ΔT is the air-sea temperature difference.

No direct empirical expression can be given to estimate the corresponding expression for the coverage due to passive foam formations coverage with thicknesses between *h* and *h+dh* at wind speed *WS*. However, it can be evaluated numerically as function of *h* and *WS*, as described in [13]. As well, the air-sea stratification impact is accounted for in the paramerization through an exponential correction term similar to the one in (14) but with modified numerical constants α_s and β_s.

The parameters α and β of the thermal correction factors were determined in [13] for both 'crest-foam' and 'static-foam' by best fitting the model to Monahan and Woolf [1989]'s empirical laws [19]. Using a least-square method, the determined numerical values for α and β are:

α_c = 0.198 and β_c = 0.91 for 'crest-foam coverage',

and,

α_s = 0.086 and β_s= 0.38 for 'static-foam coverage'.

According to that model, the fractional sea surface covered by foam-layers with thicknesses between *h* and *h+dh* at wind speed *WS* used in Equation (1) is finally function of:

- the foam-layers thicknesses *h*[m]
- the wind speed *WS* at 10 meter height [m/s]
- the temperature difference between air and sea ΔT [°C]

4.5.2. Mathematical description

The total contribution of foam formations to the sea surface brigthness temperature measured at L-band as given in Eq. (1) will be mathematically expressed for implementation into the processor using:

1) Three Look-Up tables (LUTs) that will provide (1) the foam-induced sea surface brigthness temperature (one LUT1 for H and LUT2 for V polarization) and (2) an additional LUT (LUT3) that will also provide the total foam-coverage.

LUT1 and LUT2 will be provided as function of the following parameters (with associated ranges):

- the incidence angle θ_i at SMOS pixel [deg], (0→ 75°)
- the sea surface temperature T_s [K], (269.15→ 309.15 K)
- the prior sea surface salinity SSS [psu] (0 → 40 psu)
- the wind speed *WS* at 10 meter height [m/s],(0 → 30 m/s) and,

- the temperature difference between air at 2 m height and sea surface :

$\Delta T=T_a-T_s$, [°C]],(-35 → 25°C*)

LUT3 will be provided as function of the following parameters (with associated ranges):

- the wind speed *WS* at 10 meter height [m/s],and,
- the temperature difference between air at 2 m height and sea surface :

$\Delta T=T_a-T_s$, [°C]],(-35 → 25°C*)

LUT1 and LUT2 will provide directly Tb_foam (H or V) , expressed as the result of the integral in Eq. 1 times SST. The reason why we provide LUT3 as well is that in Eq 1, only incremental foam coverages dF as function of thickness are included and NOT the total foam coverage, namely F(U). However the processor will need the later to evaluate the total surface contribution including foam and no-foam surface contributions (flat+rough), as follows:

$$Tb_{surface}=(1-F)(Tb_{flat}+Tb_{rough})+Tb_{foam}$$

Note that in the mathematical expression for $e^{typ}_{Bf,}$ the numerical values for r_p, the most probable bubble radius, for δ, the bubble's water coating thickness, for κ, the bubble's packing coefficient, and for f_a, the void fraction beneath the foam layer will be assigned constant values derived by best-tunning the model to the data observed during FROG campaign [12]. These values are not provided yet in the draft ATBD but will be given later.

2) Multi-dimensional interpolation schemes

Given the four values of the "geophysical" auxiliary parameters estimated at a given SMOS pixel, namely T_{si}, SSS_i, *WS* and ΔT, plus the series of incidence angles ($\theta_{i=1,...,N}$) associated to the L1C product considered, a multi-dimensional cubic spline interpolation scheme will be applied to LUT1 ands LUT2 to evaluate, the values of $T^{(n)}_{Bf,i=1,...,N}$, at both H and V polarization. An additional 2D cubic spline interpolation scheme will be applied to LUT3 as function of *WS* and ΔT, to determine the total foam coverage.

4.5.3. Error budget estimates

Inter-comparison between the FROG measurements [12] of the foam emissivities scaled at 100% coverage and the theoretical values computed with the model described above for e^{typ}_{Bf} using as inputs the measured foam parameters have been perfomed in [12]. The values of the stickiness parameter κ, which were not measured during FROG, used in the model are the optimum ones found at each salinity, which in general increases with SSS as the bubbles are more densely packed.

The rms error between the measured data and the theoretical foam emissivity model was found to vary from 0.008 to 0.017 at H-polarization, and from 0.011 to 0.033 at V-polarization. In general the agreement is much better at H-polarization than at V-polarization. At V-polarization, the measured values show a larger variation with the incidence angle than the model predictions, which requires further analysis and refinement of the model. At H-polarization the agreement is excellent, except at low salinities, where there is a bias between the measured and predicted emissivites at all incidence angles.

A much higher uncertainty source in the model is the whitecap coverage model. Indeed, the model derived by [13] to parameterize *F(U,h)* is constructed to match the empirical laws derived by [20]. Is is well known that extremeley large scatter in the whitecap coverage data as reported from one author to the other, which might yield to uncertainties of 100% to 600 % on empirical fits for *F(U,h)*. However, being the only source of validation we have, these empirical fits shall be used here as the basis for modeling.

Accounting for an error of 100% in the foam coverage and assuming a maximum coverage of 10%, we expect a maximum rms error budget on the foam emissivity contribution modelling of about:

$$Max\left(Rms\ error\right)\left(\begin{bmatrix} e^{typ}{}_{Bfh}(\theta_i) \\ e^{typ}{}_{Bfv}(\theta_i) \end{bmatrix}\right) \leq \begin{bmatrix} 1.7\times10^{-3} \\ 3.3\times10^{-3} \end{bmatrix}$$

This transaltes into about 0.5 K and 0.9 K maximal errors at H and V polarization, respectively.

4.5.4. Practical consideration

The model is not expected to provide significant contribution for wind speeds less than about 10 m/s. We could practically consider to perform that correction only for wind speeds more than that threshold value, using the decision tree.

Note as well that when foam correction is applied to SMOS Tbs, the foam-free surface contribution (i.e. flat sea surface+ roughness correction) as to be weighted by 1-F(U), the free foam fractional surface so that F is an output of the present forward model.

4.5.4.1. Calibration and validation

Calibration and validation of the forward foam emissivity model for roughness correction will be done during the comissionning phase, and later-on, by perfoming residual analysis of the future SMOS measurements and using a formalism proposed for and applied to NASA scatterometer (NSCAT), Special Sensor Microwave Imager (SSM/I) and ESA/ERS scatterometer measurements [see 21].

Using in situ SSS, SST and wind (TAO, Argo drifter+ satellite SST and winds and ECMWF model winds) and SMOS co-localized data, the first step will be to remove the modelled flat sea surface and free-foam roughness contributions from the SMOS surface bightness temperature data (i.e., corrected for atmospheric, ionospheric, galactic and sunglint conribution) in order to estimate the residual foam impact. This shall be done in selected ocean area with strong winds (southern ocean and North seas). The in situ and satellite SSS, SST and wind data will be the chosen reference. In addition, ECMWF analysis winds will be used as a thrid data source to completely determine the errors via a multiple collocation analysis. The main objective will be to present observed correlations between regional and seasonal model predictions of the foam correction factors errors and nonwind oceanic and atmospheric factors such as the surface current and sea state. Following the methodology applied in [30], we shall explicitely take into account the errors in the reference datasets as well as in the foam correction factors retrieved estimates. The gain shall come in more accurate assessment of bias and variance and less possible systematic contamination that can obscur geophysically driven impacts not accounted for by the foam model.

4.5.4.2. Quality control and diagnostics

As explained in section 4.5.5 below, the foam correction model based on fixed geophysical parameters (bubbles radius, stickiness factors, etc ..) which might generate biases on the estimated correction.
The model can be applied as it is at launch but we expect that the CAL/VAL activities will provide after commisionning phase a possible tunning for these parameters.

4.5.4.3. Exception handling

In presence of very stormy conditions (Hurricane like situations) it is likely that high foam coverage will be associated with high rain rates. Foam correction in that case would be non-physical if no atmospheric correction to account for rain absorptivity is also provided by the processor.

4.5.5. Assumption and limitations

*: Note that there is no impact of stratification when atmopshere is stable, i.e., $\Delta T < 0$ so that, the tables will be computed only for ranges where it has an impact and where the model is thought to be valid, i.e., ΔT: 0 → 15°C. Out of this range, the LUTS will duplicate values at extreme borders of the validity range.
A strong limitation may come from the fact that the numerical values for r_p, the most probable bubble radius, for δ, the bubble's water coating thickness, for κ, the bubble's packing coefficient, and for f_a, the void fraction beneath the foam layer are assigned constant values derived by best-tunning the model to the data observed during FROG campaign [12]. This is a strong assumption, as these parameters clearly evolve as function of the synoptic wind and wave forcing conditions.

References

[1] Rosenkranz, P. W., and D. H. Staelin, Microwave emissivity of ocean foam and its effect on nadiral radiometric measurements, J. Geophys. Res., 77, 6528-6537, 1972.
[2] Stogryn, A., The emissivity of sea foam at microwave frequencies, J. Geophys. Res., 779, 1658-1666, 1972.
[3] Ross, D. B., and V. Cardone, Observations of oceanic whitecaps and their relation to remote measurements of surface wind speed, J. Geophys. Res., 79, 444-452, 1974.
[4] Smith, P. M., The emissivity of sea foam at 19 and 37 ghz, IEEE Trans. Geosci. and Remote Sens., 26, 541-547, 1988.
[5] Kunkee, D. B., and A. J. Gasiewski, Simulation of passive microwave wind direction signatures over the ocean using an asymmetric-wave geometrical optics model, Radio Sci., 32, 59-78, 1997.
[6] Guo, J., L. Tsang, W. Asher, K.-H. Ding, and C.-T. Chen, Applications of dense media radiative transfer theory for passivemicrowave remote sensing of foam covered ocean, IEEE Trans.Geosci. and Remote Sens., 39, 1019-1027, 2001.
|7] Monahan, E., Oceanic whitecaps: Sea surface features detectable via satellite that are indicators of the air-sea gas transfer coefficient, in Proc. Indian Acad. Sci. (Earth Planet Sci.), vol.111, pp. 315-319, 2002.
[8] Anguelova, M., Whitecaps, sea-salt aerosols, and climate, Ph.D. thesis, Graduate College of Marine Studies, University of Delaware, Lewes, Delaware, 2002.

[9] Droppleman, J. D., Apparent microwave emissivity of sea foam, J. Geophys. Res., 79,696-698, 1970.
[10] Barber, R. P., and J. Wu, Sea brightness temperature effects of spray and whitecaps, J. Geophys. Res., 102, 5823-5827, 1997.
[11] A. Camps, J. Font, M. Vall-llossera, C. Gabarro, R. Villarino, L. Enrique, J. Miranda, I. Corbella, N. Duo, F. Torres, S. Blanch, J. Arenas, A. Julia, J.Etcheto, V. Caselles, A. Weill, J. Boutin, S. Contardo, R. Niclos, R. Rivas, S. Reising, P. Wursteisen, M. Berger, and M. Martn-Neira, The WISE 2000 and 2001 Campaigns in support of the SMOS Mission: Sea surface L-band Brightness Temperature Observations and their application to Multi- Angular Salinity Retrieval, *IEEE Trans. Geosci. Remote Sensing*, vol. 42, no. 4, pp. 1039-1048, 2004.
[12] A. Camps, M. Vall-llossera, R. Villarino, N. Reul, B. Chapron, I. Corbella, N. Duff, F. Torres, J. Miranda, R. Sabia, A. Monerris, R. Rodríguez, "The Emissivity Of Foam-Covered Water Surface at L-Band: Theoretical Modeling And Experimental Results From The Frog 2003 Field Experiment", *IEEE Transactions on Geoscience and Remote Sensing*, vol 43, No 5, pp 925-937, 2005.
[13] N.Reul and B. Chapron, "A model of sea-foam thickness distribution for passive microwave remote sensing applications", *J. Geophys. Res.,* 108 (C10), Oct, 2003.
[14] N.Reul and B. Chapron, "Effects of foam on the emissivity of the sea surface at L-band", WP1300 Report, ESA contract N°15165/01/NL/SF, April 2001.
[15] V. Cherny and V. Y. Raizer, *Passive Microwave Remote Sensing of Oceans*, wiley-praxis series in remote sensing ed. Wiley, 1998.
[16] Dombrovskiy, L. A., and V. Y. Raizer, Microwave model of a two-phase medium at the ocean surface*, Izvestiya, Atmospheric and Oceanic Physics*, 28, 650-656, 1992.
[17] L. M. Zurk, L. Tsang, K. H. Ding, and D. P. Winebrenner, .Monte carlo simulations of the extinction rate of densely packed spheres with clustered and non-clustered geometries,. *J. Opt. Soc. America*, vol. 12, pp. 1772.1781, Aug. 1995.
[18] L. A. Dombrovskiy, .Calculation of the thermal radiation emission of foam on the sea surface,. *Izvestiya, Atmospheric and Oceanic Physics*, vol. 15, no. 3, pp. 193.198, 1979.
[19] J. Wu, .Variation of whitecap coverage with wind stress and water temperature,. *J. Phys. Oceanogr.*, vol. 18, pp. 1448.1453, 1988.
[20] Monahan, E., and D. K. Woolf, Comments on variations of white-cap coverage with wind stress and water temperature, J. Phys.Oceanogr., 19, 706-709, 1989.
[21] Y. Quilfen, B. Chapron and D. Vandemark, "The ERS Scatterometer Wind measurement accuracy: evidence of seasonal and regional biases", *Journal of Atmopsheric and Oceanic Technology*, vol 18, p 1684-1697, 2001.

4.6. Galactic noise contamination

4.6.1. Theoretical description

This section has been written with the help of [*LeVine and Abraham,* 2004] and [*Delahaye et al.,* 2002] papers.

Formatted: Font: 12 pt

4.6.1.1. Physics of the problem

At L-band, radiation from celestial sources is strong and spatially variable; they have been reviewed by *Delahaye et al.* (2002), *Le Vine and Abraham* (2004), and associated corrections needed to interpret L-band radiometric measurements have been thoroughly described by *Le Vine and Abraham* (2004). Radiation originates from three types of sources. The hydrogen line emission corresponds to a hyperfine atomic transition in neutral hydrogen: the radiation is maximum around the plane of the galaxy, most of the time less than 2 K. The cosmic background is a remnant signal of the origin of the universe and is almost constant in space and time (2.7 K). In addition to the almost constant cosmic background, a very variable (in space) continuum radiation (up to more than 10 K) is due to emissions from discrete radiosources.
As in the case of atmospheric emission, the cosmic background adds a contribution to the radiometric temperature that depends on the incidence angle linked to the reflection of the signal on the sea surface.
The two other types of sources add a signal that varies according to the incidence and azimuth angle of the measurement.

4.6.1.2. Mathematical description of algorithm

4.6.1.2.1. Data conversion

The common practice in passive microwave remote sensing of the earth is to consider equivalent brightness temperatures. Thence, for the purpose L-band radiometry, it is common to present data from radioastronomy surveys in the form of equivalent black-body temperatures, i.e., as if they were from an equivalent thermal source with total power:

$$P = kT_B \Delta B \qquad (1)$$

where k is the Boltzmann constant and ΔB is the bandwidth of the receiver used for the survey, or as a total power integrated over a frequency range as in the case of the hydrogen line emission.

a) Hydrogen Line emission:

The line emission has a relatively narrow spectrum. For hydrogen at rest, it occurs at a frequency associated with the hyperfine transition at 21.106cm. However the line is shifted by the motion of the hydrogen relative to the observer (Doppler shift) and spread by thermal energy of the gas (collisions and vibrations). Nevertheless the spectrum is relatively narrow: Leiden/Dwingeloo survey [*Hartmann and Burton,* 1997] in the Northern hemisphere and IAR survey in the southern hemisphere [*Arnal et al.,* 2000] cover the velocity range from -450 to +400km/s which corresponds to a frequency range of 4.025MHz (see below) about the center frequency of 1.42GHz of hydrogen at rest. The integrated power reported in

radioastronomy survey, P, is given in Kelvin kilometers per second (K-km/s). In order to convert it to a brightness temperature that will be recorded by a radiometer having a bandwidth ΔB, it is necessary to convert it in Kelvin-MHz using the line emission bandwidth and then to calibrate it with respect to the radiometer bandwidth.
Given the standard form for Doppler shift:

$$\nu = \nu_0 (1 - \mathrm{v}/c)$$

with ν_0 the center frequency (1.42GHz), ν the frequency associated with the velocity v and c the light speed, a velocity range from -450 to +400km/s corresponds to a frequency bandwidth of 4.025MHz.
Thence the integrated power reported in radioastronomy survey corresponding to a velocity range of 850km/s, Pint, can be converted in Kelvin-MHz using:

$$\mathrm{Pint(K\text{-}MHz)} = \mathrm{Pint(K\text{-}km/s)} \cdot 4.025/850 = \mathrm{Pint(K\text{-}km/s)} \cdot 4.735\ 10^{-3}$$

Since the SMOS radiometer bandwidth, ΔBsmos in MHz, is well above 4MHz, this value can be converted to get an equivalent Tb for SMOS, as follows:

$$\mathrm{Tb} = \mathrm{Pint(K\text{-}MHz)}/\Delta\mathrm{Bsmos} = \mathrm{Pint(K\text{-}km/s)} \cdot 4.735\ 10^{-3}/\Delta\mathrm{Bsmos}$$

b) Continuum radiation and cosmic background

These radiations are usually given in terms of effective brightness temperature, Tb, i.e. they include the correction for the bandwith of the survey (e.g. Reich and Reich maps). Thence, as these radiations are supposed to be homogeneous over the frequency range of SMOS bandwidth, there is no need to correct Tb deduced from radioastronomy surveys.

4.6.1.2.2. Galactic noise reflected towards the radiometer

In the following we will call the effective brightness temperature of the galactic radiation, Tbgal, as the sum of the hydrogen emission line plus the continuum radiation plus the cosmic background.

First it is necessary to determine the location in the celestial sky from which incident radiation will be reflected from one point in the field of view into the antenna. Given ϑ_i and φ_i respectively the incidence and the azimuth (0 towards the north; positive westward) angles of one radiometer measurement at this point, the incident galactic ray that will be specularly reflected towards the radiometer comes from an incidence angle, ϑ_{igal}:

$$\vartheta_{igal} = Arc\sin\left(\frac{\mathrm{Re} + h_{rad}}{\mathrm{Re}}\sin(\vartheta_i)\right)$$

where Re is the earth radius and h_{rad} is the altitude of the radiometer.

The elevation angle (in degrees; 0 towards the horizon and positive above the horizon) is defined as:

$$\mathrm{el} = 90 - \vartheta_{igal}$$

Usually celestial maps are given in celestial coordinates system (declination, δ, and right ascension, α). It is therefore necessary to derive δ and α from the latitude, lat, longitude, lon, sideral time, T, ϑ_i and φ_i. This can be done by solving the following implicit equations:

$$\tan(\varphi) = \frac{-\sin(H)}{\tan(\delta)\cos(lat) - \cos(H)\sin(lat)}$$

$$\sin(el) = \sin(lat)\sin(\delta) + \cos(lat)\cos(\delta)\cos(H)$$

where H is the sidereal angle (see for instance Appendix C of *Le Vine and Abraham* (2004)) defined as:

H= T-lon-α

In the following we consider three cases:

a) a simple case assuming a flat sea

b) a simple case assuming a rough sea and an homogeneous sky

c) a more complicated case where we take into account the sea surface roughness and the sky inhomogeneity.

In the following we will distinguish two polarizations for Tbgal. At present, existing galactic maps do not distinguish between V and H pol but there is suspicion about a possible polarization dependency.

a)Assuming a flat sea:

The galactic noise reflected towards the radiometer, Tbgal_refl, can be computed as:

Tbgal_refl(lat,lon, T, ϑ_i , φ_i,p) =Tbgal(δ,α,p).Rfresnel(ϑ_{igal} , SSS, SST,p)

where p is one of the polarisation (H or V).

b)Assuming an homogeneous sky:

In that case the reflection coefficient computed for estimating Tbrough, Rrough, can be used:

Tbgal_refl(lat,lon, T, ϑ_i , φ_i,p) =Tbgal(δ,α,p).(Rfresnel(ϑ_{igal} , SSS, SST,p) +Rrough(ϑ_{igal} , SSS, SST,p))

where Rrough=-Tbrough/SST (Rrough is negative)

If the sky were homogeneous, it is expected that the introduction of the roughness would have a small effect in most cases: for instance, for a 10m/s wind speed, (the reflection coefficient is modified by about 2.5% (at nadir)) and a galactic noise of 5K, neglecting the roughness effect would introduce an error of less than 0.08K. Thence it is expected that Tbgal_refl estimated using a) and b) will be very close except in case of large galactic noise which is usually associated with large inhomogeneities. However, because of the inhomogeneities in the galactic maps, it is necessary to take into account the roughness when dealing with celestial points close to the galactic plane. Therefore case a) will not be considered.

Deleted: may be

Deleted: (TBD)

c)Taking into account the roughness of the sea:

Introducing bistatic reflection coefficients that can be extracted from 2-scale or from SSA models, σ_0 , in theory the galactic noise over the whole sky should be convoluted with these scattering coefficients. However since they are expected to decrease rapidly

outside of the specular reflection, the integration could be done over an interval +/-$d\vartheta_{igal}$ which value needs TBD:

$$\text{Tbgal\_refl}(\text{lat},\text{lon},\text{T},\vartheta_i,\varphi_i,\text{v}) = \frac{1}{4\pi\cos(\vartheta_i)}$$
$$\int_0^{2\Pi}\int_{\vartheta_{igal}}^{\vartheta_{igal}+\delta\vartheta_s}\left(\sigma^0_{vv}(\vartheta_s,\varphi_s,\vartheta_i,\varphi_i)Tbgal(\vartheta_s,\varphi_s,\text{v})+\sigma^0_{vh}(\vartheta_s,\varphi_s,\vartheta_i,\varphi_i)Tbgal(\vartheta_s,\varphi_s,\text{h})\right)\sin(\vartheta_s)d\vartheta_s d\varphi_s$$

$$\text{Tbgal\_refl}(\text{lat},\text{lon},\text{T},\vartheta_i,\varphi_i,\text{h}) = \frac{1}{4\pi\cos(\vartheta_i)}$$
$$\int_0^{2\Pi}\int_{\vartheta_{igal}}^{\vartheta_{igal}+\delta\vartheta_s}\left(\sigma^0_{hh}(\vartheta_s,\varphi_s,\vartheta_i,\varphi_i)Tbgal(\vartheta_s,\varphi_s,\text{h})+\sigma^0_{hv}(\vartheta_s,\varphi_s,\vartheta_i,\varphi_i)Tbgal(\vartheta_s,\varphi_s,\text{v})\right)\sin(\vartheta_s)d\vartheta_s d\varphi_s$$

Both cases b) and c) should be kept. A switch will allow to select the desired case.

4.6.1.2.3. Integration over the antenna beam

In addition it is necessary to integrate the reflected brightness temperature over the antenna pattern to obtain Tbgal_refl_lobe, which is the quantity measured by the radiometer :

$$\text{Tbgal\_refl\_lobe}(\vartheta_i,\varphi_i) = \int_0^{2\Pi} d\varphi_i \int_{\vartheta i-\Pi/2}^{\vartheta i+\Pi/2} d\vartheta_i' \int \text{Tbgal\_refl}(\vartheta_i')P_{lobe}(\vartheta_i' - \vartheta_i,\varphi_i)$$

where Plobe is the normalized power pattern of the antenna. In case Plobe is an axially symmetric pattern, according to *Le Vine and Abraham* (2004)) it is possible to make the integration on δ and α and thence to precalculate galactic maps integrated over the antenna pattern before computing the reflection over the sea surface. Since the SMOS lobe varies accross the FOV and is not symmetric, it will be necessary to test if such an approximation is acceptable.

4.6.1.3. Error budget estimates (sensitivity analysis)

The main uncertainty is expected to come from inaccuracies of the galactic noise maps. [*Reich and Reich,* 1986] estimate the accuracy on their maps (due to the calibration of the instrument) of 0.5K. From SRS study, a constant bias of 0.5K on galactic noise map will induce a mean bias on retrieved SSS of 1psu.
In addition to a constant bias, uncertainties are likely to appear on these maps close to the equatorial galactic plane. Comparisons between the maps derived from the Stokert survey, commonly called the Reich and Reich map, and the ones deduced from the Effelsberg survey are in progress to better apprehend the error on these maps. Both maps include the continuum radiation and the cosmic background; Stockert survey was performed with a 34mn angular resolution instrument while Effelsberg used a 9mn angular resolution instrument. Stockert map for the northern hemisphere and Effelsberg maps are available on the http://www.mpifr-bonn.mpg.de/survey.html site; the Stokert map for southern hemisphere was provided by ESA. Stockert maps are global but region around Cassiopeia is excluded (no data) and strong sources are suspected to be underestimated; Effelsberg survey is concentrated close to the equatorial plane (cygnus excluded).

4.6.2. Practical considerations

4.6.2.1. Calibration and validation

As suggested before, it may be necessary to introduce a calibration factor proportional to Tbgal during the Cal/Val phase to correct for calibration and saturation problems of the existing surveys.

4.6.2.2. Quality control and diagnostics

Looking towards North (azimuth=0) with an incidence angle equal to the elevation of the observer, one looks towrds the celestial North pole which location is invariant.

4.6.3. Assumption and limitations

Depending on the reliability we can put on galactic noise maps (TBD), it could be necessary to discard some SMOS Tb affected by radiation coming from the galactic plane if it is demonstrated that this radiation is very badly known. Tests are in progress to estimate the impact of radiation errors in the galactic plane (as estimated from the difference between Effelsberg and Stockert surveys) on the retrieved SSS.

Deleted: The a) model assumes a specular reflection over the ocean surface. Because galactic noise is inhomogeneous spatially, especially close to the galactic plane, this may be not completely justified. Whether this assumption is acceptable needs to be checked; nevertheless, this limitation is expected to be of second order with respect to uncertainties on galactic noise maps.¶

Bibliography

Arnal, E.M., E. Bajaja, J.J. Lararte, R. Morras, and W.J.L. Poppel, A high sensitivity HI survey of the sky at δ<=–25°, *Astron. Astrophys. Suppl. Series*, *142*, 35-40, 2000.

Delahaye, J.Y., P. Golé, and P. Waldteufel, Calibration error of L-band sky-looking ground-based radiometers, *radio science*, *37*, 10.1029/2001RS002490, 2002.

Hartmann, D., and W.B. Burton, *Atlas of galactic neutral hydrogen*, 235 pp., Cambridge university press, New York, 1997.

LeVine, D.M., and S. Abraham, Galactic noise and passive microwave remote sensing from space at L-Band, *IEEE Transactions on Geoscience and Remote Sensing*, *42*, 119-129, 2004.

Reich, P., and W. Reich, A radio continuum survey of the northern sky at 1420 MHz, *Astron. Astrophys. Suppl. Ser.*, *63*, 205-292, 1986.

4.7. Sunglint contamination

4.7.1. Theoretical description

4.7.1.1. Physics of the problem

Beyond geophysical sources of error, Yueh et al. [1] noticed that the solar radiations pose a significant challenge for the remote sensing of ocean surface salinity. The sun is indeed an extremely strong radiation source at L-band, exhibiting a time-dependent blackbody temperature that ranges between 100000 K and 10 million K, depending on the solar activity [2] and the next solar maximum is expected in 2010, that is 3 years after SMOS launch.
Two distinct mechanisms may contribute to the solar radiation intercepted by a radiometer antenna: one is the reflection of sun radiations by the earth-surface (sunglitter effects) and the other is the direct leakage into the antenna. Here, we only focussed on the modeling for the reflected contamination over the ocean, direct contaminations being addressed by the Level 1 processor.
In [3a, 3b], it was shown that the centre of the sun's glitter pattern will never be located in the area of SMOS' synthesized field of view. However the expected range of surface wind speeds (zero wind is very uncommon) will cause the sun's glitter pattern to spread within the alias free field of view which might contamine the useful measured signals. More specifically, frequent pixel contaminations are expected around winter solstices when the the centre of the sun's glitter pattern will lye close to the right-hand border of the FOV.
Experimental evidences of the sunglitter strong impacts on the passive microwave sensing of the ocean using L-band radiometers was first given by Swift [4] in 1974, who analyzed the forward scattering of sun microwave radiations from the Cape Code Canal in Massachusetts. Data were collected at 1.4, 4.0, and 7.5 GHz for horizontal and vertical polarization at a fixed nadir viewing angle of 40°. As the sun passed through the main beam of the antennas, Swift found that the excess temperature due to reflected solar radiation increased dramatically with decreasing frequency and was polarization dependent. The sun was found to be such a dominating source at 1.4 GHz that the horizontally polarized component saturated the radiometer.
As shown by Wentz [5], these sun-glitter effects might be modelled using approximate scattering models to compute the forward scattering of the sun radiations from the rough water surface. Sun glitter does not occur frequently in practice. However, when it does, this phenomenon may have severe effects on the brightness temperature signals measured by spaceborne L- band radiometers.

If an incremental rough sea surface area *dA* located within the MIRAS antenna field of view is illuminated by the sun radiations along the direction of the unit vector $\vec{n}_i$, part of the intercepted energy might be scattered in the direction $\vec{n}_s$, i.e., toward the radiometer antenna. The solar energy scattered by *dA* in the direction $\vec{n}_s$ at time *t* is represented by the radiometric temperatures $T_{ss}(\vec{n}_s, t)$, given for h and v-polarization respectively by:

$$T_{ss}(\vec{n}_s,h,t)=\frac{1}{4\pi\cos\theta_s}\int_0^{2\pi}\int_0^{\beta_{sun}/2}\left[\sigma^o{}_{hh}(\vec{n}_s,\vec{n}_i)+\sigma^o{}_{hv}(\vec{n}_s,\vec{n}_i)\right]T_{sun}(\vec{n}_i,t)d\Omega_i$$

$$T_{ss}(\vec{n}_s,v,t)=\frac{1}{4\pi\cos\theta_s}\int_0^{2\pi}\int_0^{\beta_{sun}/2}\left[\sigma^o{}_{vv}(\vec{n}_s,\vec{n}_i)+\sigma^o{}_{vh}(\vec{n}_s,\vec{n}_i)\right]T_{sun}(\vec{n}_i,t)d\Omega_i \quad (1)$$

where $\sigma^o{}_{hh},\sigma^o{}_{vv},\sigma^o{}_{vh}$ *and* $\sigma^o{}_{hv}$, are the bistatic scattering coefficients of the sea surface at 1.4 GHz for HH, VV, VH and HV polarizations, respectively, at scattered direction $\vec{n}_s$ and incident direction $\vec{n}_i$. The scattering elevation angle is denoted θ_s. The integration limits is over the solid angle subtented by the sun where $\beta_{sun}/2$ is the angular radius of the sun as viewed from the earth. At 1.4 GHz, $\beta_{sun}/2 \approx 0.293°$, which is 10% greater than the optical angular radius [6]. $T_{sun}(\vec{n}_i,t)$ is the brightness temperature of the sun at 1.4 GHz in the direction $\vec{n}_i$ and at time *t*.

Equations (1) show that in order to estimate the contamination due to sunglint temperature at a given SMOS pixel with node corresponding to position *T* on the earth surface, determined by the latitude ϕ and longitude ψ of the observer, and at a given time *t*, the following parameters are needed:

1) $\vec{n}_i$: the direction (incidence and azimuth angles) of sun radiations at the considered earth surface position and time T =(ϕ,ψ,t),

2) $\vec{n}_s$: the direction (incidence and azimuth angles) of observation from MIRAS at target T=(ϕ,ψ,t)

3) $T_{sun}(\vec{n}_i,t)$: the brightness temperature of the sun at 1.4 GHz in the direction $\vec{n}_i$ and at time *t*, and,

4) $\sigma^o{}_{hh},\sigma^o{}_{vv},\sigma^o{}_{vh}$ *and* $\sigma^o{}_{hv}$, : the bistatic scattering coefficients of the sea surface for HH, VV, VH and HV polarizations, respectively, at scattered direction $\vec{n}_s$, incident direction $\vec{n}_i$, and corresponding to the sea state conditions at target T=(ϕ,ψ,t).

Parameters 1) can be obtained from accurate ephemerides and parameters 2) are easily deduced from SMOS observation geometry. The main difficulties in estimating $T_{ss}(\vec{n}_s,t)$ therefore consist in providing accurate estimates for the brightness temperature of the sun at 1.4 GHz and for the sea surface bistatic coefficients at L-band. The brightness temperature of the sun at 1.4 GHz being considered here as an auxiliary parameter, we ony focussed on the physical description of the bistatic coefficients model.

In the present algorithm, the bistatic scattering coefficients of the rough sea surface needed in Equations (1) are estimated using the Small Slope Approximation theory ([7], [8]), which is known to work well from moderate to high incidence angles ($40° \le \theta_i \le 80°$). The lower order-approximation (referred to as the SSA-1) is used here and is appropriate for both large- (the Kirchhoff regime) and small scale (the Bragg regime) roughness within a single theoretical scheme.

The calculation yields the following expression for a dimensionless scattering cross section $\sigma^{o}{}_{\alpha\alpha_o}$ for scattering of the wave of polarization α into the wave of polarization α_o:

$$\sigma^{o}{}_{\alpha\alpha_o}(\vec{n}_s,\vec{n}_i)=\frac{1}{\pi}\left|\frac{2q_k q_i}{q_k+q_i}B_{\alpha\alpha_o}(\vec{n}_s,\vec{n}_i)\right|^2 e^{-(q_k+q_i)^2\rho(0)}\iint\left\{e^{\left[(q_k+q_i)^2\rho(\vec{r})\right]}-1\right\}e^{\left[-i(\vec{n}_s-\vec{n}_i)\bullet\vec{r}\right]}d\vec{r} \quad (2)$$

where (q_k,q_i) represent the vertical projections of the wave vectors and the kernel functions $B_{\alpha\alpha_o}(\vec{n}_s,\vec{n}_i)$ are given in Appendix of [9]. These kernels are geometric functions of the dielectric constant: we used the Klein and Swift's model [10] to estimate the dielectric constant of sea water at L-band.

Here, the function $\rho(\vec{r})$ is defined by the relation:

$$\left\langle\exp\left[iQ(h(\vec{r}_1)-h(\vec{r}_2)\right]\right\rangle=\exp\left[-Q^2\left(\rho(0)-\rho(\vec{r}_1-\vec{r}_2)\right)\right]$$

where <…> means averaging over the space homogeneous statistical ensemble of sea surface roughness, described by the surface elevation signal $h(\vec{r}_1)$, and $Q=q_k+q_i$. For Gaussian statistics ρ represents the correlation function of roughness and can be expressed strictly in terms of a roughness spectrum:

$$\rho(\vec{r})=\int_0^{2\pi}\int_0^{\infty}W(\vec{k})\exp\left[i\,\vec{k}\cdot\vec{r}\right]d\vec{k}$$

where $W(\vec{k})$ is the directional wavenumber spectrum of the rough sea surface at surface wavenumber vector $\vec{k}$.

In the present work, sea surface statistics is assumed Gaussian and ρ is obtained from the sea surface spectrum model of Kudryavtsev al. [11]. In our approach, the calculation of $\sigma^{o}{}_{\alpha\alpha_o}$ is performed using an azimuthal harmonic decomposition for the autocorrelation function. Moreover, to calculate accurately the autocorrelation function, we introduced a sufficiently dense net on the surface wavenumber vector plane within the range $10^{-3}\le k\le 10^{3}$ rad/m, applying a uniform step with respect to *log(k)* rather than to *k*.

4.7.2. Mathematical description

An additional model simplification is used to estimate the amount of solar energy scattered by the sea surface and impinging the MIRAS antenna. We assumed than within the solid angle subtended by the sun as seen from any of the observed terrestrial targets, the local sun direction $\vec{n}_i$ is almost constant, so that, at any target *T*, the radiometric sunglint temperatures $T_{ss}(\vec{n}_s,\alpha)$ of a sunglint Stokes vector component, can be approximated locally at polarization α, by:

$$T_{ss}(\vec{n}_s,t,\alpha)\approx\frac{T_{sun}(t)\,\Omega_{sun}}{4\pi\cos\theta_s}\left[\sigma^{o}{}_{\alpha\alpha}(\vec{n}_s,\vec{n}_i)+\sigma^{o}{}_{\alpha\alpha_o}(\vec{n}_s,\vec{n}_i)\right] \quad (3)$$

where $\vec{n}_s$ and $\vec{n}_i$ are the local MIRAS observation and sun illumination directions at target T, respectively. Ωsun is the solid angle intercepting the sun as seen from the earth, and with $\beta_{sun}/2$ ≈0.293° at 1.4 GHz:

$$\Omega_{sun} = 2\pi\left[1-\cos(\beta_{sun}/2)\right] = 8.2\times10^{-5}\ sr$$

To evaluate $T_{ss}(\vec{n}_s,\alpha)$ using equation (3) at a given earth position and time, one need the following parameters as inputs:

1) $[\theta_i, \phi_i]$ the local sun angles (incidence and azimuth angles) at the considered earth surface position and time, given by T =(ϕ,ψ,t);

2) $[\theta_s, \phi_s]$: the local observation angles (incidence and azimuth angles) from MIRAS antenna at target T=(ϕ,ψ,t)

3) $T_{sun}(t)$: the brightness temperature of the sun at 1.4 GHz and at time *t*,

4) the following ocean surface parameters at target T=(ϕ,ψ,t).:

- ***a)*** the prior sea surface salinity SSS [psu],
- ***b)*** the sea surface temperature SST [°C],
- ***c)*** the wind friction velocity U* [m/s], and,
- ***d)*** the wind direction φ_u [in rad].

Assuming that the main factors influencing the spread and intensity of the sunglint pattern will be the sun brightness temperature, the wind (friction) velocity and direction, we assume for the processor algorithm constant values for SSS=35 psu and for SST=15°C.
The processor shall therefore evaluate mathematically Equation (3), using a LOOK-UP Table for the bistatic scattering coefficients and as inputs :

Input parameters	**Range of values**
Sun incidence angle θ_i [deg]	30°->90°
Relative azimuth angle between sun and MIRAS observation angle ϕ_i - ϕ_s [deg]	0°->180°
MIRAS observation incidence angle θ_s [deg]	0°->90°
Wind friction velocity [m/s]	0->1 m/s
Local 10 meter height wind direction φ_u [deg]	0°->360°

Table I: *Input parameters for computing the sunglint Stokes vector using Eq 3 and bistatic coefficients LUTS*

Comment [JF9]: As well as for galactic noise, I guess an integration over the SMOS antenna beam needs also to be taken into account.
(J. Boutin)

4.7.3. Error budget estimates

Main sources of errors in the estimation of $T_{ss}(\vec{n}_s,\alpha)$ using Eq. (3) will be

- ✓ Errors on the estimation of the bistatic scattering coefficients of the sea surface at L-band, and
- ✓ Errors on the estimation of the sun brightness temperature at 1.4 GHz the SMOS time of acquisition.

An estimates of the errors on the modelling of the bistatic scattering coefficients of the sea surface at L-band can be based on the errors on the asymptotic electromagnetic, namely the SSA-1 approximation. SSA-1 gives qualitatively correct 3D bistatic scattering coefficient when compared to exact numerical simulation using the Method of Moment with a general agreement between SSA-1 and MoM within 3dB in VV and within 1.5 dB in HH polarizations [12]. In average, SSA-1 overestimate HH and underestimates VV so that SSA-1 systematically overestimates the H/V ratio with a mean of order +20%. The errors on the sea surface roughness statistics are difficult to estimate but will clearly have an important impact as well.
A complete error budget estimate can not be provided without any estimate of the error on the auxiliary sun brightness temperature data at 1.4 GHz. If it comes out of L1 processor, we need an error budget on the estimate of that parameter from L1.

4.7.4. Practical consideration

4.7.4.1. Calibration and validation

Dedicated CAL/VAL activities should be envisaged for the SMOS sunglint model with two main components:

-an earth-based campaign aiming at measuring precisely the sunglint scattering at L-band (e.g., experiment similar to [4]), with high-quality concomitant auxiliary solar fluxes measurements at 21 cm as well as surface roughness information to calibrate and validate the bistatic-scattering coefficient models.

-a SMOS-data based analysis. Re-analysis of all flagged pixels and brightnesses for which good quality (close in time and space) co-localized auxiliary wind and solar flux data at 21 cm are available shall be performed to assess the efficiency of the model.

4.7.4.2. Quality control and diagnostics

Assuming the major source of error in the model shall be the estimation of the sun brightness temperature at 1.4 GHz, quality control and diagnostics will strongly depend on the accuracy for that auxiliary data.
If it comes out of L1 processor (without a priori geophysical input), a complementary quality check shall be performed for that auxiliary data using earth-based solar flux measurements available at 1.4 GHz. These are available from sun-tracker radiometers by the US Air Force, at Sagamore Hill(Massachusetts), since 1966. They can be obtained through the National Geophysical Data Center at Boulder, Colorado. These data sets also include other solar fluxes measurements conducted at 1415 MHz since 1988 from radiometers in Palehua (Hawaii), San Vito (Italy) and Learmonth (Australia), and 1GHz data are also collected daily at Nobeyama Radio Observatory (Japan). If high temporal resolution solar fluxes can be obtained, the closest data in time from SMOS acquisitions shall be used to monitor quality controls, as sun brightness temperature values might evolve very significantly over short time scales. The so-called R-components of the sun brightness temperature indeed consist of the second and minute-duration bursts produced by the active sun components: sunspots (manifestations of magnetically disturbed conditions at the sun's visible surface), flares (huge explosions on the surface of the sun) and other transient activity. This high-temporal varaibility of the sun signals might strongly affect the quality of the forward model estimates.

4.7.4.3. Exception handling

If there is no estimation of the sun brightness temperature at 1.4 GHz output from L1 processor (e.g., sun eclipsed by MIRAS), there is a need for other source of that auxiliary data.

4.7.5. Assumption and limitations

First assumption in the model is that within the solid angle subtented by the sun as seen from any of the observed terrestrial targets, the local sun direction $\vec{n}_i$ is almost constant. This is not a strong assumption. However, it is as well assumed that the sun brightness temperature at 1.4 GHz is not polarized and homogeneous within the solar disc. This is known to be unrealistic [2] and certainly will limitate somehow the applicability of the predicted sunglint pattern polarized features.

Another source of limitation is the bistatic coefficient modeling. The SSA-1 approximation is by essence a first-order small slope perturbation approach so that it is not expected to correctly estimate the roughness impact for sea surfaces exhibiting large slopes and most importantly, large curvature. Therefore, is it expected to fail in strong frontal conditions (strong wave-wave, wave-current or wind-wave interaction conditions) and does not account for breaking wave and foam impacts. Moreover, the sea surface state model (i.e. Kudryavtsev et al) is only accounting for wind seas and should be valid only for wind seas generated by winds stronger than about 2 m/s and less than 15 m/s. Out of these limits, it is not expected that the physics of air-sea interaction is correctly accounted for.

Therefore, we do not expect the model to perform well in presence of either strong swells, strong currents, very small and unsteady winds as well as stormy conditions. We expect however that accounting for the impact of waves on the drag coefficients will help better characterizing the impact of these parameters on roughness.

References

[1] S. H. Yueh, R. West, W. J. Wilson, F. K. Li, E. G. Njoku, and Y. Rahmat-Samii, Error sources and feasibility for microwave remote sensing of ocean surface salinity, *IEEE Trans. Geosci. and Remote Sens.*, vol. 39, no. 5, pp. 1049-1060, 2001.

[2] G. A. Duck and D. E. Gary, The sun at 1.4 GHz, *Astron. Astrophys.*, vol. 124, pp. 103-107, 1983.

[3a] N. Reul, WP1500 : support for solar effects in "Retrieval Concept and Architecture Document for Sea Surface Salinity Retrieval for SMOS mission", ref. SMOS-TN-ACR-LOD-001, Issue 1, Revision 2, Dated 17/08/2004. Appendix A (contract CCN-2 of 16027/02/NL/GS)

[3b] B. Picard, N. Reul, P.Waldeufel, and E. Anterrieu, "*Impacts of Solar Radiations on sea surface salinity remote sensing from Synthetic Aperture Imaging Radiometers*", proceeding of IGARRS 2004.

[4] C. T. Swift, Microwave radiometer measurements of the Cape Cod Cannal, Radio Sci., vol. 9, no. 7, pp. 641-653, 1976.

[5] F. Wentz, The forward scattering of microwave solar radiation from a water surface, *Radio Sci.*, vol. 13, no. 1, pp. 131-138, 1978.

[6] J. Aarons*, Solar System Radio Astronomy*. Plenum, 1965.

[7] A. G. Voronovich, Small-slope approximation in wave scattering by rough surfaces, *Sov. Phys.-JETP*, vol. 62, pp. 65-70, 1985.

[8] A. G. Voronovich, Small-slope approximation for electromagnetic wave scattering at a rough interface of two dielectric half-spaces, *Waves in Random Media*, vol. 4, pp. 337-367, 1994.
[9] A. G. Voronovich and V. U. Zavorotny, Theoretical model for scattering of radar signals in ku and c-bands from a rough sea surface with breaking waves,*Waves in Random Media*, vol. 11, pp. 247-269, 2001.
[10] Klein L.A., and C.T. Swift, An improved model for the dielectric constant of sea-water at microwave frequencies, IEEE Trans. Antennas and Propag., AP-25, 1043-111, 1977.
[11] Kudryavtsev V.N., Makin V. K. and Chapron B., Coupled sea surface-atmosphere model. 2. Spectrum of short wind waves, J. Geophys. Res, C4, 7625-7639, 1999.

[12] N Reul, CA Guerin, G. Soriano, E. Bachelier, P. Borderies, F. Mattia, C. Ruiz and N. Floury, "On the Use of Rigorous Microwave Interaction Models to Support Remote Sensing of Natural Surfaces" , ESA contract 17335/03/NL/AG, 2005.

4.8. Moon contamination

This module will not be implemented in a first version of the algorithm, due to being considered a second order effect

4.9. Atmospheric effects

4.9.1. Theoretical description

This section of the ATBD takes advantage of the analysis reported in an ESA study [1: Peichl et al, 2004].

4.9.1.1. Physics of the problem

4.9.1.1.1. The radiative transfer equation

This section assumes a bare surface, and ignore the sky contribution as well as ionospheric effects. The geometrical rotation from the surface to the SMOS antenna is not considered either.

Several components of the atmosphere are radiatively active, which generates effects to be accounted for in the **radiative transfer equation** (RTE).

In the absence of atmosphere, the measured brightness temperature Tb_m is simply the upwelling brightness temperature from the surface Tb_s:

$Tb_m = Tb_s = T_s\, e_s$	(1)

Where

- T_s is the physical surface temperature
- e_s is the surface emissivity

Introducing the atmosphere, the RTE equation is written:

$Tb_m = Tb_s\, e^{-\tau} + Tb_{up} + \boldsymbol{\Gamma}\, Tb_{down}\, e^{-\tau}$	(2a)

Where

- Tb_{up} is the brightness temperature self-emitted by the atmosphere upwards
- Tb_{down} is the brightness temperature self-emitted by the atmosphere downwards
- $\boldsymbol{\Gamma}$ is the surface reflection coefficient, with $\boldsymbol{\Gamma} = 1 - e_s$;
- τ is the equivalent optical thickness of the atmosphere.

Comparing both equations, it is seen that the atmosphere will generate 3 corrective terms, which are best seen when writing equation (2) as follows:

$Tb_m = Tb_s + \mathbf{Tb_s\,(e^{-\tau} - 1)} + \mathbf{Tb_{up}} + \boldsymbol{\Gamma}\, \mathbf{Tb_{down}}\, \mathbf{e^{-\tau}}$	(2b)

There are 4 atmospheric components to be considered: dry atmosphere, water vapor, clouds and rain. Ideally, the quantities to be known in equation (2) (τ , Tb_{up} , Tb_{down}) are the sums of the 4 corresponding contributions.

In every case, the basic quantity from which atmospheric contributions can be estimated is normally the **lineic absorption coefficient κ**, generally expressed in dB/km.

4.9.1.1.2. Dry atmosphere

The radiatively active component in dry atmosphere is **molecular oxygen**.Oxygen molecules have a permanent magnetic moment; therefore absorption and radiation in the microwave region occur due to magnetic interactions with the incidence field. This interaction produces a family of rotation absorption lines in the vicinity of 60GHz (known as the oxygen complex) and an additional isolated line at 118.8GHz [Crane, 1971]. Due to pressure characteristics of the lower part of the Earth's atmosphere, pressure broadening causes the complex of lines to blend together to a continuous absorption band centered around 60GHz.

The oxygen absorption and radiation change due to changes in the meteorological parameters, and are dependent on the pressure P(z) and the temperature T(z) of the gas as a function of the height z.

A model for the absorption by oxygen for lower frequencies is described in [2: Ulaby, 1981]. For frequencies below 45GHz, the contribution from the 118.75GHz oxygen absorption line can be neglected, and thereby we only have the contribution from the 60GHz absorption line. Then the lineic absorption from oxygen at f=1.413 GHz can be written in dB/km as:

$$\kappa_{OX} = 1.110^{-2} f^2 \left(\frac{P}{1013}\right)\left(\frac{300}{T}\right)^2 \gamma\left(\frac{1}{(f-f_0)^2+\gamma^2}+\frac{1}{f^2+\gamma^2}\right) \quad \text{(a3)}$$

where

- f is the frequency (1.413 GHz)
- f_0 is the absorption line frequency (60 GHz)
- P is the pressure in hectoPascal (hPa)
- T is the physical temperature in K
- γ is the line width parameter written in GHz as:

$$\gamma = \gamma_0\left(\frac{P}{1013}\right)\left(\frac{300}{T}\right)^2 \quad \text{(3b)}$$

Where the line width γ_0 is pressure dependent:

γ_0 = 0.59 above 333 hPa, 1.18 below 25 hPa, and varies linearly with P between 333 and 25 hPa

4.9.1.1.3. Water vapor

In the microwave region, water vapor has rotational absorption lines at 22.235 GHz and at 183.31 GHz. Furthermore there are also some absorption lines above this region, which contributes to the microwave absorption spectrum. For calculation of the absorption at L band one can, according to [Ulaby, 1981], group the contributions from the 183.31GHz and all the absorption lines above in a residual term through the use of low frequency approximation. The resulting absorption coefficient κ_{H2O} can then be written as a sum of the contribution from the 22.235 GHz absorption line κ_{22} and a residual term κ_r:

According to [4: Waters, 1976]:

$\kappa_{22} = 2f^2 \rho_v \left(\frac{300}{T}\right)^{5/2} e^{-644/T} \left(\frac{\gamma_1}{(494.4 - f^2)^2 + 4 f^2 \gamma_1^2}\right)$	(4a)

Where

- ρ_v is the water vapor density (gm^{-3})
- γ_1 is the line width parameter (GHz):

$\gamma_1 = 2.85\left(\frac{P}{1013}\right)\left(\frac{300}{T}\right)^{0.626}\left(1 + 0.018\frac{\rho_v T}{P}\right)$	(4b)

Concerning the residual term, according to [2: Ulaby, 1981]:

$\kappa_r = 2.4\,10^{-6} f^2 \rho_v \left(\frac{300}{T}\right)^{3/2} \gamma_1$	(4c)

And finally:

$\kappa_{H2O} = \kappa_{22} + \kappa_r$	(4d)

4.9.1.1.4. Clouds

When electromagnetic radiation interacts with particles such as those in snow, clouds, fog and rain, it involves absorption and scattering. But if only drops, which have a diameter much smaller than the wavelength, are considered – which is the case for 1.4GHz - then scattering is unimportant, and the absorption coefficient can be calculated from the Rayleigh approximation.

The particles are assumed to be randomly distributed within the volume, and therefore the contribution of the individual particles can be summed assuming an incoherent process.

Furthermore, it is also assumed that the particles are spherical, which is a reasonably assumption for most atmospheric water and ice droplets. The scattering and absorption characteristics of a spherical particle are governed by three factors: electromagnetic wavelength, index of refraction, and particle radius.

Clouds are complex phenomena, which consists of water either in liquid or in frozen form. The amount of water and the phase of the water in the cloud depend on the altitude, the temperature and indirectly of the pressure. The clouds are described by cloud base, cloud top, the mass density of the liquid water in the cloud and principal composition of the cloud. The water content of a cloud is according to [Ulaby, 1981] typically less than $1 g/m^3$.

Radiative effects of ice clouds are negligible at L Band. Concerning liquid water clouds, according to [1] and [2], empirical expressions have been developed by [5: Benoit, 1968] for the lineic absorption coefficient. It appears that the only cases where the overall radiative effect at L Band might not be negligible concerns deep cumuli. However there is no reliable auxiliary data allowing select a depth for these clouds. In addition, they are mostly associated with rain events, which are dealt with next.

4.9.1.1.5. Rain

Physically, rain occurrence is similar to clouds. However the problem is complicated by several factors:

- Due to the size of raindrops, the Rayleigh approximation is no longer strictly valid, hence a dependence appears with the granulometry of rain, which is variable and not accurately known;
- Large raindrops are not spherical
- While ice particle do not contribute to atmospheric extinction, there is often a melting zone (just below the 0°C isotherm which is very poorly predicted and may not be negligible in terms of radiative effects
- Finally the rain is often expressed in rainfall intensity, whereas the relevant quantities are lineic densities (liquid water content) in the atmosphere.

For all these reasons, it does not seem practical to correct for rain. According to [1], rain in the atmosphere producing a non negligible radiative contribution when the rain intensity exceeds about 10 mm/hr; this is estimated to happen less than 0.2% of the time over all latitudes, up to less than 0.65% of the time over equatorial areas (these figures may be pessimistic for a 06h local time).

One should also mention the more in depth analysis carried out by Schultz [6].

Formatted: Not Highlight

Therefore rain occurrences are a matter for flagging rather than correcting. As stated above, the heavy clouds should be associated with rain events.

However, there are obviously cases for which rain attenuation effects will be significant. This will deserve further studies, including an attempt to build and a forward model for the rain contribution, an special attention for calibration operations. This is all the more true since rain is a major component of the global water cycle, in which the SMOS mission is expected to bring improved insights.

Formatted: Not Highlight

4.9.1.2. Mathematical description of algorithm

Deleted: *Can we consider this issue closed and then remove the highlights in blue and delete the comment?*¶

4.9.1.2.1. Ratiative transfer for gaseous components

From section 1.1, it is concluded that atmospheric contribution should be computed for oxygen and water vapor.

Numerical simulations show that, for L band, the $Tb_{up} + Tb_{down}$ radiative contributions are extremely close one to each other and can be assumed equal to a single value Tb_{atm} in equation (2). Therefore what is needed is:

$\tau_{atm} = \tau_{O2} + \tau_{H2O}$	(5a)
$Tb_{atm} = Tb_{O2} + Tb_{H2O}$	(5b)

Equations (2a) and (2b) can be written again:

$Tb_m = Tb_s\, e^{-\tau atm} + Tb_{atm}\,(1 + \Gamma\, e^{-\tau atm})$	(5c)
$Tb_m = Tb_s + Tb_s\,(e^{-\tau atm} - 1) + Tb_{atm}\,(1 + \Gamma\, e^{\tau atm})$	(5d)

Contributions to absorption come from the whole thickness of the atmosphere. However, for oxygen it is not necessary to consider altitudes higher than a level ZM ≈ 30 km (TBC), where absorption becomes completely negligible. For water vapor, the altitude range to be considered is limited to ZM ≈ 10 km (TBC).

Over the required altitude range, the exact computation requests knowledge of altitude profiles for T and P; then, the atmosphere is divided in slices δz. For each slice and for each

component, the elementary optical thickness $\delta\boldsymbol{\tau}_G$ (where G is replaced by either O2 or H2O) is computed from the lineic absorption coefficient $\boldsymbol{\kappa}_G$:

$\delta\tau_G = 1 - 1/10^{\kappa_G \, \delta z/10}$	(6a)

The effect of **incidence angle ι** on optical thickness must be introduced in the above equation:

$\delta z(\iota) = \delta z_{NADIR} / \cos(\iota)$	(6b)

The total optical thickness $\boldsymbol{\tau}_G$ is obtained by summing the $\delta\boldsymbol{\tau}_G$ over the relevant altitude range:

$\tau_G = \sum_{Z=0 \to ZM} \delta\tau_G(z)$	(6c)

The radiative contribution Tb_G is (taking the upwelling case) computed as follows:

$BT_G = \sum_{Z=0 \to ZM} T(z)\, \delta\tau_G(z) \exp[- \sum_{Z'=Z \to ZM} \delta\tau_G(z')]$	(6d)

This formulation yields the upwelling oxygen contribution. As mentioned earlier, the downwelling contribution is found very close, with differences well below 0.01K.

Assuming the attenuation through an elementary layer is very small, and that the physical temperature variation at this scale is linear, the estimate for the physical temperature T(z) in (6d) can be taken as the **average** between T values for the bottom and the top of the elementary layer.

4.9.1.2.2. Further simplifications

From equation (5c), it is seen that the 2 quantities linked to atmospheric radiative contributions $\boldsymbol{\tau}_{atm}$ and Tb_{atm} are fixed during the retrieval. Looking at equation (5d), it is seen however that the atmospheric contribution will vary with Tb_s and $\boldsymbol{\Gamma}$; therefore, strictly speaking, this contribution cannot be considered as a fixed additive correction.

The **oxygen** overall contribution is by far the largest atmospheric contribution. It may reach up to 6 K and beyond, is described in [1]. As shown above, after some simplifications, integrations along the vertical still remain necessary in the equations. Three ways are identified to compute $\boldsymbol{\tau}_{O2}$ and Tb_{O2} :

1. Carry out the **integrations** as indicated in equations (6). The necessary altitude range and the necessary number of levels are TBC.
2. **Tabulate** $\boldsymbol{\tau}_{O2}$ and Tb_{O2} as functions of the surface (atmospheric) temperature P0, the surface pressure P0 and some parameter still TBD describing the structure of the temperature profile, and then interpolate from these tables.
3. Build **empirical laws** to compute $\boldsymbol{\tau}_{O2}$ and Tb_{O2}. Actually, the most efficient (and physically meaningful) way to do this consists in writing the oxygen emission as the product of optical thickness by an equivalent layer temperature:

$Tb_{atm} = (T0 + DT_{O2})\, \boldsymbol{\tau}_{O2}$	(7)

Then, empirical laws are needed to compute both optical thickness and the **difference** DT_{O2} between the equivalent layer temperature and the surface temperature. Preliminary tests suggests that this will be achieved fairly easily, except that again a parameter still TBD describing the temperature profile structure and its possible variations is needed.

For **water vapor**, the atmospheric contribution is seldomly significant, only for very moist atmosphere. Hence, although basically the 3 approaches mentioned for O_2 still need be considered, it is expected that it will be possible to characterize water vapor by a single parameter: either the surface value, or the columnar content, and then to process using the empirical law approach. This is TBD.

In order to update this section of the ATBD, what is needed is to perform a series of test based on representative atmospheric profiles concerning temperature and water vapor.

References

[1] M Peichl, V. Wittmann, E Anterrieu, B Picard, N Skou and S. Sobjaerg: Final report: SCIENTIFIC INPUTS FOR THE SMOS LEVEL 1 PROCESSOR DEVELOPMENT, in response to ESA contract No. 10508/02/NL/GS. The section referred to here was written by Skou and Sobjaerg.

[2] Ulaby, Fawwaz T. and Richard K. More and Adrian K. Fung, (1981), "Microwave Remote Sensing – Active and Passive", Artech House Inc. , Vol. 1 & 3

[3] Crane R.K. (1971)."Propagation Phenomena Affecting Satellite Communication Systems Operation in the Centimeter and Millimeter Wavelength Bands", Proceedings of the IEEE, 59, pp 173-188.

[4] *Waters, J. W.* (1976), "Absorption and Emission of Microwave Radiation by Atmospheric Gases", in Methods of Experimental Physics, M.L. Meeks, ed. 12, Part B, Radio Astronomy, Academic Press, Section 2.

[5] *Benoit, A.* (1968) "Signal attenuation Due to Neutral Oxygen and Water Vapor, Rain and Clouds", Microwave Journal, 11, pp. 73-80

[6] *J. Schulz,* in WP1200*:* "Impact of rain on sea surface brightness temperature", Scientific requirements and impact of space observations of ocean salinity for modeling and climate studies, *ESA study 14273/00/NL/DC, 2002, p51-43.*

Formatted: Not Highlight

4.9.1.3. Error budget estimates (sensitivity analysis)

The method selected for computing gazeous radiative contributions has to be selected in such a way that the resulting error on upwelling brightness temperatures due to approximating the effect of physical atmospheric properties (pressure, temperature, water vapor concentration) never exceeds 0.05 K for SMOS operating conditions. It is expected that this goal is compatible with computing power/time requirements.

Then, the major error source will be due to estimates of absorption cross sections, which in turn reflect the uncertainty on spectroscopic measurements. This uncertainty is estimated around 5% .

4.9.2. Practical considerations

4.9.2.1. Calibration and validation

Since the uncertainty on absorption cross sections cannot be overcome, the resulting error will have to be corrected within the overall SMOS validation process. However, the variation with incidence angle offers a possibility to discriminate among other effects.

Assuming one succeeds in determining correctly the absorption cross sections, the resulting uncertainty would be permanently eliminated.

4.9.2.2. Quality control and diagnostics

In case a simplified algorithm is applied (see § 1.2.2), care must be applied, based on considering a representative sample of experimental atmospheric data or analyses, in order to ensure that either tables or empirical laws cover the whole ranges of physical situations.

4.9.3. Assumption and limitations

Assumptions are related to laboratory knowledge of spectral properties of atmospheric gases.

Limitations concern the presence of liquid (cloud or rain) water in the atmosphere, for which a flagging approach is suggested rather than a correction.

4.10. Swell and other unknown effects

This module will not be implemented in a first version of the algorithm, due to being considered a second order effect

4.11. Bias correction

This potential correction at L2 comes from a problem in level 1: A scene dependent bias of a few Kelvin in brightness temperatures has been detected in simulations of SMOS observations and processing (Camps et al., 2005 and also confirmed by other groups). It appears that L1c products may likely not be calibrated according to specifications, and then hamper the determination of absolute ocean salinity. This serious issue has been raised to the SMOS project management, and the following action line has been proposed and accepted:

Deleted: will

An activity will be initiated to first confirm such scene dependant biases, understand its causes, and attempt to correct it at L1. In the event that the L1 correction is insufficient, the L2 SSS team will investigate the possibility of minimizing the impact of such errors, based on a TN - to be provided by the project - describing in detail the source of such scene dependant bias, the limitation of the corrections performed at L1, and any other analysis and /or necessary information needed by a non-instrument cognisant engineer/scientist to understand the problem.

Deleted: The L2 team proposes that the project initiates a

This module of the ATBD describes a correction to be applied at L2 just in case the problem is not solved at L1. It will be behind a switch. Alternative correction schemes are being investigated by the ESLs

4.11.1. Theoretical description

4.11.1.1. Physics of the problem

From Camps et al. (Radio Science, 2005):

"The properties of the brightness temperature images obtained from SEPS exhibit an excellent agreement with the SMOS error budget predictions in terms of radiometric accuracy and sensitivity [Camps et al., 2003c]. However, when comparing these images with respect to the ideal ones (same angular resolution but without noise and instrumental errors), there is often a bias.

Three sources of bias have been identified:

1. Instrumental inaccuracies in the noise injection radiometers (NIRs) used to measure the antenna temperature (average value of the scene). These errors are: thermal noise (DT~0.2 K), offset, and linearity errors. While the offset causes a scene-independent brightness temperature bias, the linearity error causes a brightness temperature error, which is dependent on the antenna temperature corresponding to the scene being imaged. These terms are also temperature-dependent and therefore depend on satellite's argument of the latitude.
2. Inherent difference between the antenna temperature (average value of the brightness temperature of the scene in the unit circle) and the average brightness temperature in the AF-FOV since the AF-FOV does not cover the whole space. This error has been found to be more important in inhomogeneous scenes (e.g., near the coastline).

3. Sun contribution to the antenna temperature. Even though some image reconstruction algorithms include Sun brightness temperature estimators and cancellators such as Camps et al. [2004b], Sun cancellation is never perfect and there is always a residual error which appears as ripples (''tails'' of the quasi-impulse response) and a residual contribution to the antenna temperature.

If the sensitivity of the brightness temperature at nadir to the sea surface salinity is DT/DSSS ~ 0.5 K/psu at 25ºC (even smaller at lower temperatures) and the goal is to achieve an SSS error of 0.1 psu, the absolute accuracy of a real aperture radiometer should be 0.05 K, which is very challenging for any type of radiometer. This level of accuracy is very unlikely in a MIRAS-type of instrument with internal calibration only [Torres et al., 1996; Corbella et al., 1998], and therefore some sort of external calibration must be envisaged.

The use of one or several tie points to match the retrieved brightness temperature does not produce satisfactory results since the radiometric sensitivity of MIRAS is ~2.4 K at boresight, and worsens away from this direction [Camps et al., 2004c]. The proposed external calibration technique relies on the use of ancillary SST and WS data, and SSS estimates to predict the brightness temperature of nadir pixels (0_ incidence angle), for all the snapshot images containing the pixels where the SSS is going to be retrieved. For the whole series of snapshots, the nadir brightness temperatures at both polarizations are added together to form the estimated first Stokes parameter at nadir (^In), and finally the ^In values corresponding to each snapshot are then averaged (I model) to reduce its noise.

The same procedure is followed with the measured data. Finally, the average bias for the set of snapshots used in the retrieval is computed as DI = I data – I model, which is then subtracted from In data, for all image pixels, and for all the snapshots in which the píxel is visible.

The performance of this technique improves with: (1) the number of visible snapshots (N observations) with nadir pixels corresponding to sea, and (2) homogeneous brightness temperature scenes (smaller antenna temperature bias value from second source), which is the case of the ocean. (Nadir land pixels are not considered since their brightness temperature depends on more geophysical parameters and exhibit a much larger variability than in the case of sea.)"

What is proposed here is not a modification of the modelled Tb at surface level (contribution to the forward model) as in most of modules in section 4, but a correction of the measured Tb. That is the salinity retrieval would not be performed from the L1c product as provided by the L1 processor, but from these corrected values.

To take better into account that this Tb bias is scene-dependent, a second approach for the correction has also been proposed by UPC (A. Camps, personal communication). Instead of using a series of consecutive nadir measurements, the averaging is made over all the grid points in a single snapshot. The ocean area included in an AF-FOV is expected to have a bias that we propose to remove by comparing the average of both the instantaneously measured Tb and the modelled Tb (at the corresponding incidence angle) for all the grid points classified as ocean. This technique can be improved by not including in the computation of the average those points lying far from boresight and hence having the maximum noise (the threshold should be defined by a trade-off between number of observations and level of noise).

4.11.1.2. Mathematical description of algorithm

For each snapshot Tb values at antenna reference frame in those grid points that have been marked as "Ocean OK" (no land or sea ice contamination + theoretical radiometric sensitivity below threshold L0) are averaged, either I=Tx+Ty or Tx and Ty separately (and Txy = Tyx in case of full-pol). Tb_mean_data is/are obtained.

The same forward model and auxiliary data to be used in the salinity retrieval are applied to each one of the marked grid points (using climatology for SSS) and its Tb is computed at the incidence angle that corresponds to the specific snapshot considered. Then all the terms for additional contributions are applied (atmospheric, galactic noise …) and resulting Tbs transported to antenna reference frame. All the I=Tx+Ty (alternatively Tx and Ty, or plus Txy if full-pol) of the snapshot are averaged. Tb_mean_model is/are obtained.

Finally the scene dependent bias is computed as DTb = Tb_mean_data – Tb_mean_model, and the measurements for all points changed to I corrected = I_data – DI (alternatively Tx corrected = Tx_data – DTx, Ty corrected = Ty_data – DTy, or even Txy corrected = Txy_data – DTxy = Tyx corrected).

Sequence (for I in dual-pol):

1- After one pair of snapshots (1.2 + 1.2 s) examine all grid points in the AF-FOV
2- Check if they are "Ocean OK"
3- If total number N of "Ocean OK" points is above minimum N0, then continue
4- For each ocean grid point I_data = Tx + Ty measured taken from L1c (detailed description of this equation in module 13)
5- I_mean_data = 1/N Σ I_data (1 to N "Ocean OK" grid points)
6- In parallel, for every "Ocean OK" grid point compute I_model from SST, WS (and if necessary other parameters for roughness description) as provided by the auxiliary data set (same to be used in the retrieval) and SSS provided by climatology, following the complete forward model described in this ATBD (see module 13). The result is I_model at antenna level
7- I_mean_model = 1/N Σ I_model (1 to N "Ocean OK" points)
8- DI = I_mean_data – I_mean_model
9- For every ocean grid point (not only "Ocean OK", but also those above noise threshold) I_data_corrected = I_data – DI
10- Go to next snapshots (pair of Tx and Ty measurements)

Thresholds TBD, e.g. L0 = 4K, N0 = 50 points. (L0 is called Min_Rad_Acc_SBC and N0 is called Min_Num_SBC in the output procut table).

The same procedure applies for A1, A2 and A3 if necessary

Note: this bias correction has to be made using exactly the same options (roughness model, swell correction, etc.) that will be used in the further SSS retrieval

4.11.1.3. Error budget estimates (sensitivity analysis)

The application of this bias correction module does not modify the measurements noise and is expected to reduce significantly the scene-dependent bias. In Camps et al. (2005) the application of the first approach to the bias correction (named there as external calibration) in a simulation for an area of the equatorial Pacific on 4 February 2003 results in a bias correction of about 4 K, that implies a reduction of SSS error from 5.5 psu to less than 1 psu in a swath width of approximately +- 700 km. The second approach has not yet been tested with SEPS.

4.11.2. Practical considerations

4.11.2.1. Calibration and validation

This bias correction will probably not be complete and a second bias removal will be necessary once SSS has been computed. But this is a problem that lies in the cal/val domain, beyond the scope of the L2 processor.

We have to consider that, having used a climatological SSS for the correction, it is likely that an additional small bias can have been introduced to Tb. However, the spatial distribution of SSS (gradients) as measured by SMOS will not be altered, and best values can be recovered through this cal/val second bias removal.

4.11.2.2. Quality control and diagnostics

The scenes that are considered not to have enough "Ocean OK" grid points to proceed with the bias correction, have to be flagged accordingly. The SSS retrieved from these scenes will initially be not reliable, but depending on availability of in situ information a further correction during cal/val can be attempted

4.11.3. Assumption and limitations

This module has to be systematically applied to all scenes that include a significant part of ocean. The definition of "significant" here should come from the minimum number of observations necessary to allow computing the average. My guess is that this number can be low, just enough for an average of noisy data to have sense.

Bibliography

Camps, A., I. Corbella, F. Torres, N. Duffo, and M. Vall-llossera (2003c), SMOS system performance model and error budget, Rep. SO-TN-UPC-PLM-02, Eur. Space Res. and Technol Cent., Noordwijk, Netherlands.

Camps, A., M. Vall-llossera, L. Batres, F. Torres, N. Duffo, and I. Corbella (2005) Retrieving sea surface salinity with multiangular L-band brightness temperatures: Improvement by spatiotemporal averaging. Radio Science, 40, RS2003, doi: 10.1029/2004RS003040

Camps, A., M. Vall-llossera, N. Duffo, M. Zapata, I. Corbella, F. Torres, and V. Barrena (2004b), Sun effects in 2D aperture synthesis radiometry imaging and their cancellation, IEEE Trans. Geosci. Remote Sens., 42(6), 1161–1167.

Camps, A., M. Zapata, I. Corbella, F. Torres, M. Vall-llossera, N. Duffo, C. García, and F. Martín (2004c), SMOS radiometric performance evaluation using SEPS: Evaluation of thermal drifts, paper presented at International Geoscience and Remote Sensing Symposium IGARSS 2004, Inst. of Electr. and Electron. Eng., Anchorage, Alaska.

Corbella, I., F. Torres, A. Camps, and J. Bará (1998), A new calibration technique for interferometric radiometers, Proc. SPIE, 3498, 359–366.

Torres, F., A. Camps, J. Bará, I. Corbella, and R. Ferrero (1996), On-board phase and modulus calibration of large aperture synthesis radiometers: Study applied to MIRAS, IEEE Trans. Geosci. Remote Sens., 34, 1000–1009.

4.12. Transport ground level Tb to antenna level

4.12.1. Theoretical description

4.12.1.1. Physics of the problem

The iterative process to retrieve salinity from SMOS measurements requires comparing the measured data with Tb modeled through the algorithms described in this ATBD. All the different sub-models are describing the processes that contribute to sea surface L-band emission (flat sea, roughness, foam, …), the effects of incoming radiation that need to be added to this emission (sun, moon, cosmic and galactic background, …), plus the modifications to this radiation in its transit through the atmosphere. The result is the modeled value of Tb on top of the atmosphere expressed in the Earth reference frame.

The next step is to transport this Tb to the SMOS antenna reference frame, considering both the change in geometry and the ionospheric effects (Faraday rotation), to allow the comparison with the measured Tb.

4.12.1.2. Mathematical description of the algorithm

With the viewing geometry as defined in ACRI Reqts_L2Draft-2.doc (see figure and annex)

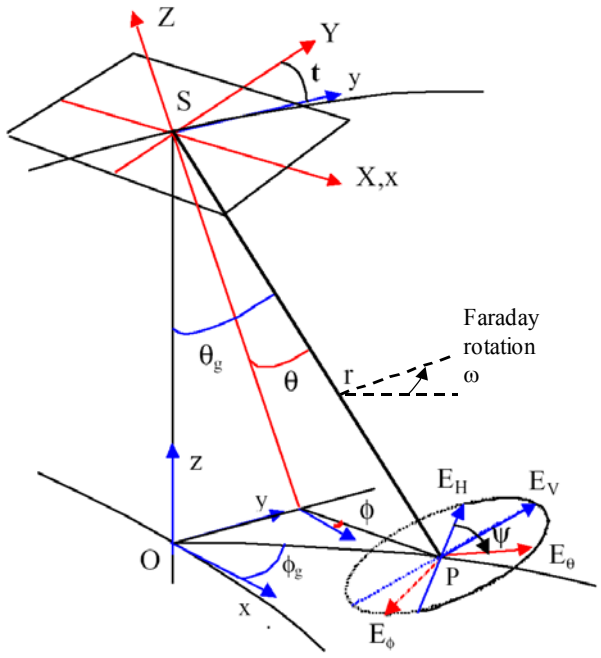

that follows the conventions described in Earth Explorer CFI Software Mission Convention Document (Deimos), we introduce the mathematical expressions for the angles to be used in the transport from ground to antenna reference frames.

for $-\pi/2 \le \phi_g \le \pi/2$:

$$\theta = Arc\cos\left[\sin t \sin\theta_g \sin\phi_g + \cos t \cos\theta_g\right]$$

$$\phi = -Arc\sin\left[\frac{-\sin t \cos\theta_g + \cos t \sin\theta_g \sin\phi_g}{\sin\theta}\right]$$

$$\psi = \pi - Arc\sin\left[\frac{\cos t \sin\theta_g - \sin t \cos\theta_g \sin\phi_g}{\sin\theta}\right]$$

for $\pi/2 \le \phi_g \le 3\pi/2$: ϕ has to be replaced by $\pi - \phi$ and ψ by $\pi - \psi$

We define the rotation angle $\alpha = -\phi - \psi - \omega$, being ω the Faraday rotation angle. Then, following ACRI Reqts_L2Draft-2.doc

Dual polarization mode:

Direct transformation from surface reference frame to antenna reference frame is

$$\begin{bmatrix} A1 \\ A2 \end{bmatrix} = \begin{bmatrix} \cos^2(\alpha) & \sin^2(\alpha) & -\cos(\alpha)\sin(\alpha) \\ \sin^2(\alpha) & \cos^2(\alpha) & \cos(\alpha)\sin(\alpha) \end{bmatrix} \begin{bmatrix} T_H \\ T_V \\ T_3 \end{bmatrix} = [MR2] \begin{bmatrix} T_H \\ T_V \\ T_3 \end{bmatrix}$$

If T3 is assumed to be zero then the equation becomes:

$$\begin{bmatrix} A1 \\ A2 \end{bmatrix} = \begin{bmatrix} \cos^2(\alpha) & \sin^2(\alpha) \\ \sin^2(\alpha) & \cos^2(\alpha) \end{bmatrix} \begin{bmatrix} T_H \\ T_V \end{bmatrix} = [MR2] \begin{bmatrix} T_H \\ T_V \end{bmatrix}$$

There is a singularity problem if $\cos(\alpha) = \sin(\alpha)$, i.e. $\alpha = \pm\pi/4$ or $\pm 3\pi/4$. In such a configuration, A1 = A2 = $(T_H + T_V)/2$ and it is not possible to derive T_H and T_V from A1 and A2.

Full polarization mode:

$$\begin{bmatrix} A1 \\ A2 \\ A3 \\ A4 \end{bmatrix} = \begin{bmatrix} \cos^2(\alpha) & \sin^2(\alpha) & -\cos(\alpha)\sin(\alpha) & 0 \\ \sin^2(\alpha) & \cos^2(\alpha) & \cos(\alpha)\sin(\alpha) & 0 \\ \sin(2\alpha) & -\sin(2\alpha) & \cos(2\alpha) & 0 \\ 0 & 0 & 0 & 1 \end{bmatrix} \begin{bmatrix} T_H \\ T_V \\ T_3 \\ T_4 \end{bmatrix} = [MR4] \begin{bmatrix} T_H \\ T_V \\ T_3 \\ T_4 \end{bmatrix}$$

No singularities appear in this mode.

As it has been shown by simulation studies and experimental data that over the ocean Thv ≈ Tvh ≈ 0, the third Stokes parameter at Earth reference frame is considered also to be 0 at first approximation. . However, theoretical models provide non zero T3 and T4 so we recommend to keep the possibility of taking into account non zero T3, even in dual pol mode. Then the different sub-models provided in this SSS ATBD are valid either for dual-pol or full-pol formulation.

If the first Stokes parameter is used for the iterative retrieval I = A1 + A2 = Th + Tv and there is no need to apply any of the above described transformations.

References

ACRI, Reqts_L2Draft-2c.doc

Camps, A., M. Vall-llossera, N. Duffo, F. Torres, and I. Corbella (2005), Performance of Sea Surface Salinity and Soil Moisture retrieval algorithms with different auxiliary datasets in 2-D L-band aperture synthesis interferomètric radiometers, IEEE Trans. Geosci. Remote Sens., 43(5), May 2005

Claassen, J.P., and A.K. Fung, The Recovery of Polarized Apparent Temperature Distributions of Flat Scenes from Antenna Temperature Measurements, IEEE Transactions on Antennas and Propagation, AP-22 (3), 433-442, 1974.

Waldteufel, P. et Caudal, G. Off-axis Radiometric Measurements; Application to Interferometric Antenna Design. IEEE TGARS, 40, 6, juin 2002, 1435-1439

Waldteufel, P, Floury, N., Dinnat, E., Caudal, G., Ionospheric Effects for L-abnd "-D Interferometric Radiometry, IEEE TGARS, 42, 1, janvier 2004, 105-118

4.13. Sum of contributions

4.13.1. Theoretical description

4.13.1.1. Physics of the problem

This module consists in the addition of all the sub-models used to compute the brightness temperature of a specific ocean grid point at antenna level. Then it includes the forward model for L-band emissivity of a flat sea, plus correction for surface roughness (3 different options are considered by now, that can incorporate additional terms for foam, swell effects or others), the introduction of galactic noise contamination, sun glint and moon contamination, atmospheric effects, and finally transport from ground level to antenna level.

The input to module 13 are the equations provided by modules 1 to 12 and will be applied to those grid points that have been selected as adequate for SSS retrieval in the Decision Tree step.

4.13.1.1.1. Note on first Stokes parameter computation

As information to the rest of modules, we indicate here the detail of the first Stokes parameter (I=Th+Tv=A1+A2) computation from a SMOS measurement snapshot (2.4 s), in fact a pair of two consecutive measurements in orthogonal polarisations:

As A1 and A2 are measured in two consecutive (in case of dual-pol) 1.2 s slots, the incidence angle for a specific grid point is not exactly the same for both, but will differ (in case of dual-pol) in some 0.6º (approx. 8 km displacement at 756 km height). A little bigger in case of full-pol. To build I a correction is needed to have both components shifted to a unique incidence angle. Although this correction is for sure much below the noise of the measurement, and then is not expected to have a very significant impact, it is worth computing it routinely and in a future evaluation of the algorithm check if it is necessary to keep the correction or just bypass it to save computing time.

As the variation of Tb on incidence angle is very similar for the flat sea model or in any roughness parameterisation, the angular correction will be implemented using the flat sea case for simplicity.

Let's assume that for a specific grid point A1 is measured under θx and A2 under θy. We want to shift both measurements to a value that corresponds to the angle that is just in the middle of θx and θy ("mean angle"). The approximation consists in calculating for each polarisation the difference between Tb emitted by a flat sea (computed with SST from the auxiliary data set and SSS from climatology) at the measured angle and at the "mean angle", and add this difference to the actually measured value.

i1) θ_mean=(θx+θy)/2
i2) A1(θ_mean)=A1(θx)-A1_flat(θx)+A1_flat(θ_mean)
i3) A2(θ_mean)=A2(θy)-A2_flat(θy)+A2_flat(θ_mean)
i4) I(θ_mean)=A1(θ_mean)+A2(θ_mean)
where A1 and A2 are provided by L1 and A1_flat and A2_flat are computed using the flat sea model (described in 4.1) with auxiliary SST for the specific grid point and SSS from climatology.

As noise in A1 and A2 is uncorrelated, $\sigma^2 I = \sigma^2 A1 + \sigma^2 A2$

Alternative approach: To avoid the possible introduction of any bias on Tb due to the use of climatological SSS, the interpolation to the mean angle could be done based on accumulated SMOS data versus incidence angle statistics.

Comment [JF10]: Proposed by N. Reul

Third approach: At SRR meeting in ACRI it was proposed to define a 'pseudo Stokes' vector, with the first parameter defined as A1+A2, where A1 and A2 have slightly different geometries, since having been acquired in different instants, and therefore with different incidence angles. However, this parameter might be sensitive to Faraday rotation (TBC).

Comment [JF11]: Definition of pseudo-Stokes (proposed by J.L. Vergely if I am not wrong) should be checked

This issue needs to be clarified A switch should allow selecting one of these options.

4.13.1.1.2. Sum of modules

The iterative method for salinity retrieval requires computing Tb with expected SST, SSS and roughness descriptors values at the adequate incidence angle, correct it for the presence of all envisaged contaminations (galactic, sun, moon and atmospheric), and transport the resulting value to antenna level for comparison with the measured Tb (level 1c) that has been previously corrected for bias. This series of computations will be made following the different sub-models described in sections 4.1 to 4.12 of this ATBD.

When an angular dependence is present, the computations are made for θ_mean.

Comment [C12]: . No, in case we don't use the first Stokes parameter, this is not necessary, we can keep thetax and thetay. In case using the first Stokes parameter, the correction for theta_mean could be done at the end after step 8?

1- Tb_1 = Tb_flat computed with equation described in 4.1
2- Tb_2 = Tb_1 + Tb_rough computed with surface roughness sub-model described in 4.2, 4.3 or 4.4. It is clear that from this step three versions of the Tb exist in parallel
3- Tb_3 = Tb_2 with corrections for foam and/or swell if applicable, following sub-models described in 4.5 and 4.10 (description of these modules includes instructions on applicability, depending on roughness sub-model used and on auxiliary information, e.g. wind speed)
4- Tb_4 = Tb_3 modified for sun glint contamination as described in 4.7
5- Tb_5 = Tb_4 modified for moon contamination as described in 4.8 (if necessary)
6- Tb_6 = Tb_5 modified for reflected galactic noise contamination as described in 4.6, which is attenuated by the atmosphere, when down-welling (described in 4.9).
7- Tb_7 = Tb_6 modified by the reflected down-ward atmospheric emission as described in 4.9.
8- Tb_8= Tb_7 attenuated by the atmosphere (described in 4.9).
9- Tb_9=Tb_8 modified by the atmosphere self emission direct to antenna (described in 4.9).
10- Tb_10 = Tb_9 transported from ground to antenna level as described in 4.12

This Tb_10 is the brightness temperature that has to be included as "Tb mod" in the iterative convergence module (4.14) where it is compared with the "Tb meas" measured by SMOS

We have to indicate that the choice of retrieving SSS using I or using Th and Tv separately does not affect modules 4.1 to 4.11, that are mathematically described using Th and Tv. It is only in step 10 above when either the Tb to be transported is Th+Tv (then equal to A1+A2) or both components are transported separately and then the Faraday rotation has to be taken into account.

4.13.1.2. Mathematical description of algorithm

The Sum of contributions can be expressed mathematically as follows:

Firstly the brightness temperature of the sea at the bottom of the atmosphere is computed. Latter the atmosphere and extraterrestrial sources are applied, and finally the transport from ground to antenna is considered.

The brightness temperature at the ground level (BOA) due to sea surface emission *(at BOA there is also the reflection of atm. signal + galactic signal etc)* is as follows:

$$Tb_{sea} = (Tb_{flat} + Tb_{rough})(1 - F) + Tb_{foam} \qquad [4.13.1]$$

Tb_{flat} is the Tb for a flat sea, as described in module 1 of the ATBD, and Tb_{rough} is the contribution of the roughness of the sea, which is described by 3 different modules in 2, 3 and 4. F is the fraction of sea foam coverage that mainly depends on the wind speed (WS) and is given in module 5. Tb_{foam} is the brightness temperature due to the foam and described also in module 5. If the empirical model is chosen, then F and Tb_{foam} must be set to 0, since the empirical model takes already into account the foam effect. The effect of foam is only appreciable for wind speeds higher than 12 m/s. However, the terms envolving the foam contribution (F and Tb_{foam}) should be applied always, independently from the wind speed value, and it is already considered in the definition of F and Tb_{foam} in module 5.

Then atmosphere and extraterrestrial sources are considered:

$$Tb_{BOA} = Tb_{sea} + Tb_{reflected} = Tb_{sea} + (Tb_{DN}\Gamma + (Tgal\_refl)e^{-\tau_{atm}}) \qquad [4.13.2]$$

where $Tb_{reflected}$ is the radiometric temperature from the sky and atmosphere scattered by the surface, which is the addition of two terms; the downward emitted atmospheric radiation (Tb_{DN}) and the brightness due to extraterrestrial sources. The extraterrestrial sources considered here (Tgal) are the hydrogen line, and the cosmic and galactic contribution, as explained in part 6 of this document. The atmospheric contribution term is multiplied by Γ, that is the reflection coefficient computed by the Fresnel equation. And T_{gal} is multiplied by an attenuation factor due to the atmosphere, since its formulation is at top of the atmosphere.

To compute Tb at top of the atmosphere (without considering Faraday rotation) in the Earth reference frame:

Comment [EL13]: Why not using here for Gamma the real estimation of surface reflectivity from combined flat+rough emissivity models ? (N. Reul)

Comment [JF14]: Tb_{DN} does not speak to me: There is a need to adjust notations with atmospheric part but maybe BTatm is not a good choice; I would prefer Tbatm for the Tb coming from atm. emission. (J. Boutin)

Deleted: Tb_{glint} is the contribution of the sun glint and it is defined in module 7.

$$Tb_{TOA}^{EARTH} = Tb_{BOA}\, e^{-\tau_{atm}} + Tb_{UP} \qquad [4.14.3]$$

where Tb_{UP} is the atmospheric self emission direct to the antenna (but computed at TOA and with Earth reference frame) and $e^{-\tau_{atm}}$ is the attenuation produced by the atmosphere. Section 4.9 specifies that Tb_{UP} and Tb_{DN} are very close, and considered equal to Tbatm, which is defined in that section..

Comment [JF15]: After discussion at PDR: we have to decide whether we consider TOA below ionosphere or at satellite level

Finally to compute this temperature at the antenna reference frame, the geometrical transformation and the ionospheric effect should be considered, following module 12, as:

$$Tb^{ANTENNA} = [MR4] \cdot Tb_{TOA}^{EARTH} \qquad [4.13.4]$$

where MR4 is the matrix that describes the geometrical transformation plus the Faraday rotation

4.13.1.3. Error budget estimates (sensitivity analysis)

The addition of the different modules implies an analysis of the impact of the individual errors on the overall error budget. This was planned in the ESL proposal as WP2600 and expected to be finished by the end of the study.

4.13.2. Practical considerations

4.13.2.1. Calibration and validation

The validation of this module can be done by running some tests cases with exactly the same configuration (in terms of sub-models switched on and use of auxiliary data) with the summation module used in the SRS study and the equivalent used by UPC from SEPS, to check that the result is the same

4.13.2.2. Quality control and diagnostics

The range of validity of this module comes from the intersection of the corresponding ranges for all sub-models.

4.13.3. Assumption and limitations

The module has to be applied to all grid points selected as good for salinity retrieval at the Decision tree.

4.14. Iterative Scheme

4.14.1. Theoretical description

4.14.1.1. Physics of the problem

The iterative method Levenberg and Marquard is choosen to use in the inverse algorithm. This method was already implemented in the simulator for soil moisture study and gives very similar results to the [*Jackson*, 1972] method used in SR1600. The mathematical problem is described below in detail.

Set of measurements are brightness temperatures Tb_i^{meas} observed for a single pixel at different incidence angles, θ_i. These data need to be fitted into a direct model to find the solution of the parameters.

$$T_b^{\mathrm{mod}} = f(\theta, SSS, SST, P_{rough})$$

where P_{rough} is a vector that includes the parameters used in each model to describe the sea roughness.

This implies minimization of the following cost function :

$$\chi^2 = \sum_{i=0}^{Nm-1} \frac{\left[T_{b\,i}^{\ meas} - T_{bi}^{\mathrm{mod}}(\theta, P)\right]^2}{\sigma_{T_{bi}}^{\ 2}} + \sum_{j=0}^{Np-1} \frac{\left[P_j - P_j^{\ prior}\right]^2}{\sigma_{P_j}^{\ 2}} \qquad [4.14.1]$$

Being P_j, the j parameters that influence the T_b: SSS, SST, WS, and depending on the cases, also significant wave height Hs, wind direction ϕ, wave-age Ω, and TEC parameter in case of not using first stoke, etc.

$P_{j\ prior}$ is a value of that parameter known a priori to the measurements, and known with an uncertainty σ_{Pj} (Waldfteufel, 2003, Gabarró, 2004). θ_i is the incidence angle of measurements from nadir.

Some experiments seem to advise not using SSS as one of the parameters P_j, as the retrieved value tends to the a priori value. A way of avoiding this is by setting the uncertainty of SSS as a high value (i.e. σ_{SSS}=99999), to not consider this term in practice.

Note: As mentioned in section 4.4 the empirical model that describes the Tb due to sea roughness is linearly dependent on the incidence angle. Then it is only possible to retrieve two roughness parameters for each polarisation. In the case of using H and V polarisation independently, the maximum number of retrieved is 4. If the first Stokes is used, then only 2 parameters can be retrieved.

Deleted: c

Comment [EL16]: Might be u* should be used as THE wind roughness retrieval parameter as it is used as imput by the three forward models NR

We tried it with the empirical model and gave worst results than WS JF

Formatted: Font: (Default) TimesNewRoman, Do not check spelling or grammar, Lowered by 21 pt

Comment [C17]: It may be dangerous to minimize over all the parameters entering in the f() function; for the 2-scale model part, I propose to minimize on the components of WS in neutral atmosphere (that includes information of u* + influence of wind direction), on SSS and on SST. It is better to consider wind components instead of wind speed as wind components errors better satisfy the gaussian condition contrary to the WS parameter JB

4.14.1.2. Mathematical description of algorithm

Mathematically the above equation can be written as follows:

$$\chi^2 = (T_b^{meas} - T_b^{\mathrm{mod}}(\theta, \overrightarrow{P_j}))^T C_{T_B}^{-1} (T_b^{meas} - T_b^{\mathrm{mod}}(\theta, \overrightarrow{P_j})) + (P_j^{prior} - P_j)^T C_{P_j}^{-1} (P_j^{prior} - P_j) \quad [4.14.2]$$

Where the T_b^{meas} are the N_m observations performed at different incidence angles, ^{T} represents the transposition operation, and C_{Tb} is the variance/covariance matrix for T_b. The diagonals of this matrix are the radiometric sensitivity of T_b measurements. Off diagonal elements are 0 in the antenna frame.

P_j are different parameters that should be retrieved, P_j^{prior} are the a priori knowledge of the parameters (obtained from models or satellites, the auxiliary information), and C_{Pj} is the variance/covariance matrix of these parameters. The diagonal of the matrix are the uncertainties on the a priori parameters.

Finally the above equation can be expressed as follows:

$$\chi^2 = (X - X\,\mathrm{mod})^T C_z^{-1} (X - X\,\mathrm{mod}) \quad [4.14.3]$$

Where C_Z matrix is built by aligning along the main diagonal the matrixes C_{Tb} and $C_{Pj;}$ the vector X has a Nm+Np length and consists on:

$$X = \begin{pmatrix} T_b(1) \\ T_b(2) \\ \ldots\ldots \\ T_b(Nm) \\ P_{prior}(1) \\ p_{prior}(2) \\ \ldots\ldots \\ p_{prior}(Np) \end{pmatrix} \quad [4.14.4]$$

Where P_{prior} is the a priori information of the parameter; X_mod has the same length as X and is defined as:

$$X\_\mathrm{mod} = \begin{pmatrix} T_b^{\mathrm{mod}}(1,p) \\ T_b^{\mathrm{mod}}(2,p) \\ ..... \\ T_b^{\mathrm{mod}}(Nm,p) \\ p(1) \\ p(2) \\ ..... \\ p(Np) \end{pmatrix} \qquad [4.14.5]$$

Where P is the parameter to be retrieved that will change at each iteration. It is the first guess value at the first iteration.

Let's call *a* to the vector of Np parameters to be retrieved (for example a= [SSS, SST, WS, Hs, Ω]).

Sufficiently close to the minimum the cost function is approximated by a quadratic form:

$$\chi^2(a) = \gamma - d \cdot a + \frac{1}{2} \cdot a \cdot D \cdot a \qquad [4.14.6]$$

Then jumping from current trial parameters a_{cur} (equal to a first guess value for step 0) to a minimizing one a_{min} is done by the inverse Hessian method:

$$a_{\min} = a_{cur} + D^{-1} \cdot \left[-\nabla\chi^2(a_{cur}) \right] \qquad [4.14.7]$$

But if the minimum functions couldn't be approximated by a quadratic form, a *steepest decent method* has to be used:

$$a_{next} = a_{cur} + constant \nabla\chi^2(a_{cur}) \qquad [4.14.8]$$

The gradient (d) and the Hessian (D) of χ^2 need to be calculated:

$$d = \frac{\partial\chi^2}{\partial a_k} \qquad D = \frac{\partial^2\chi^2}{\partial a_k \partial a_l} \qquad [4.14.9]$$

Let,

$$\alpha_{kl} = \frac{1}{2} D \qquad \beta_k = -\frac{1}{2} d \qquad [4.14.10]$$

The *inverse Hessian method* can then be written as:

$$\sum_{i=0}^{Nm-1} \alpha_{kl} \delta a_l = \beta_K \qquad [4.14.11]$$

And the *steepest decent method* can be rewritten as:

$$\delta a_k = constant \times \beta_k \qquad [4.14.12]$$

With $\delta a = a_{min} - a_{cur}$ or $\delta a = a_{next} - a_{cur}$ and $k \in [0:Np-1]$

The Levenberg & Marquardt method put forth a method for varying smoothly between the extremes of the *Inverse-Hessian method* and the *steepest decent method* using a factor λ.
This factor will replace the constant term in the *steepest descent method:*

$$\delta a_k = \frac{1}{\lambda \alpha_{kk}} \beta_k \quad with \quad k \in [0 : Np-1] \qquad [4.14.13]$$

and then if we define a new matrix α', by the following prescription:

$$\begin{cases} \alpha'_{jj} = \alpha_{jj}(1+\lambda) \\ \alpha'_{jk} = \alpha_{jk} \quad (j \neq k) \end{cases} \qquad [4.14.14]$$

the two methods can be expressed as:

$$\sum_{i=0}^{Nm-1} \alpha'_{kl} \, \delta a_l = \beta_K \qquad [4.14.15]$$

When λ is very large, the matrix α' is forced into being diagonally dominant, so method is like *steepest descent method* and as λ approaches 0 method is like *Hessian gradient method*.

Given an initial guess for the set of fitted parameters *a*, the iterative method consists of:

1 Compute $\chi^2(a)$.
2 Select an initial modest value for λini, say λini = 0.001.
3 Solve the linear equations for δa and evaluate $\chi^2(a+\delta a)$.
4 If $\chi^2(a+\delta a) \geq \chi^2(a)$, increase λ by a factor Kd and go back to 3.
5 If $\chi^2(a+\delta a) < \chi^2(a)$, decrease λ by a factor Kd, update the trial solution a=a+δa and go back to 3.

This iteration loop is stopped when χ^2 is decreased with respect the previous iteration by less than a *threshold* δ_χ as an absolute value. It can be considered as a first approach to be: $\delta_\chi = 10e^{-5}$ (Press, 1986; Marquardt 1963). (See also 'Retrieval Concept and Architecture for Sea Surface Salinity Retrieval for SMOS Mission' document from the CNN2 of contract

Deleted: 10
Deleted: 10
Deleted: *threshold*
Formatted: Subscript

16027/02/NL/GS). This threshold should be easy modifiable and should be calibrated once the satellite will be flying.

Also the step at the first iteration, this is, λ_{ini}, can be adjusted to better values, to optimize the computing time. By default it will be set to 0.001.

Deleted: the first value of

The maximum number of iterations allowed to the system is jt_max, and should be also modifiable. It could be changed once the computing time for each grid point will be better known. By default Nmax can be set to 20.

Deleted: N_{max}

The first guesses of each parameter need to be adjusted. It is proposed to use for the first guess of salinity a fixed value of 35. For the other parameters the first guess could be the a priory value + 10%. TBC

Comment [C18]: I don't understand why is the first guess not equal to the a priory value?. JB

Once the acceptable minimum has been found, then λ should be set to 0, and compute the covariance matrix as:

$$[C] = [\alpha]^{-1}$$

However, in some circumstances, the estimation can "get stuck," and as a result, we would see a very large value of the loss function. Therefore a FLAG should be raised to inform that the inversion is probably incorrect.

No boundaries will be applied in the inversion process, therefore the retrieved parameters should be considered as effective values, since, they could result in physically impossible values (i.e. negative wind speeds).

4.14.1.3. Error budget estimates (sensitivity analysis)

The algorithm will iterate until χ^2 decrease less than a threshold between two consecutive iterations. Another reason to stop the iterative process is if the number of iterations is higher than an Nmax which is previously defined.

Therefore it is impossible to obtain better results if any of the two conditions described above have been accomplished.

4.14.2. Practical considerations

4.14.2.1. Calibration and validation

The adjustments to be done to the model once it is working with real values, as it is explained in 4.14.1.2, will have to do with:

- first value of λ_{ini};
- threshold δ_{χ};
- maximum number of iterations it_max.

Formatted: Subscript
Deleted: Nmax
Formatted: Not Superscript/ Subscript

The validation of the retrieved SSS may also consider the quality of the retrieved auxiliary parameters adjusted during the minimization process.

4.14.2.2. Quality control and diagnostics

If convergence is not achieved after it_max iterations, this is, if once it_max iterations are performed, the condition $\chi_{i+1}^2-\chi_i^2 < \delta_{\chi}$ is not true, then a FLAG should be raised, and the parameters given by the algorithms should be the value obtained in the last iteration. TBC

Deleted: N_{max}
Deleted: N_{max}
Deleted: *threshold*

4.14.3. Assumption and limitations

Assumptions:

- We are assuming that all the measurement errors are Gaussian and that all the parameters follow a Gaussian distribution.

Limitations:

- If the number of observations of a pixel (observed with different incidence angles) is less than Nm_{min} (could be set to 10), then the inversion process cannot be performed. This is because with not enough measures, the inversion process could lead to retrieved values with an unacceptable precision.

Bibliography

Gabarró, C., Vall-llossera, M., Font, J., and Camps, A. (2004b). Determination of Sea Surface Salinity and Wind Speed by L-band Microwave Radiometry from a fixed Platform. Internation Journal of Remote Sensing, 25(1):111–128.

Marquardt, D. (1963). An algorithm for least-squares estimation of non-linear parameters. Journal on Applied mathematics, 11(2):431–441.

Press, W, Teukolsky, S., Vetterling, W., Fannery, B. (1986) Numerical Recipes. Ed: Cambridge University press.

Waldteufel, P, Boutin, J., Kerr, Y. (2003) Selecting an optimal configuration for the Soil Moisture and Ocean Salinity mission. Radio Science, Vol. 38, No. 3, 8051, doi:10.1029/2002RS002744.

4.15. Brightness temperature at surface level

One of the outputs of the SMOS SSS L2 processor has to be to provide, for each grid point, the set of brightness temperatures measured by MIRAS that have been used to compute salinity. But, unlike in L1c product, these have to be values at surface level (not antenna level) that can be used for example for assimilation in general circulation models.

In this module we will describe how these values have to be computed, essentially by reversing the transformation described in module 4.12 and applying the atmospheric corrections described in 4.9.

To be completed

5. Secondary algorithm description

5.1. Theoretical description

5.1.1. Physics of the problem

In the context of developing SSS inversion methodologies from the SMOS brightness temperature data, both iterative and neural networks retrieval algorithms have been studied and their performance evaluated. In [1] and [2], both inversion methods (iterative and neural) have been evaluated with respect to their robustness to noise/biases on (i) the measured brightness temperatures, (ii) the needed auxiliary geophysical parameters and (iii) to inaccuracies in the forward models.

For both inversion methodologies, it was shown that the noise on measured brightness temperatures, if it is conform to what currently expected, seems not to be an issue. This is not the case for a bias on the measured brightness temperatures that will provide a strong retrieval error using both methodologies.

The sensitivity of inversion accuracy to auxiliary parameters (sea surface temperature, wind speed, surface roughness, a priori values for the salinity) reveal that both methods are very sensitive to the accuracy of the auxiliary parameters. It is especially true for an iterative method, in which, the search of the minimum of the cost function is constrained inside an interval of width equal to plus and minus a given standard deviation for each auxiliary parameter around first guess values. If these auxiliary parameters are known with an accuracy equal or better than 1°C, 1psu and 2 m/s for SST, SSS and wind speed, respectively, the salinity error should match the Level 2 processor requirements. But if it is not the case (for example in regions with strong SSS, SST and wind variability), the iterative inversion is too much constrained by these first guesses. The neural inversion seems to be less sensitive to these auxiliary parameters: they are used in the calculation of the retrieved salinity but do not define a domain for the search of the solution.

To provide an estimation of the impact of the imperfections in the direct models, measured brightness temperatures were simulated and inverted with two different emissivity models, which were nevertheless very close (same dielectric constant for sea water, same wave spectrum for roughness corrections). The retrieval accuracy was found to be strongly reduced for both methods revealing a clear impact of the forward model on the retrieved SSS accuracy.

Therefore, if one consider the complete error budget of the salinity retrieval including errors in the measured brightness temperatures, errors in forward emissivity models, errors in the inversion methods and errors in the auxiliary parameters, it is clear that a secondary, purely empirical, inversion algorithm (which do not need a direct surface emissivity model), shall provide a useful added-value salinity product, at least at the beginning of the mission to help

tuning the forward surface emissivity models. A Neural Network (NN) formulation is particularly adapted to the development of such algorithms.

The two major difficulties in implementing a neural network inversion algorithm for SMOS are

1) the definition of **the network topology**, since the number of incidence angles and their values varies with pixel's distance to the ground track, and are different for the same pixel in different overflights. Therefore, it should be expected to define and train as many neural networks as independent pixels are in a swath width, with the added difficulty of training neural networks with noisy data at the swath edges.

2) The generation of geophysical databases. The choice for generating a learning database to train the NN is known to be crucial in the development of a neural inversion algorithm. Whereas in the iterative method no major off-line component is identified (leaving aside external calibration), in the NN a major off-line component is necessary with the data used to build **the learning basis** and the software necessary to train the networks. Two other important off line geophysical databases are needed to develop the algorithm: first, a validation database to control the quality of the algorithm and the capacity of generalization during the learning phase, and, second a testing and independent database to evaluate the performances of the algorithm where it has not learnt.

Concerning the network topology, it is not clear that NN can handle incidence angle dependant fractions in retrieval as provided in SMOS Level 1C data. Incidence angle coverage of Tb must be therefore interpolated/averaged to categories to be defined and NN will be developed for each category. These categories will certainly be dependent on the dwell line position of the considered input brightness data (probably a few tens).

The geophysical databases required to estimate the statistical relationship between the SSS and the SMOS Tb's at surface level will be built during the commissioning phase with collocated in-situ SSS and surface Tb's estimated from SMOS measurements (i.e., corrected for atmospheric and ionospheric effects), as well as "all" possible sets of other pertinent geophysical parameters.

Both the NN topology and the geophysical databases are not yet defined, therefore only the interface for a neural network algorithm is defined here in order to populate this net at a later date.

5.1.2. Mathematical description of the algorithm

The algorithm shall use as inputs multi-angular brightness temperature data at the surface level ,i.e, Level 1C data corrected for atmospheric and ionospheric contributions. The mathematical implementation of the Neural Network inversion algorithm, as it is anticipated now, will consist in three main processing steps:

1) A data preprocessing step to provide adapted inputs to the NN algorithm. Multi-angular brightness temperature data at the surface level will be categorized as function of their incidence angle coverage and/or corresponding pixel dwell line positions (categories still to be defined). The incidence angle coverage of Tb's will be therefore interpolated/averaged to these categories.

2) An internal decision tree. Assuming there will be several neural networks developed for each identified input data category (based on input data dwell line position and/or incidence angle coverage), the decision tree shall determine which sub-Neural Network will be used for retrieving SSS from those data.

3) An output processing step to deliver SSS from a final expression given by the combination of the transfer function with weights and biases corresponding to the neural network selected by the decision tree.

Inputs to the algorithm shall be:

1) SMOS brightness temperatures at the surface level,i.e., corrected for atmospheric, ionospheric and galactic contributions, in H and V polarization if the instrument is operated in dual mode or the full-stokes data in full polarimetric mode.

2) Category definitions of SMOS brightness temperatures at the surface level used in the data preprocessing and decision tree,

3) Auxiliary sea surface temperature, wind speed module at 10 meter height and a priori SSS estimate,

4) Lookup table of coefficients (biases and weights in the network) for all sub-networks corresponding to a given input data category.

There will be one Lookup table of coefficients (biases and weights) for each sub-network, corresponding to each data category.

Ecah sub-neural network is defined by the number of layers, the number of neurons for each layer and the transfer function associated to each neuron.

There are n inputs: the categorized multi-angle brightness temperatures at surface level and one output the salinity and its associated error. The information goes forward in one of the developed network from the inputs X to the output Y. All the information between two neurons is quantified by a weight W.

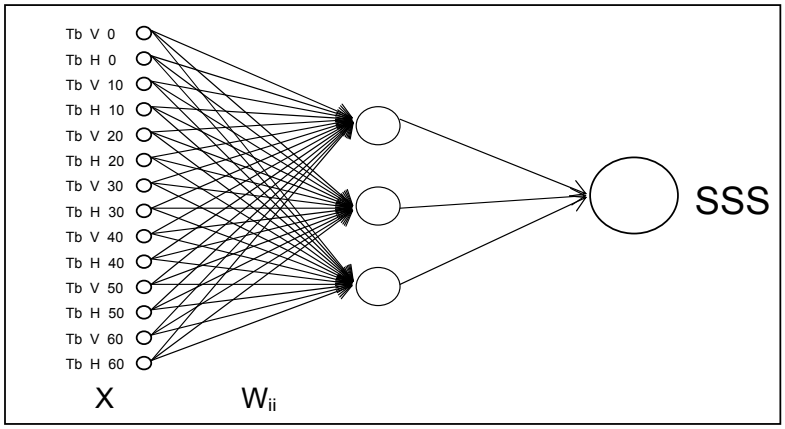

Fig: *Example of a network with one single layer of 3 neurons and 14 inputs*

For one given neuron i, its output Si is expressed by :

$$S_i = f\left(\sum_{j=1}^{p} W_{ij} S_j - W_{i0}\right)$$

Where

- Sj are the contributions of the p other neurons in the previous layer
- Wij is the weight between neuron i and neuron j
- Wi0 is the bias of neuron i
- f is the transfer function associated to the neuron.

The transfer function that will be used is the sigmoid function:

$$f(x) = \frac{\exp(x) - 1}{\exp(x) + 1}$$

It is the function generally used for neural networks because it has good properties : it is a symmetric function bounded between -1 and 1.
There is no mathematical rule to fix the number of neurons. However, the number of neurons is linked to the number of samples in the database since the number of weights and biases has to be proportional to the amount of data used to train the network. The determination of the adapted architecture is done in an empirical way, testing for various architectures.

The network output has a final expression given by the combination of the transfer function with weights and biases :

$$Y = \sum_{i=1}^{n} W_i . f_i\left(\sum_{j=1}^{p} W_{ij} X_j + W_{i0}\right) + W_0$$

5.1.3. Error budget estimates (sensitivity analysis)

Testing Database	Neural Network	
	Bias	Stdev
Tbs without noise Auxiliary parameters with noise (1 psu, 1°C, 2m/s)	-0.29	0.52
Tbs without noise (θ) Auxiliary parameters with noise (1psu,1°C,2m/s)	-0.29	0.56
Tbs with a bias of 1K Auxiliary parameters with noise (1 psu,1°C,2m/s)	-0.70	0.50
Tbs with noise (θ) Auxiliary parameters perfectly known	-0.27	0.44
Tbs with noise (θ) Auxiliary parameters with noise (2 psu, 2°C, 4m/s)	-0.34	0.84
Tbs with noise (θ) Independent auxiliary parameters	-0.24	0.47
Tbs simulated with the SSA model with noise (θ) Auxiliary parameters with noise (1 psu, 1°C, 2m/s)	-0.27	0.54

Table 1. In each tested configurations bias and standard deviation (psu) between retrieved and reference salinity.

Table 1 summarizes results (bias and standard deviation on retrieved SSS) obtained in [2] from different tested configurations for SSS retrieval from neural Networks. For these tests, SMOS Tb's were simulated through a forward model. In almost all simulated cases, the standard deviation error on retrieved salinity is lower than 0.9 psu with the neural inversion.. The neural inversion has the advantage to be much less sensitive to a priori values for auxiliary data than an iterative method. It is also less sensitive to the noise and to a possible bias on the brightness temperatures. Nevertheless, the results obtained with the neural algorithm are not perfect. In particular, the behavior of the algorithm for low and high salinity that results in a systematic slope, can be greatly improved.

While these results are indicative of expected retriveal errors using Neural Networks, it is still difficult to provide at that step of processor development a correct error budget. Indded, the network that be used later will be based on real SMOS data and real in situ SSS, which shall provide quite different functionnal relationship than the one predicted by a forward emissivity model.

5.2. Practical considerations

5.2.1. Calibration and validation

The performance of the global empirical salinity neural network algorithm will evaluated by comparing *in situ* SSS salinity with retrieved salinity. The correlation between algorithm results and in situ data, limited with regression coefficients, will allow adjustments to be done to the Neural network biases and weigths for classified SMOS brightness temperature categories.

Therefore, we will have to perform a post launch adjustment of the coefficients for salinity parameter retrieval. Salinity validation will be performed over selected test sites for different sea surface conditions (cold, warm, high and low winds, rainy, wind seas, wind seas+swell, frontal area) to assess the accuracy of the algorithm under different salinity conditions. Test sites associated with the salinity classes will be selected where in situ information is most readily available (e.g., ARGO float locations).

5.2.2. Quality control and diagnostics

The first step in quality control will be visual examination of the salinity products products to ensure that the SMOSs are consistent with our understanding of climate, and no gross errors are being made. We will further compare retrieved. We will utilize the kriging process ([3],[4]) to construct statistical relationships from the widely scattered in situ SSS measurements. We will continue comparing ocean model generated salinities of a basin and sub-basin with estimates derived from the algorithm. We will also compare SMOS with Aquarius derived salinities (if available) for comparison. When a particular assumption is found to be deficient (e.g. category choice for incidence angle coverage, network toipology), we will employ a better procedure to correct the problem.

Diagnostic checks for out-of-range data or unreasonable results will be used in the algorithms to determine whether the output should be flagged as unacceptable. Some diagnostic checks may trigger alternative decision tests in the algorithm. An example of such diagnostics is determination of salinity at the sea-ice border or under strong rainfalls. The retrieval algorithms are not expected to be reliable in these conditions, but they may be used with appropriate adjustments. A diagnostic test may determine, for example, the amount of rain in a pixel scene, and based on that determination we can proceed with the salinity decision tests or mark the data as ’salinity under rain”.

5.2.3. Exception handling

Occasional missing pixel data or missing lines of data may be worked around by flagging that missing data and proceeding with the algorithm, carrying that missing data flag through to the output data set. In cases where input data files are unavailable but necessary for completing intermediate calculations, the algorithm should not proceed until those data are available.

Numeric errors and out-of-range values are errors that may arise from equations in the algorithm. Numeric errors will be handled by flagging them, i.e., filling with a code value and continuing with processing the rest of the data set. Intermediate calculations will probably be checked for out-of-range values and filled with a code value if out-of-range values are detected.
If sunglint or sea ice is present for an entire sub-cycle period (3 days) over a pixel or group of pixels, no usable salinity data could be generated and that will be indicated on the SMOS products.

Other predicted exceptions are as follows:
(a) Abnormal program termination: Unless the program termination code is set to normal termination, the appropriate error message will be sent to the operator. This will require immediate corrective action as needed.
(b) Files not found: The program will terminate and the appropriate error message will be sent to the operator.
(c) Fatal computation error: This will result in an abnormal termination.
(d) Non-fatal computation error: Warning messages will be sent to the operator who will decide whether to halt the processing or continue the processing until the problem can be resolved.

References

[1] Zanifé, O. Z., Reul, N., Chapron, B., Obligis, E., Boone, C., Labroue, S., Sagen, H. and Evensen, G., "*SMOS Salinity Data Processing Study*", ESA contract 15165/01/NL/SF, 2001.

[2] Camps, A., Font, J., Gabarró, C., Miranda, J., Obligis, E., Labroue, S., Boone, C., Sabia, R., Vall-llosera, M., Reul, N., Technical report WP1100: A review on practical issues for SSS retrieval, ESA contract 4505/03/NL/Cb, 2004.

[3] Matheron, G., The theory of regionalized variables and its applications. Techn. Rep. Fascicule 5, Les cahiers du centre de morphologie Mathématique de Fontainebleau, Ecole supérieure des Mines, Paris, 1971.

[4] Servain J., Gohin F., and A. Muzellec, Wind fields at the surface determined from combined ship and satellite altimeter data, J. Atmos. Oceanic. Technol., 10,6, 880-886, 1993.

6. Output Product

Two L2 Salinity Output files will be provided for each SMOS half orbit: a User Data Product (UDP), including information to be distributed to all users, and a Data Analysis Report (DAR), with auxiliary information on data processing for specific users working on algorithms improvement and products validation. Both files have a unique Headers section plus a series of Binary fields (one per ESEA grid point, maximum 82257)

User Data Product

- Headers

FH: Fixed Header

MPH: Main Product Header — Same fields as in L1C

SPH: Specific Product Header

- Product_Location
- Quality_Information_Of_L1C_Input_Data
- Input_Data_Information — L1C, ECMWF, DGG, Galaxy map, land_sea mask, time correlation model, configuration files
- List_Of_DataRecord_Description count=2+3xNumber_Of_Retrieval_Schemes
- L2_Product_Location — Boundaries, centres, Sub-satellite points
- User_Data_Product_Quality_Summary

- Binary fields of UDP (three SSS retrievals)

GPILB: Grid Points Info List Binary

GPD: Grid Point Data — includes land/sea/ice flags

IGP: Input Geophysical Parameters — Input geophysical parameters at grid point, derived from ECMWF and auxiliary data map)

List_of_Retrieval_Schemes count=3 — **Number of retrieval schemes / SSS in a L2 product is still TBD**

RRB: Retrieval Results Binary

- UDD: User Data Descriptor
  - Flags — Configuration of retrieval scheme
  - Descriptors
  - Initial_Conditions — Prior, uncertainty on prior and first guess (optional) of SSS, SST and param1 to 4
- CDD: Confidence Data Descriptor
- PSD: Process Status Descriptor

RRB: Retrieval Results Binary

RRB: Retrieval Results Binary

Data Analysis Report

- Headers

FH: Fixed Header

MPH: Main Product Header Same fields as in L1C and UDP MPH

SPH: Specific Product Header

- Binary fields of DAR (three SSS retrievals)

Formatted: Bullets and Numbering

GPILB: Grid Points Info List Binary

GPD: Grid Point Data Same as in UDP

M1: Measurement 1 Data on measurement basis, shared by all forward models (e.g. atmosphere, L2 flags on measurements) or from L1C (angles, flags of L1C)

Mn: Measurement n=Nb_InputMeas_valid+Nb_InputMeas_invalid

List_of_Retrieval_Schemes count=3

RAR: Retrieval Analysis Report Binary

RAR: Retrieval Analysis Report Binary

RAR: Retrieval Analysis Report Binary

Formatted: Font: 12 pt

Formatted: Heading 2

Sizing:

Table below gives estimates of product sizes assuming UDP includes three SSS values.

	Typical	Maximum
Number of grid points in Sea	44912	82257
Number of measurements	$3.93\ 10^6$	$7.20\ 10^6$
UDP	**22.3Mb**	**40.8Mb**
DAR	**1.44Gb**	**2.63Gb**

Mb: 10^6 bytes
Gb: 10^9 bytes

A detailed list and description of the different fields included in these two files is now under revision and will be provided in ATBD issue 1

7. ANNEX: AUXILIARY DATA PROCESSING

See attached file Annex7_ATBD-AGDP_v1.pdf

Formatted: Heading 1

8. ANNEX: SMOS L1c product requirements for sea surface salinity retrieval at level 2

This note describes the needs of L2 prototype processors in terms of brightness temperature, radiometric uncertainty, geometry of observations and synthetic antenna pattern.
Section 0 gives definitions of all quantities needed by L2 prototype processor. Section 0 gives a textual description of L2 processor needs for Sea Surface Salinity and Soil Moisture retrievals. Section 0 reports the current understanding of L1 product content and details our proposal for interfacing L1 and L2 processing. Section 0 addresses other operation modes like the strip adaptive processing.

Definitions

Reference frames

Satellite reference frame

The Satellite reference frame is defined in section 5.2.1 of Earth Explorer CFI Software Mission Convention Document[1]: "*The Zs axis points along the radial satellite direction vector, positive from the centre of the TOD reference frame towards the satellite, the Ys axis points along the transversal direction vector within the osculating orbital plane (i.e the plane defined by the position and velocity vectors of the satellite), orthogonal to the Zs axis and opposed to the direction of the orbital motion of the satellite. The Xs axis points towards the out-of-plane direction vector completing the right hand reference frame.*" Figure 3 of Earth Explorer CFI Software Mission Convention Document is reproduced below for clarity:

Deleted: 0
Deleted: 0
Deleted: 0
Deleted: 0
Deleted: 0
Deleted: 0
Deleted: 0
Deleted: 0
Formatted: Normal, Indent: Left: 0 cm, First line: 0 cm, Tabs: Not at 0.63 cm
Formatted: Font: 14 pt, Underline, English (U.K.)
Formatted: English (U.K.)
Formatted
Formatted: Font: 14 pt, English (U.K.)
Formatted: Normal, Indent: First line: 1.25 cm
Formatted: Font: 14 pt, No underline
Formatted: English (U.K.)

[1] ESA ref CS-MA-DMS-GS-001 version 1.3 dated 15-07-2003.

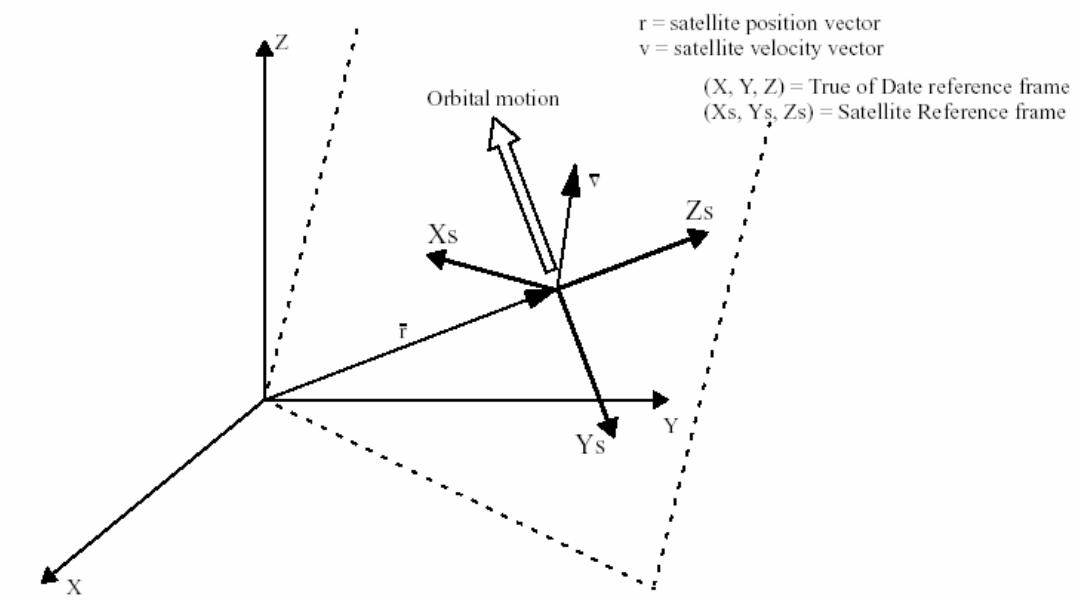

Figure 2: The Satellite Reference Frame as defined in EE CFI Mission Conventions Document

Antenna reference frame

The antenna reference frame is a satellite relative reference frame, as defined in section 5.2.2 of Earth Explorer CFI Software Mission Convention Document. The antenna reference frame is obtained by rotating the Satellite Reference Frame by two rotations because no rotation around –Ys is necessary, i.e. (Xs,Ys,Zs) = (X^1s,Y^1s,Z^1s). First rotation is around -X^1s, with a pitch angle $\xi>0$ equal to the antenna tilt angle. The second rotation around Z^2s (i.e the rotated Z^1s axis) over a yaw angle $\zeta=\pi$, so that the angle between the orbital motion vector and Y's axis is the tilt angle.

In the antenna frame, the director cosines are often used. They are defined by

$$\xi = \sin(\theta)\cos(\varphi) \qquad \eta = \sin(\theta)\sin(\varphi) \qquad \text{Eq. 1}$$

where θ is the angle between the light of sight and –Z's. φ is the azimuth of the line of sight in the antenna reference frame, with $\varphi=0$ for the X's axis and $\varphi=\pi/2$ for the Y's axis.

Target reference frame

At surface level, topocentric[2] reference frames are adopted, where the line of sight hit the Earth's surface.

From antenna reference frame to target reference frame

Reference frames adopted in this note are depicted in . The antenna reference frame is noted (S,X,Y,Z) instead of (X's,Y's,Y's).

Formatted: Font: 14 pt, English (U.K.)
Formatted: Normal, Indent: First line: 1.25 cm
Formatted: Normal, Indent: First line: 1.25 cm
Formatted: Font: 14 pt, English (U.K.)
Formatted: Font: 14 pt
Formatted: English (U.K.)
Formatted: Normal
Formatted: Font: 14 pt, English (U.K.)
Formatted: Font: 14 pt

[2] See section 5.1.7 of Earth Explorer CFI Software Mission Convention Document

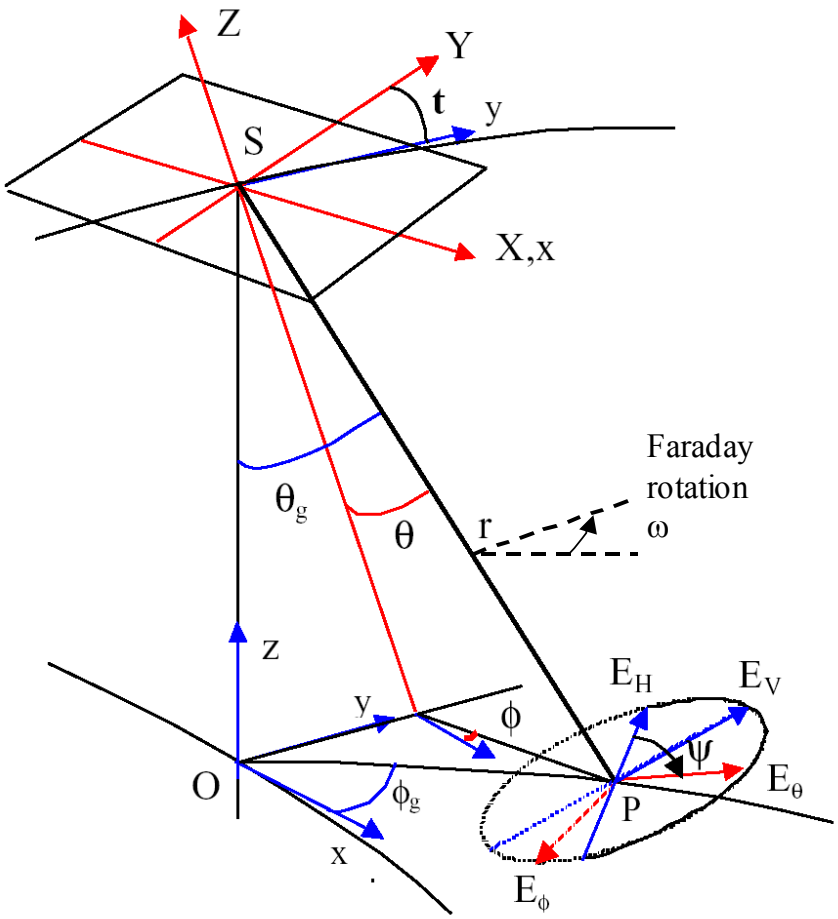

Figure 3: Definition of viewing geometry

In the surface reference frame, the horizontal (H) polarization direction is perpendicular to the incidence plan and is the product of two unit vectors that are collinear with $\overrightarrow{PS}$ and $\overrightarrow{OP}$ directions. The vertical (V) polarization direction is perpendicular to both $\overrightarrow{PS}$ and the H polarization direction.

In the antenna reference frame, the X polarization direction is along X=X's axis and the Y polarization direction is defined by the Y=Y's axis.

To link directions of polarization at surface and at antenna levels, two angles ψ and ϕ are considered, together with an intermediary angle θ. For $-\pi/2 \leq \phi_g \leq \pi/2$:

$$\theta = Arc\cos\left[\sin t \sin\theta_g \sin\phi_g + \cos t \cos\theta_g\right] \qquad \text{Eq. 2}$$

$$\phi = -Arc\sin\left[\frac{-\sin t \cos\theta_g + \cos t \sin\theta_g \sin\phi_g}{\sin\theta}\right] \qquad \text{Eq. 3}$$

$$\psi = \pi - Arc\sin\left[\frac{\cos t \sin\theta_g - \sin t \cos\theta_g \sin\phi_g}{\sin\theta}\right] \qquad \text{Eq. 4}$$

If $\pi/2 \leq \phi_s \leq 3\pi/2$, and give $\pi-\phi$ and $\pi-\psi$ respectively, instead of ϕ and ψ. It is worth noting that for ϕ and ψ rotation angles are define along the SP direction (toward the Earth), positive counterclockwise.

Faraday rotation

If the antenna looking toward the Earth sees a fully polarized electromagnetic waves propagating from the surface, the polarization directions rotate while the electromagnetic waves cross the ionosphere because the medium contains free electrons and is under the influence of Earth magnetic field[3]. The rotation angle is:

$$\omega = \text{constant} \int_{\text{surface}}^{\text{satellite}} N(l) B_{//}(l) dl \qquad \text{Eq. 5}$$

where N is the electron number density and $B_{||}$ is the component of the magnetic field parallel to the propagation direction. From the antenna reference frame, ω angle is positive counterclockwise.

Brightness temperatures

Brightness temperatures in the antenna frame in X and Y polarization directions are noted A1 and A2, instead of T_X ad T_Y respectively. This convention avoids confusion in full polarization mode: Stokes parameters 3 and 4 at the antenna level are noted A3 and A4 (A like Antenna), whereas they are noted T_3 and T_4 at surface level.

Dual polarization mode

Direct transformation from surface reference frame to antenna reference frame is as follows:

$$\begin{bmatrix} A1 \\ A2 \end{bmatrix} = \begin{bmatrix} \cos^2(a) & \sin^2(a) \\ \sin^2(a) & \cos^2(a) \end{bmatrix} \begin{bmatrix} T_H \\ T_V \end{bmatrix} = [MR2] \begin{bmatrix} T_H \\ T_V \end{bmatrix} \qquad \text{Eq. 6}$$

where[4]

$a = -\omega - \phi - \psi$There is a singularity problem if $\cos(a) = \sin(a)$, i.e. $a = \pm \pi/4$ or $\pm 3\pi/4$. In such a configuration, A1 = A2 = $(T_H + T_V)/2$ and it is not possible to derive T_H and T_V from A1 and A2.

Full polarization mode

$$\begin{bmatrix} A1 \\ A2 \\ A3 \\ A4 \end{bmatrix} = \begin{bmatrix} \cos^2(a) & \sin^2(a) & -\cos(a)\sin(a) & 0 \\ \sin^2(a) & \cos^2(a) & \cos(a)\sin(a) & 0 \\ \sin(2a) & -\sin(2a) & \cos(2a) & 0 \\ 0 & 0 & 0 & 1 \end{bmatrix} \begin{bmatrix} T_H \\ T_V \\ T_3 \\ T_4 \end{bmatrix} = [MR4] \begin{bmatrix} T_H \\ T_V \\ T_3 \\ T_4 \end{bmatrix} \qquad \text{Eq. 7}$$

No singularities appear in this mode. T_3 and T_4 are expected to be equal to 0. If Faraday rotation is not removed (ω =0), T_3 becomes different of 0. T_4 is always equal to 0.

[3] See http://farside.ph.utexas.edu/teaching/jk1/lectures/node60.html for details.
[4] Signs of this sum are TBC because they depend on sign conventions.

Formatted: Normal, Indent: First line: 1.25 cm
Formatted: English (U.K.)
Formatted
Formatted: English (U.K.)
Formatted: Normal
Formatted: English (U.K.)
Formatted
Formatted: English (U.K.)
Formatted: Normal

Radiometric uncertainty

Formatted: English (U.K.)
Formatted
Formatted: Normal

The most adequate reference although not complete is:
Camps A., Corbella I., Bara J and Torres F.: Radiometric sensitivity computation in aperture synthesis radiometry, IEEE trans. Geosci. Rem Sens., 36, pp 680-685, March 1998
Radiometric uncertainty gives the amplitude of radiometric noise in K. It is derived from the total scene temperature, the system temperature and is a function of viewing direction according to the average LICEF receiver gain. It depends on the integration time and the receiver bandwidth as well as other parameters of the receiving channels.

$$\sigma_T \approx G \frac{\sqrt{3}}{2} d^2 \frac{(T_{sys} + T_{scene})}{\sqrt{(B \tau_{eff})}} \alpha_W f_{rd} \sqrt{N_V}$$ Eq. 8

- G is the gain of the antenna element. Expressed linearly (rather than in dB): G ≈ 7.2 **TBC** — Formatted: Bullets and Numbering
- d is the spacing ratio: d = (distance between elements) / wavelength; d = 0.875
- T_{sys} is the system temperature (K); T_{sys} ≈ 215K, for a 2.4 dB noise figure
- T_{scene} is the scene temperature (K)
- B is the equivalent receiving bandwidth in Hz; B ≈ 19 10^6 Hz
- τ_{eff} is the effective integration time for a given polarization: $\tau_{eff} = \tau / c_{eff}$, where τ is the actual integration time. In the dual pol mode τ is always equal to 1.2s. In full pol mode, for the four Stokes components, the 4 τ values alternate between (1.2, 0.4, 0.4, 0.4) and (0.4, 1.2, 0.4, 0.4) (see Martin Neira, M., Polarimetric mode of MIRAS, *IEEE Transactions on Geoscience and Remote Sensing*, *40*, 1755-1768, 2002) **TBC**. The coefficient c_{eff} accounts for the 1 bit correlation (dominant factor 2.46), for oversampling (factor 0.74) and for the hermiticity of the cross visibilities hv and vh : c_{eff} ≈ 1.81 for Tv and Th, c_{eff} ≈ 1.81/2 for the third and fourth Stokes parameters.
- α_W is a coefficient which accounts for integration over the apodization window. For a rectangular window, α_W = 1; for an exact Blackman window, α_W ≈ 0.452 in the SMOS case. for Kaiser window with parameter = 13, α_W ≈ 0.365 **TBC**
- f_{rd} is a factor to account for redundant visibilities: f_{rd} ≈ 0.82 **TBC**
- N_V is the total number of visibility samples: $N_V = 6 N_{EL}^2 + 6 N_{EL} + 1$, where N_{EL} is the number of elements per arm. In the SMOS case, N_{EL} = 23 and sqrt(N_V) = 52.7

In full polarimetric mode, T_{scene} is taken equal to 0.

The 2 or 4 σ_T values computed using the radiometric sensitivity equation yield the radiometric sensitivity on **boresight**.
It makes sense to request one separate value per Stokes parameter, as changes are expected in antenna gains and in scene temperatures.
When applying the visibility equation, it is seen that reconstructed Tb are weighted by the inverse product of element directional gains: $GV_k(\theta,\phi)\, GV^*_l(\theta,\phi)$, where GV are **voltage** directional gains. Similarly, the std on the Tb must be corrected. In this case however, it is not necessary to account for differences between elements, and an average directional pattern is all that is needed.

With $\overline{G}(\theta,\phi)$ the average LICEF receiver directional **power** gain function, normalized so that max(G) = 1 on boresight, the radiometric uncertainty on brightness temperature AP in polarization direction P=1, 2, 3 or 4 is given by:

$$\sigma_{AP(\theta,\phi)} = \sigma_T / \overline{G}(\theta,\phi) \qquad \text{Eq. 9}$$

Therefore the map of $\overline{G}(\theta,\phi)$ is needed for L2 processing. This is a static map. It can be expressed either in polar coordinates in the antenna frame, or conveniently in the director cosines, provided they are part of the L1 output.

For brightness temperatures at surface level, the radiometric uncertainties on T_H and T_V are given by:

$$\begin{bmatrix} \sigma^2_{T_H} & \mathrm{cov}(T_H,T_V) \\ \mathrm{cov}(T_H,T_V) & \sigma^2_{T_V} \end{bmatrix} = \left([MR2]^{-1}\right)^T \begin{bmatrix} \sigma^2_{A1} & 0 \\ 0 & \sigma^2_{A2} \end{bmatrix} [MR2]^{-1} \qquad \text{Eq. 10}$$

The matrix described by σ^2_{TH} and σ^2_{TV} is the variance/covariance matrix of brightness temperatures in surface reference frame and $([MR2]^{-1})^T$, the transposed matrix of $[MR2]^{-1}$. The variance/covariance matrix carries the radiometric uncertainties associated with T_H and T_V on its diagonal and the correlation coefficient between T_H and T_V (covariance) on the non-diagonal terms. The non-diagonal terms are equal. While *A1* and *A2* are mainly uncorrelated (ignoring correlations due to common channels), T_H and T_V are strongly correlated because they are derived from *A1* and *A2* through linear relationships.
In case MR2 is singular, σ_{T_H} and σ_{T_V} tend towards infinity;
$\mathrm{cov}(T_H,T_V)$ tends towards: $-\sigma_{T_H}\sigma_{T_V}$

In full polarimetric mode, no singularity is expected at the ground level.

$$\begin{bmatrix} \sigma^2_{T_H} & \mathrm{cov}(T_H,T_V) & \mathrm{cov}(T_H,T_3) & \mathrm{cov}(T_H,T_4) \\ \mathrm{cov}(T_H,T_V) & \sigma^2_{T_V} & \mathrm{cov}(T_V,T_3) & \mathrm{cov}(T_V,T_4) \\ \mathrm{cov}(T_H,T_3) & \mathrm{cov}(T_V,T_3) & \sigma^2_{T_3} & \mathrm{cov}(T_3,T_4) \\ \mathrm{cov}(T_H,T_4) & \mathrm{cov}(T_V,T_4) & \mathrm{cov}(T_3,T_4) & \sigma^2_{T_4} \end{bmatrix} = \left([MR4]^{-1}\right)^T \begin{bmatrix} \sigma^2_{A1} & 0 & 0 & 0 \\ 0 & \sigma^2_{A2} & 0 & 0 \\ 0 & 0 & \sigma^2_{A3} & 0 \\ 0 & 0 & 0 & \sigma^2_{A4} \end{bmatrix} [MR4]^{-1} \qquad \text{Eq. 11}$$

Synthetic antenna pattern

Formatted: English (U.K.)
Formatted
Formatted: Normal

Function S gives the synthetic antenna pattern as a function of (ξ,η) that are small variations around the viewing direction (ξ_0,η_0) in the director cosine frame[5]:

$$S(\xi,\eta) = \frac{\sqrt{3}}{2} d^2 \sum_{l=1}^{L} \sum_{c=1}^{C} W \exp\left[-\pi W_r^2 (U\xi + V\eta)^2\right] \exp\left[j2\pi(U(\xi-\xi_0)+V(\eta-\eta_0))\right] \qquad \text{Eq. 12}$$

Where:

- $U(l,c)$ and $V(l,c)$ are coordinates of visibilities.
- ξ_0 and η_0 are director cosines of viewing direction.

Formatted: Bullets and Numbering

[5] This is equation C.3 page 218 of SEPS ADDD v4.1 ref SO-TN-GMV-PLM-003 dated 18-12-2003. In SEPS documentation, the synthetic antenna pattern is called equivalent array factor.

- d is the spacing ratio: distance between LICEF receivers in wavelength (d=0.875)
- $j = \sqrt{-1}$
- $W_r = \frac{B_{\min}}{f_0}$ with $B_{\min}$ is receiver bandwidth and f_0 is the receiver center frequency (1413.5MHz)
- W is the apodization function computed where coordinates of visibilities are provided.

The weighting function to be applied at surface level is derived from S(ξ,η) after geometrical transformations:

- from (ξ_0+ξ,η_0+η) frame to (θ,φ) frame according to .
- from (θ,φ) frame to (longitude, latitude) using Earth Explorer CFI.
- Introducing the smearing effect along the track.

Formatted: Bullets and Numbering

Needs for L2 prototype processing

Formatted: Heading 2, Indent: Left: 0 cm, First line: 0 cm, Tabs: Not at 0.63 cm

Formatted: Font: 14 pt

Formatted: Normal

For sea surface salinity retrieval

Formatted: Font: 14 pt, English (U.K.)

The final report (ref SMOS-TN-ACR-LOD-006 v1 dated 21-03-2005) of the sea surface salinity retrieval study (contract 16027/02/NL/GS) recommends that the TEC is a constrained parameter in the iterative process. This means that Faraday rotation shall not be corrected at level 1 processing.

The SSS L2 processor needs brightness temperature in the antenna reference frame (A1 and A2 for dual pol; A1, A2, A3 and A4 for full pol), along with radiometric uncertainties (σ_{A1} and σ_{A2}, for dual pol; σ_{A1}, σ_{A2}, σ_{A3} and σ_{A4} for full pol), and one angle, $(\phi + \psi)$, which depends on observation geometry. These needs are compliant with SMOS product definition baseline (see page 9 of SO-TN-ESA-GS-1250, v1.3 dated 28-01-2005).

The Faraday rotation angle ω will be computed and adjusted during level 2 processing. This angle depends on the geomagnetic field and the Total Electronic Content (TEC) of the ionosphere[6]. The TEC data will be used to compute the initial guess for Faraday rotation angle.

The SSS L2 processor needs all orbital data necessary to use the Earth Explorer CFI software. All requirements in terms of geometry (angles) shall be covered by EE CFI software.

The SSS L2 processor needs a way to compute the weighting function to be applied at surface level for estimating land or ice contamination for flagging and possibly account for them.

The SSS L2 processor takes in charge surface reflected terms such as galactic background or Sun glint, but not their possible side effects due to the reconstruction process.

Formatted: Normal

For soil moisture retrieval

Formatted: Font: 14 pt, English (U.K.)

To be completed by ARRAY.

Interface with L1 processing

Formatted: Heading 2, Indent: Left: 0 cm, First line: 0 cm, Tabs: Not at 0.63 cm

Formatted: Normal

Understanding of L1c products

Formatted: Font: 14 pt, English (U.K.)

[6] See Appendix A of SEPS ADDDv4.1, ref SO-TN-GMV-PLM-0003 dated 18-12-2003.

Our understanding of the content of L1C products, based on

- SMOS L1 Processor Input/Output Definition ref. SO-IS-DME-L1PP-014 v2.1 dated 22-02-05
- SMOS L1 Product Format Specification ref. SO-IS-DME-L1PP-0002 v1.1 dated 22-02-05
- SMOS L1 Auxiliary Data Specification Format ref. SO-IS-DME-L1PP-0003 v1.1 dated 22-02-05

is that they include

- T_H and T_V[7] + eventually U and V
- all information to compute $(\phi + \psi)$ using Earth Explorer CFI,[8]
- Geomagnetic field [9] and TEC[10] data in auxiliary data products.
- Apodization function[11]

The L1c products do not suit the needs on L2 processors. Radiometric uncertainties are not provided. For sea surface salinity retrieval, correction of Faraday rotation is not needed.

Proposed interface with SSS prototype processor

For sea surface retrieval, it is proposed that the L1c products include in dual polarization:

- A1 and A2
- σ_{A1} and σ_{A2}

and for full polarization:

- A1, A2, A3 and A4
- σ_{A1}, σ_{A2}, σ_{A3} and σ_{A4}

For each set of brightness temperature reconstructed for one element of the SMOS grid:

- A reference to the apodization function used during reconstruction.
- Acquisition time
- Integration time (for smearing effects).

For sea surface retrieval, it is proposed that the L1c auxiliary products include:

- Synthetic antenna patterns S (see), tabulated for $|\xi|<2/7$ and $|\eta|<2/7$ (TBC[12]) and sampling is TBD. Each Synthetic antenna pattern table is referenced and the reference number is found in the L1c product. This referencing is used in case the apodization function changes or the strip adaptive approach is adopted (see section 0).
- Orbit information (see inputs of Earth Explorer CFI).
- The SMOS fixed grid (ISEA grid).

Extension to other operating modes

Strip-adaptive processing

[7] See Table 26 of SO-IS-DME-L1PP-0002 page 69.
[8] See Table 25 of SO-IS-DME-L1PP-0002 page 65.
[9] TBD, see section 4.16 of SO-IS-DME-L1PP-0003 page 45.
[10] TBD, see section 4.15 of SO-IS-DME-L1PP-0003 page 44.
[11] TBD, see section 4.17 of SO-IS-DME-L1PP-0003 page 45.
[12] In first approximation, with a spacecraft at 700km altitude, to cover an area 200km around the target, we have $\sin(\theta-\theta_0)<200/700$ at nadir. Knowing that φ ranges from 0 to 2π, indicates that the condition is $|\xi|<2/7$ and $|\eta|<2/7$.

Formatted: Bullets and Numbering
Formatted: Bullets and Numbering
Formatted: Normal, Indent: First line: 1.25 cm
Formatted: Font: 14 pt, English (U.K.)
Formatted: Font: 14 pt
Formatted: English (U.K.)
Formatted: Bullets and Numbering
Formatted: Bullets and Numbering
Formatted: Bullets and Numbering
Formatted: Bullets and Numbering
Deleted: 0
Deleted: 0
Formatted: Normal, Indent: Left: 0 cm, First line: 0 cm, Tabs: Not at 0.63 cm
Formatted: Font: 14 pt, English (U.K.)
Formatted: Font: 14 pt
Formatted: English (U.K.)
Formatted: English (U.K.)
Formatted: English (U.K.)

The strip-adaptive processing, also known as equi-pixel processing, uses different apodization functions in the reconstruction process in order to minimize distortions of SMOS footprints. This means that the Synthetic antenna pattern S is not unique. It is proposed that L1 processing provides a series of Synthetic antenna pattern S, referenced by a number, and that this reference number is included in the L1c product. The number of Synthetic antenna functions S is estimated to be less than several thousands.

Formatted: Heading 1

9. ANNEX: TABLE OF VARIABLES

to be written

Deleted: ¶

Deleted: ----------Page Break----------

ANNEX: SMOS L1c product requirements for sea surface salinity retrieval at level 2¶

¶

This note describes the needs of L2 prototype processors in terms of brightness temperature, radiometric uncertainty, geometry of observations and synthetic antenna pattern.¶

Section 0 gives definitions of all quantities needed by L2 prototype processor. Section 0 gives a textual description of L2 processor needs for Sea Surface Salinity and Soil Moisture retrievals. Section 0 reports the current understanding of L1 product content and details our proposal for interfacing L1 and L2 processing. Section 0 addresses other operation modes like the strip adaptive processing.¶

Definitions¶

Reference frames¶

Satellite reference frame¶

The Satellite reference frame is defined in section 5.2.1 of Earth Explorer CFI Software Mission Convention Document[13]: "*The Zs axis points along the radial satellite direction vector, positive from the centre of the TOD reference frame towards the satellite, the Ys axis points along the transversal direction vector within the osculating orbital plane (i.e the plane defined by the position and velocity vectors of the satellite), orthogonal to the Zs axis and opposed to the direction of the orbital motion of the satellite. The Xs axis points towards the out-of-plane direction vector completing the right hand reference frame.*" Figure 3 of Earth Explorer CFI Software Mission Convention Document is reproduced below for clarity:¶

... [50]

Formatted: Heading 1, Tabs: 0.63 cm, List tab

Page 96: [1] Formatted	**Caro**	**03/10/2005 17:13:00**

Font: 12 pt

Page 96: [2] Formatted	**Caro**	**03/10/2005 17:13:00**

Heading 2, None

Page 96: [3] Change	**Caro**	**03/10/2005 16:36:00**

Formatted Bullets and Numbering

Page 96: [4] Formatted	**Caro**	**03/10/2005 17:23:00**

Font: 10 pt, Bold

Page 96: [5] Formatted	**Caro**	**03/10/2005 17:23:00**

None

Page 96: [6] Formatted	**Caro**	**03/10/2005 17:23:00**

Font: 10 pt, Bold

Page 96: [7] Formatted	**Caro**	**03/10/2005 17:23:00**

None

Page 96: [8] Formatted	**Caro**	**03/10/2005 17:23:00**

Font: 10 pt, Bold

Page 96: [9] Formatted	**Caro**	**03/10/2005 17:23:00**

None

Page 96: [10] Formatted	**Caro**	**03/10/2005 17:24:00**

Font: 10 pt

Page 96: [11] Formatted	**Caro**	**03/10/2005 17:24:00**

None

Page 96: [12] Formatted	**Caro**	**03/10/2005 17:24:00**

Font: 10 pt

Page 96: [13] Formatted	**Caro**	**03/10/2005 17:24:00**

None

Page 96: [14] Formatted	**Caro**	**03/10/2005 17:24:00**

Font: 10 pt

Page 96: [15] Formatted	**Caro**	**03/10/2005 17:24:00**

None

Page 96: [16] Formatted	**Caro**	**03/10/2005 17:24:00**

Font: 10 pt

Page 96: [17] Formatted	**Caro**	**03/10/2005 17:24:00**

None

Page 96: [18] Formatted	**Caro**	**03/10/2005 17:24:00**

Font: 10 pt

Page 96: [19] Formatted	**Caro**	**03/10/2005 17:24:00**

None

Page 96: [20] Formatted	**Caro**	**03/10/2005 17:25:00**

Font: 10 pt

Page 96: [21] Formatted	**Caro**	**03/10/2005 17:25:00**

None

Page 96: [22] Change	**Caro**	**03/10/2005 16:36:00**

Formatted Bullets and Numbering

Page 96: [23] Formatted	**Caro**	**03/10/2005 17:26:00**

Font: 10 pt, Bold

Page 96: [24] Formatted	**Caro**	**03/10/2005 17:26:00**

Font: 10 pt, Bold

Page 96: [25] Formatted	**Caro**	**03/10/2005 17:26:00**

None

Page 96: [26] Formatted	**Caro**	**03/10/2005 17:27:00**

Font: 10 pt

Page 96: [27] Formatted	**Caro**	**03/10/2005 17:26:00**

None

Page 96: [28] Formatted	**Caro**	**03/10/2005 17:26:00**

None

Page 96: [29] Formatted	**Caro**	**03/10/2005 17:27:00**

Font: 10 pt

Page 96: [30] Formatted	**Caro**	**03/10/2005 17:27:00**

Font: 10 pt, Bold

Page 96: [31] Formatted	**Caro**	**03/10/2005 17:27:00**

Font: 10 pt, Bold

Page 96: [32] Formatted	**Caro**	**03/10/2005 17:27:00**

None

Page 96: [33] Formatted	**Caro**	**03/10/2005 17:27:00**

Font: 10 pt

Page 96: [34] Formatted	**Caro**	**03/10/2005 17:27:00**

None

Page 96: [35] Formatted	**Caro**	**03/10/2005 17:27:00**

Font: 10 pt

Page 96: [36] Formatted	**Caro**	**03/10/2005 17:27:00**

None

Page 96: [37] Formatted	**Caro**	**03/10/2005 17:27:00**

Font: 10 pt

Page 96: [38] Formatted	**Caro**	**03/10/2005 17:27:00**

None

Page 96: [39] Formatted	**Caro**	**03/10/2005 17:27:00**

Font: 10 pt

Page 96: [40] Formatted	**Caro**	**03/10/2005 17:27:00**

None

Page 96: [41] Formatted	**Caro**	**03/10/2005 17:28:00**

Font: 10 pt

Page 96: [42] Formatted	**Caro**	**03/10/2005 17:28:00**

None

Page 96: [43] Formatted	**Caro**	**03/10/2005 17:28:00**

Font: 10 pt

Page 96: [44] Formatted	**Caro**	**03/10/2005 17:28:00**

None

Page 96: [45] Formatted	**Caro**	**03/10/2005 17:28:00**

Font: 10 pt

Page 96: [46] Formatted	**Caro**	**03/10/2005 17:28:00**

None

Page 96: [47] Formatted	**Caro**	**03/10/2005 17:14:00**

Font: 12 pt

Page 96: [48] Formatted	**Caro**	**03/10/2005 17:14:00**

Heading 2, None

Page 96: [49] Change	**Caro**	**03/10/2005 16:36:00**

Formatted Bullets and Numbering

Page 109: [50] Deleted	**Caro**	**03/10/2005 16:38:00**

Page Break

ANNEX: SMOS L1c product requirements for sea surface salinity retrieval at level 2

This note describes the needs of L2 prototype processors in terms of brightness temperature, radiometric uncertainty, geometry of observations and synthetic antenna pattern.
Section 0 gives definitions of all quantities needed by L2 prototype processor. Section 0 gives a textual description of L2 processor needs for Sea Surface Salinity and Soil Moisture retrievals. Section 0 reports the current understanding of L1 product content and details our proposal for interfacing L1 and L2 processing. Section 0 addresses other operation modes like the strip adaptive processing.

Definitions

Reference frames

Satellite reference frame

The Satellite reference frame is defined in section 5.2.1 of Earth Explorer CFI Software Mission Convention Document[1]: "*The Zs axis points along the radial satellite direction vector, positive from the centre of the TOD reference frame towards the satellite, the Ys axis points along the transversal direction vector within the osculating orbital plane (i.e the plane defined by the position and velocity vectors of the satellite), orthogonal to the Zs axis and opposed to the direction of the orbital motion of the satellite. The Xs axis points towards the out-of-plane direction vector completing the right hand reference frame.*" Figure 3 of Earth Explorer CFI Software Mission Convention Document is reproduced below for clarity:

[1] ESA ref CS-MA-DMS-GS-001 version 1.3 dated 15-07-2003.

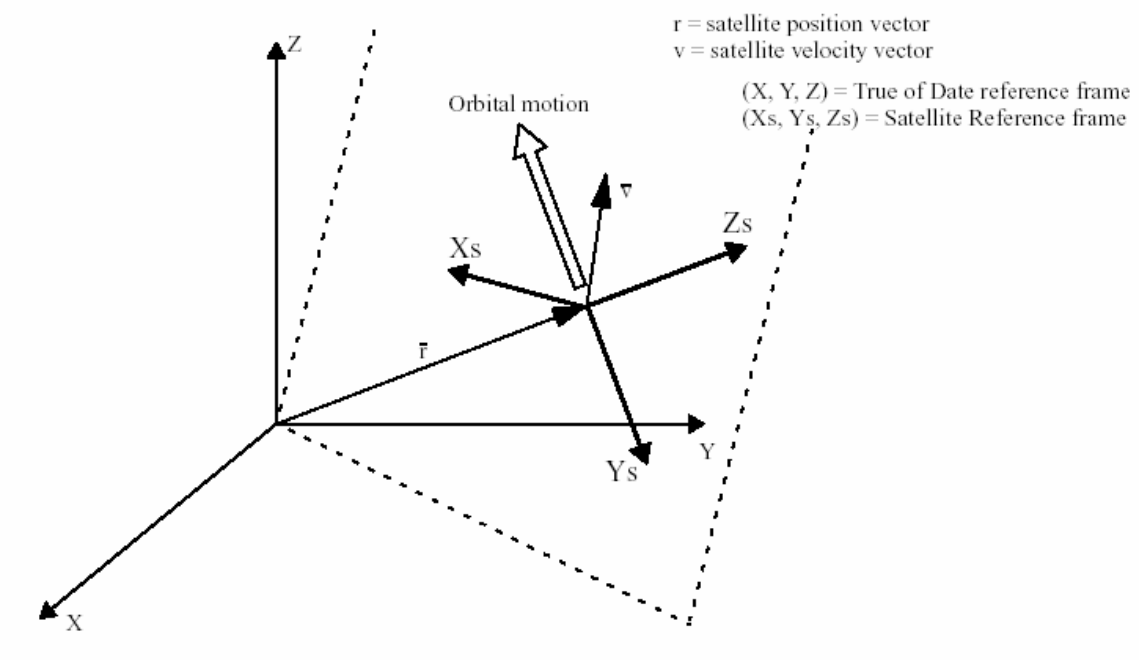

Figure 2: The Satellite Reference Frame as defined in EE CFI Mission Conventions Document

Antenna reference frame

The antenna reference frame is a satellite relative reference frame, as defined in section 5.2.2 of Earth Explorer CFI Software Mission Convention Document. The antenna reference frame is obtained by rotating the Satellite Reference Frame by two rotations because no rotation around –Ys is necessary, i.e. (Xs,Ys,Zs) = (X^1s,Y^1s,Z^1s). First rotation is around -X^1s, with a pitch angle $\xi>0$ equal to the antenna tilt angle. The second rotation around Z^2s (i.e the rotated Z^1s axis) over a yaw angle $\zeta=\pi$, so that the angle between the orbital motion vector and Y's axis is the tilt angle.
In the antenna frame, the director cosines are often used. They are defined by

$$\xi = \sin(\theta)\cos(\varphi) \qquad \eta = \sin(\theta)\sin(\varphi) \qquad \text{Eq. 1}$$

where θ is the angle between the light of sight and –Z's. φ is the azimuth of the line of sight in the antenna reference frame, with φ=0 for the X's axis and φ=π/2 for the Y's axis.

Target reference frame

At surface level, topocentric[2] reference frames are adopted, where the line of sight hit the Earth's surface.

From antenna reference frame to target reference frame

Reference frames adopted in this note are depicted in Figure 3. The antenna reference frame is noted (S,X,Y,Z) instead of (X's,Y's,Y's).

[2] See section 5.1.7 of Earth Explorer CFI Software Mission Convention Document

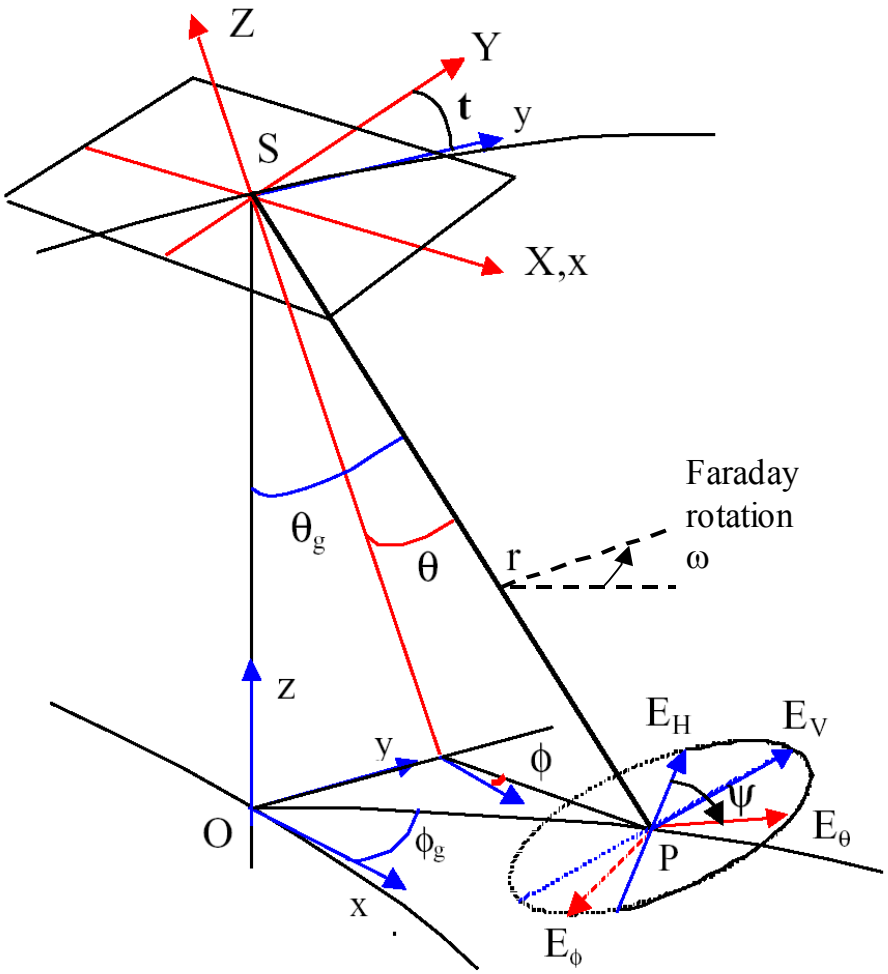

Figure 3: Definition of viewing geometry

In the surface reference frame, the horizontal (H) polarization direction is perpendicular to the incidence plan and is the product of two unit vectors that are collinear with $\overrightarrow{PS}$ and $\overrightarrow{OP}$ directions. The vertical (V) polarization direction is perpendicular to both $\overrightarrow{PS}$ and the H polarization direction.

In the antenna reference frame, the X polarization direction is along X=X's axis and the Y polarization direction is defined by the Y=Y's axis.

To link directions of polarization at surface and at antenna levels, two angles ψ and ϕ are considered, together with an intermediary angle θ. For $-\pi/2 \leq \phi_g \leq \pi/2$:

$$\theta = Arc\cos\left[\sin t \sin\theta_g \sin\phi_g + \cos t \cos\theta_g\right] \qquad \text{Eq. 2}$$

$$\phi = -Arc\sin\left[\frac{-\sin t \cos\theta_g + \cos t \sin\theta_g \sin\phi_g}{\sin\theta}\right] \qquad \text{Eq. 3}$$

$$\psi = \pi - Arc\sin\left[\frac{\cos t \sin\theta_g - \sin t \cos\theta_g \sin\phi_g}{\sin\theta}\right] \qquad \text{Eq. 4}$$

If $\pi/2 \leq \phi_g \leq 3\pi/2$, Eq. 3 and Eq. 4 give $\pi-\phi$ and $\pi-\psi$ respectively, instead of ϕ and ψ. It is worth noting that for ϕ and ψ rotation angles are define along the SP direction (toward the Earth), positive counterclockwise.

Faraday rotation

If the antenna looking toward the Earth sees a fully polarized electromagnetic waves propagating from the surface, the polarization directions rotate while the electromagnetic waves cross the ionosphere because the medium contains free electrons and is under the influence of Earth magnetic field[3]. The rotation angle is:

$$\omega = \text{constant} \int_{\text{surface}}^{\text{satellite}} N(l) B_{//}(l) dl \qquad \text{Eq. 5}$$

where N is the electron number density and $B_{||}$ is the component of the magnetic field parallel to the propagation direction. From the antenna reference frame, ω angle is positive counterclockwise.

Brightness temperatures

Brightness temperatures in the antenna frame in X and Y polarization directions are noted A1 and A2, instead of T_X ad T_Y respectively. This convention avoids confusion in full polarization mode: Stokes parameters 3 and 4 at the antenna level are noted A3 and A4 (A like Antenna), whereas they are noted T_3 and T_4 at surface level.

Dual polarization mode

Direct transformation from surface reference frame to antenna reference frame is as follows:

$$\begin{bmatrix} A1 \\ A2 \end{bmatrix} = \begin{bmatrix} \cos^2(a) & \sin^2(a) \\ \sin^2(a) & \cos^2(a) \end{bmatrix} \begin{bmatrix} T_H \\ T_V \end{bmatrix} = [MR2] \begin{bmatrix} T_H \\ T_V \end{bmatrix} \qquad \text{Eq. 6}$$

where[4]

$a = -\omega - \phi - \psi$There is a singularity problem if $\cos(a) = \sin(a)$, i.e. $a = \pm \pi/4$ or $\pm 3\pi/4$. In such a configuration, A1 = A2 = $(T_H + T_V)/2$ and it is not possible to derive T_H and T_V from A1 and A2.

Full polarization mode

$$\begin{bmatrix} A1 \\ A2 \\ A3 \\ A4 \end{bmatrix} = \begin{bmatrix} \cos^2(a) & \sin^2(a) & -\cos(a)\sin(a) & 0 \\ \sin^2(a) & \cos^2(a) & \cos(a)\sin(a) & 0 \\ \sin(2a) & -\sin(2a) & \cos(2a) & 0 \\ 0 & 0 & 0 & 1 \end{bmatrix} \begin{bmatrix} T_H \\ T_V \\ T_3 \\ T_4 \end{bmatrix} = [MR4] \begin{bmatrix} T_H \\ T_V \\ T_3 \\ T_4 \end{bmatrix} \qquad \text{Eq. 7}$$

No singularities appear in this mode. T_3 and T_4 are expected to be equal to 0. If Faraday rotation is not removed (ω =0), T_3 becomes different of 0. T_4 is always equal to 0.

Radiometric uncertainty

The most adequate reference although not complete is:

---

[3] See http://farside.ph.utexas.edu/teaching/jk1/lectures/node60.html for details.

[4] Signs of this sum are TBC because they depend on sign conventions.

Camps A., Corbella I., Bara J and Torres F.: Radiometric sensitivity computation in aperture synthesis radiometry, IEEE trans. Geosci. Rem Sens., 36, pp 680-685, March 1998

Radiometric uncertainty gives the amplitude of radiometric noise in K. It is derived from the total scene temperature, the system temperature and is a function of viewing direction according to the average LICEF receiver gain. It depends on the integration time and the receiver bandwidth as well as other parameters of the receiving channels.

$$\sigma_T \approx G \frac{\sqrt{3}}{2} d^2 \frac{(T_{sys} + T_{scene})}{\sqrt{(B \tau_{eff})}} \alpha_W \, f_{rd} \sqrt{N_V} \qquad \text{Eq. 8}$$

G is the gain of the antenna element. Expressed linearly (rather than in dB): $G \approx 7.2$ **TBC**

d is the spacing ratio: d = (distance between elements) / wavelength; d = 0.875

T_{sys} is the system temperature (K); $T_{sys} \approx 215$K, for a 2.4 dB noise figure

T_{scene} is the scene temperature (K)

B is the equivalent receiving bandwidth in Hz; $B \approx 19\ 10^6$ Hz

τ_{eff} is the effective integration time for a given polarization: $\tau_{eff} = \tau / c_{eff}$, where τ is the actual integration time. In the dual pol mode τ is always equal to 1.2s. In full pol mode, for the four Stokes components, the $4\,\tau$ values alternate between (1.2, 0.4, 0.4, 0.4) and (0.4, 1.2, 0.4, 0.4) (see Martin Neira, M., Polarimetric mode of MIRAS, *IEEE Transactions on Geoscience and Remote Sensing*, *40*, 1755-1768, 2002) **TBC**. The coefficient c_{eff} accounts for the 1 bit correlation (dominant factor 2.46), for oversampling (factor 0.74) and for the hermiticity of the cross visibilities hv and vh : $c_{eff} \approx 1.81$ for Tv and Th, $c_{eff} \approx 1.81/2$ for the third and fourth Stokes parameters.

α_W is a coefficient which accounts for integration over the apodization window. For a rectangular window, $\alpha_W = 1$; for an exact Blackman window, $\alpha_W \approx 0.452$ in the SMOS case. for Kaiser window with parameter = 13, $\alpha_W \approx 0.365$ **TBC**

f_{rd} is a factor to account for redundant visibilities: $f_{rd} \approx 0.82$ **TBC**

N_V is the total number of visibility samples: $N_V = 6\ N_{EL}^2 + 6\ N_{EL} + 1$, where N_{EL} is the number of elements per arm. In the SMOS case, $N_{EL} = 23$ and $\text{sqrt}(N_V) = 52.7$

In full polarimetric mode, T_{scene} is taken equal to 0.

The 2 or 4 σ_T values computed using the radiometric sensitivity equation yield the radiometric sensitivity on **boresight**.

It makes sense to request one separate value per Stokes parameter, as changes are expected in antenna gains and in scene temperatures.

When applying the visibility equation, it is seen that reconstructed Tb are weighted by the inverse product of element directional gains: $GV_k(\theta,\phi)\, GV^*_l(\theta,\phi)$, where *GV* are **voltage** directional gains. Similarly, the std on the Tb must be corrected. In this case however, it is not necessary to account for differences between elements, and an average directional pattern is all that is needed.

With $\overline{G}(\theta,\phi)$ the average LICEF receiver directional **power** gain function, normalized so that max(G) = 1 on boresight, the radiometric uncertainty on brightness temperature AP in polarization direction P=1, 2, 3 or 4 is given by:

$$\sigma_{AP(\theta,\phi)} = \sigma_T / \overline{G}(\theta,\phi) \qquad \text{Eq. 9}$$

Therefore the map of $\overline{G}(\theta,\phi)$ is needed for L2 processing. This is a static map. It can be expressed either in polar coordinates in the antenna frame, or conveniently in the director cosines, provided they are part of the L1 output.

For brightness temperatures at surface level, the radiometric uncertainties on T_H and T_V are given by:

$$\begin{bmatrix} \sigma^2_{T_H} & \mathrm{cov}(T_H,T_V) \\ \mathrm{cov}(T_H,T_V) & \sigma^2_{T_V} \end{bmatrix} = \left([MR2]^{-1}\right)^T \begin{bmatrix} \sigma^2_{A1} & 0 \\ 0 & \sigma^2_{A2} \end{bmatrix} [MR2]^{-1} \qquad \text{Eq. 10}$$

The matrix described by σ^2_{TH} and σ^2_{TV} is the variance/covariance matrix of brightness temperatures in surface reference frame and $([MR2]^{-1})^T$, the transposed matrix of $[MR2]^{-1}$. The variance/covariance matrix carries the radiometric uncertainties associated with T_H and T_V on its diagonal and the correlation coefficient between T_H and T_V (covariance) on the non-diagonal terms. The non-diagonal terms are equal. While *A1* and *A2* are mainly uncorrelated (ignoring correlations due to common channels), T_H and T_V are strongly correlated because they are derived from *A1* and *A2* through linear relationships.
In case MR2 is singular, σ_{TH} and σ_{TV} tend towards infinity;
$\mathrm{cov}(T_H,T_V)$ tends towards: - $\sigma_{TH}\,\sigma_{TV}$

In full polarimetric mode, no singularity is expected at the ground level.

$$\begin{bmatrix} \sigma^2_{T_H} & \mathrm{cov}(T_H,T_V) & \mathrm{cov}(T_H,T_3) & \mathrm{cov}(T_H,T_4) \\ \mathrm{cov}(T_H,T_V) & \sigma^2_{T_V} & \mathrm{cov}(T_V,T_3) & \mathrm{cov}(T_V,T_4) \\ \mathrm{cov}(T_H,T_3) & \mathrm{cov}(T_V,T_3) & \sigma^2_{T_3} & \mathrm{cov}(T_3,T_4) \\ \mathrm{cov}(T_H,T_4) & \mathrm{cov}(T_V,T_4) & \mathrm{cov}(T_3,T_4) & \sigma^2_{T_4} \end{bmatrix} = \left([MR4]^{-1}\right)^T \begin{bmatrix} \sigma^2_{A1} & 0 & 0 & 0 \\ 0 & \sigma^2_{A2} & 0 & 0 \\ 0 & 0 & \sigma^2_{A3} & 0 \\ 0 & 0 & 0 & \sigma^2_{A4} \end{bmatrix} [MR4]^{-1} \qquad \text{Eq. 11}$$

Synthetic antenna pattern

Function S gives the synthetic antenna pattern as a function of (ξ,η) that are small variations around the viewing direction (ξ_0,η_0) in the director cosine frame[5]:

$$S(\xi,\eta) = \frac{\sqrt{3}}{2} d^2 \sum_{l=1}^{L}\sum_{c=1}^{C} W \exp\left[-\pi W_r^2 \left(U\xi + V\eta\right)^2\right] \exp\left[j2\pi\left(U\left(\xi-\xi_0\right)+V\left(\eta-\eta_0\right)\right)\right] \qquad \text{Eq. 12}$$

Where:
$U(l,c)$ and $V(l,c)$ are coordinates of visibilities.
ξ_0 and η_0 are director cosines of viewing direction.
d is the spacing ratio: distance between LICEF receivers in wavelength (d=0.875)

[5] This is equation C.3 page 218 of SEPS ADDD v4.1 ref SO-TN-GMV-PLM-003 dated 18-12-2003. In SEPS documentation, the synthetic antenna pattern is called equivalent array factor.

$j = \sqrt{-1}$

$W_r = \frac{B_{\min}}{f_0}$ with $B_{\min}$ is receiver bandwidth and f_0 is the receiver center frequency (1413.5MHz)

W is the apodization function computed where coordinates of visibilities are provided.

The weighting function to be applied at surface level is derived from $S(\xi,\eta)$ after geometrical transformations:

from $(\xi_0+\xi,\eta_0+\eta)$ frame to (θ,φ) frame according to Eq. 1.

from (θ,φ) frame to (longitude, latitude) using Earth Explorer CFI.

Introducing the smearing effect along the track.

Needs for L2 prototype processing

For sea surface salinity retrieval

The final report (ref SMOS-TN-ACR-LOD-006 v1 dated 21-03-2005) of the sea surface salinity retrieval study (contract 16027/02/NL/GS) recommends that the TEC is a constrained parameter in the iterative process. This means that Faraday rotation shall not be corrected at level 1 processing.

The SSS L2 processor needs brightness temperature in the antenna reference frame (A1 and A2 for dual pol; A1, A2, A3 and A4 for full pol), along with radiometric uncertainties (σ_{A1} and σ_{A2}, for dual pol; σ_{A1}, σ_{A2}, σ_{A3} and σ_{A4} for full pol), and one angle, $(\phi + \psi)$, which depends on observation geometry. These needs are compliant with SMOS product definition baseline (see page 9 of SO-TN-ESA-GS-1250, v1.3 dated 28-01-2005).

The Faraday rotation angle ω will be computed and adjusted during level 2 processing. This angle depends on the geomagnetic field and the Total Electronic Content (TEC) of the ionosphere[6]. The TEC data will be used to compute the initial guess for Faraday rotation angle.

The SSS L2 processor needs all orbital data necessary to use the Earth Explorer CFI software. All requirements in terms of geometry (angles) shall be covered by EE CFI software.

The SSS L2 processor needs a way to compute the weighting function to be applied at surface level for estimating land or ice contamination for flagging and possibly account for them.

The SSS L2 processor takes in charge surface reflected terms such as galactic background or Sun glint, but not their possible side effects due to the reconstruction process.

For soil moisture retrieval

To be completed by ARRAY.

Interface with L1 processing

Understanding of L1c products

Our understanding of the content of L1C products, based on

[6] See Appendix A of SEPS ADDDv4.1, ref SO-TN-GMV-PLM-0003 dated 18-12-2003.

SMOS L1 Processor Input/Output Definition ref. SO-IS-DME-L1PP-014 v2.1 dated 22-02-05
SMOS L1 Product Format Specification ref. SO-IS-DME-L1PP-0002 v1.1 dated 22-02-05
SMOS L1 Auxiliary Data Specification Format ref. SO-IS-DME-L1PP-0003 v1.1 dated 22-02-05
is that they include
T_H and T_V[7] + eventually U and V
all information to compute ($\phi + \psi$) using Earth Explorer CFI,[8]
Geomagnetic field [9] and TEC[10] data in auxiliary data products.
Apodization function[11]
The L1c products do not suit the needs on L2 processors. Radiometric uncertainties are not provided. For sea surface salinity retrieval, correction of Faraday rotation is not needed.

Proposed interface with SSS prototype processor

For sea surface retrieval, it is proposed that the L1c products include in dual polarization:
A1 and A2
σ_{A1} and σ_{A2}
and for full polarization:
A1, A2, A3 and A4
σ_{A1}, σ_{A2}, σ_{A3} and σ_{A4}
For each set of brightness temperature reconstructed for one element of the SMOS grid:
A reference to the apodization function used during reconstruction.
Acquisition time
Integration time (for smearing effects).

For sea surface retrieval, it is proposed that the L1c auxiliary products include:
Synthetic antenna patterns S (see Eq. 12), tabulated for $|\xi|<2/7$ and $|\eta|<2/7$ (TBC[12]) and sampling is TBD. Each Synthetic antenna pattern table is referenced and the reference number is found in the L1c product. This referencing is used in case the apodization function changes or the strip adaptive approach is adopted (see section 0).
Orbit information (see inputs of Earth Explorer CFI).
The SMOS fixed grid (ISEA grid).

[7] See Table 26 of SO-IS-DME-L1PP-0002 page 69.
[8] See Table 25 of SO-IS-DME-L1PP-0002 page 65.
[9] TBD, see section 4.16 of SO-IS-DME-L1PP-0003 page 45.
[10] TBD, see section 4.15 of SO-IS-DME-L1PP-0003 page 44.
[11] TBD, see section 4.17 of SO-IS-DME-L1PP-0003 page 45.
[12] In first approximation, with a spacecraft at 700km altitude, to cover an area 200km around the target, we have $\sin(\theta-\theta_0)<200/700$ at nadir. Knowing that φ ranges from 0 to 2π, indicates that the condition is $|\xi|<2/7$ and $|\eta|<2/7$.

Extension to other operating modes

Strip-adaptive processing

The strip-adaptive processing, also known as equi-pixel processing, uses different apodization functions in the reconstruction process in order to minimize distortions of SMOS footprints. This means that the Synthetic antenna pattern S is not unique. It is proposed that L1 processing provides a series of Synthetic antenna pattern S, referenced by a number, and that this reference number is included in the L1c product. The number of Synthetic antenna functions S is estimated to be less than several thousands.